Title
Optimizing innate immune signals to enhance antigen-specific adaptive responses

Author
Chapon, Maxime

Publication Date
2018

Peer reviewed|Thesis/dissertation

UNIVERSITY OF CALIFORNIA

Los Angeles

Optimizing innate immune signals to enhance antigen-specific adaptive responses

A dissertation submitted in partial satisfaction of the requirements for the degree Doctor of Philosophy in Microbiology, Immunology, and Molecular Genetics

by

Maxime Chapon

2018

ABSTRACT OF THE DISSERTATION

Optimizing innate immune signals to enhance antigen-specific adaptive responses

by

Maxime Chapon

Doctor of Philosophy in Microbiology, Immunology, and Molecular Genetics

University of California, Los Angeles, 2018

Professor Genhong Cheng, Chair

The innate and adaptive immune responses are intertwined systems that require complex regulation to achieve an efficient protection from pathogens and diseases. Upon sensing of a foreign attack through specialized receptors, cells activate the transcription of cytokines such as type-I interferons to emit a danger signal and regulate their function. The strength and complexity of this signal is dependent on the type of pathogen recognition receptor (PRR) engaged. These signals can then skew the type of antigen-specific adaptive immune response that is created. In the past decade, there has been a renewed interest in using the immune system to fight cancer. A better understanding of how one can use the innate immune signals to trigger an efficacious adaptive immune response would help improve novel immunotherapies.

One of the tools used to trigger such immune response is oncolytic viruses, such as Herpes Simplex virus type 1 (HSV-1). HSV-1 has evolved proteins able to regulate the type-I interferon

response to enhance its ability to reproduce and limit attacks from the immune system. In this work, we examine the entire HSV-1 genome to determine which genes are responsible for this phenotype and characterize a novel interferon regulating protein, UL42.

Another promising pathogen that has been used to provoke anti-tumoral responses is the bacterium *Listeria monocytogenes* (Lm). Lm infection leads to a strong CD8 cytotoxic T-cell response which can be retargeted towards cancerous antigens. Here, we describe how we developed a construct to express neoantigens in Lm to trigger an antigen-specific immune response. Our results indicate that this strategy was successful *in vitro* but did not translate *in vivo*, possibly because of poor expression of the construct.

The antigen-specific T-cell receptor (TCR) repertoire can vary in diversity (breath) and individual clonal characteristics such as avidity or differentiated cell type. The extent to which the innate immune response regulates the selection of the TCR repertoire in response to a specific pathogen is poorly understood. Herein, we use an *in vivo* mouse model to investigate how different PRR ligands can affect the selection of this repertoire. Our results suggest that ligands for distinct toll-like receptors (TLR) might contribute to the selection of different TCR variable fragment families. We did not detect any difference in the complexity of the repertoire following stimulation with different TLR ligands but suggest this might be due to technical limitations associated with our *in vivo* model.

The dissertation of Maxime Chapon is approved.

Alexander Hoffman

John M Timmerman

Otto Orlean Yang

Genhong Cheng, Committee Chair

University of California, Los Angeles

2018

DEDICATION

To Andrew

For getting me through the finish line.

Et à Pepette,

The truth is out there

TABLE OF CONTENTS

LIST OF FIGURES AND TABLES

ACKNOWLEDGEMENTS

I would like to start by acknowledging Pr. Genhong Cheng for giving me the opportunity to complete my graduate studies in his laboratory. Over the years, Genhong provided me with many opportunities to work on diverse projects, help in the writing of grants, and offer my opinion on diverse ventures. I especially enjoyed our conversations regarding the field of immunotherapy as a whole and where it was headed.

I would like to thank the members of my committee, past and present: Dr. David Brooks (former), Dr. Otto Yang, Dr. John Timmerman, and Dr. Alexander Hoffman. Their support and insight during our meetings were very helpful in defining the direction of my research.

I would like to thank my collaborators Pr. Aliasger K Salem and Dr. Vijaya Joshi for providing us with the microparticles used in Chapter 4. I would also like to thank the Pr. Douglas L. Black and Dr. Yi Ying for providing me access to their MiSeq for the studies in Chapter 2.

I express my sincere gratitude to the members of the Cheng lab. In particular I would like to acknowledge Dr. Kislay Parvatyiar who was extremely helpful in defining the mechanism described in Chapter 2. I would also like to highlight Dr. Saba Aliyari who taught me many viral work techniques without which I would probably still be figuring out what project to do.

I will miss Jeffrey Zhao's undefeated enthusiasm and positive outlook on life. I am grateful for the help he and Connie Au provided me with a difficult-to-get-to-work HSV screen.

Finally, I would like to offer special thanks to Dr-Dr. Anna Reichart, Dr. Gayle Boxx, and soon-to-be doctor Sarah Christofersen. Through their support and our daily ritual of coffee sharing, they allowed me to release some of the pressure associated with grad school. I wouldn't be there without them.

Thank you to my family and friends for their constant support. Special thanks to my mother for asking me when I'll be done already. Sometimes all you need is a little nudge.

I would also like to thank my prior mentors Nadège Bercovici, Alain Trautmann, and Franck Perez for introducing me to research and shaping me into the scientist I've become.

I acknowledge the Whitcome Pre-doctoral Training Program in Molecular Biology for their financial support.

Chapter 2 is a version of the manuscript in preparation "The major HSV-1 immunoregulatory protein UL42 inhibits type-1 interferon induction and signaling". Kislay Parvatyiar participated in experimental design and performed experiments and Jeffrey S Zhao performed experiments.

I acknowledge the permission from Elsevier to reprint "Generation of a Live Attenuated Influenza Vaccine that Elicits Broad Protection in Mice and Ferrets" by Wang et al. as Appendix A.

BIOGRAPHICAL SKETCH

Education

2011-2018(exp)	**PhD candidate** in Microbiology, Immunology and Molecular Genetics
	University of California, Los Angeles
2013-2015	**Philip Whitcome fellow** in molecular biology
2008-2010	**Master degree:** "Infectiologie : Microbiologie, Virologie, Immunologie"
	Université Paris 7 Denis Diderot, France
2005-2008	**Licence degree:** "Biochimie Biologie Moléculaire"
	Université de Nantes, France

Research Experience

2011-2018	Genhong Cheng, University of California Los Angeles
	Graduate Student Researcher
February – July 11	Franck Perez lab, Institut Curie, Paris
	Consulting Engineer
2009-2010	Nadège Bercovici, Institut Cochin, Paris
	Master thesis
June 09	Nadège Bercovici, Institut Cochin, Paris
	Undergraduate Researcher
June-July 08	Nadège Bercovici, Institut Cochin, Paris
	Undergraduate Researcher

Publications and poster presentations

Maxime Chapon, Kislay Parvatiyar, Jeffrey S. Zhao, Genhong Cheng

The major HSV-1 immunoregulatory protein UL42 inhibits type-1 interferon induction and signaling.

In preparation

Maxime Chapon, Kislay Parvatiyar, Jeffrey S. Zhao, Genhong Cheng

Comprehensive mutant library reveals novel HSV-1 regulators of the interferon response

Poster presentation, 57th Midwinter Conference of Immunologists at Asilomar, 2018

Aiping Wu*, Lulan Wang*, **Maxime Chapon***, Stephanie G. Valderramos, Saba Aliyari, Chunfeng Li, Feng Ma, Natalie Quanquin, Cat-Van Tran, Yong-Qiang Deng, Hui Zhao, Xue Ji,Cheng-Feng Qin, Taijiao Jiang, Genhong Cheng

Tracking the Evolution of and Spread of Zika Virus by Footprint Analysis.

In submission

Kislay Parvatiyar, Jose Pindado, Anurupa Dev, Roghiyh Aliyari, Shivam A. Zaver, Hoda Gerami, **Maxime Chapon**, Amir A. Ghaffari, Anant Dhingra, Genhong Cheng

A TRAF3-NIK module differentially regulates DNA vs RNA pathways in innate immune signaling.

Accepted Nature Communications April 2018

Wang L*, Liu SY*, Chen HW*, Xu J*, **Chapon M**, Zhang T, Zhou F, Wang YE, Quanquin N, Wang G, Tian X, He Z, Liu L, Yu W, Sanchez DJ, Liang Y, Jiang T, Modlin R, Bloom BR, Li Q, Deng JC, Zhou P, Qin FX, Cheng G.

Generation of a Live Attenuated Influenza Vaccine that Elicits Broad Protection in Mice and Ferrets.

Cell Host Microbe. 2017 Mar 8;21(3):334-343

Wang SF, Fouquet S, **Chapon M**, Salmon H, Regnier F, Labroquère K, Badoual C, Damotte D, Validire P, Maubec E, Delongchamps NB, Cazes A, Gibault L, Garcette M, Dieu-Nosjean MC, Zerbib M, Avril MF, Prévost-Blondel A, Randriamampita C, Trautmann A, Bercovici N.

Early T cell signalling is reversibly altered in PD-1+ T lymphocytes infiltrating human tumors.

PLoS One. 2011 Mar 7;6(3):e17621

Chapon M, Randriamampita C, Maubec E, Badoual C, Fouquet S, Wang SF, Marinho E, Farhi D, Garcette M, Jacobelli S, Rouquette A, Carlotti A, Girod A, Prévost-Blondel A, Trautmann A, Avril MF, Bercovici N.

Progressive upregulation of PD-1 in primary and metastatic melanomas associated with blunted TCR signaling in infiltrating T lymphocytes.

J Invest Dermatol. 2011 Jun;131(6):1300-7

*co-first author

CHAPTER 1

Introduction

Pathogen sensing by the innate immune system

The innate immune system is the first line of defense of the body. It is characterized by a limited set of pathogen recognition receptors (PRR) able to sense defined pathogen associated molecular patterns (PAMP) [1]. Engagement of these PRR on immune and non-immune cells leads to the activation of gene programs that result in the start of a complex immune response [2]. Extracellular pathogens are detected by a set of membrane-bound sensors called toll-like receptors (TLR). Ten functional TLRs have been identified in humans, while 12 have been in mice [3].

TLR3 is responsible for recognition the genome of dsRNA viruses [1]. It can also be artificially activated by polyI:C, a synthetic RNA species. Upon binding to its ligand, TLR3 molecules in the endolysosome dimerize and recruit the adaptor molecule TIR domain-containing adapter inducing IFN-β (TRIF) [3]. TRIF then recruits TNF-receptor associated factor 6 (TRAF6) which activates transforming growth factor-β activated kinase-1 (TAK1) to activate the nuclear factor kappa-B (NF-κB) pathway [1]. TLR3 activation can also lead to type-I interferon production through activation of interferon regulatory factors IRF-3 and IRF-7 [1]. This TRIF-dependent activity is mediated through activation of TNF receptor associated factor 3 (TRAF3) which recruits the kinases TANK-binding kinase 1 (TBK1) and inhibitor of NF-κB kinase subunit epsilon (IKKε) [4]. They in turn phosphorylate IRF-3 which translocates to the nucleus where it activates the interferon-β gene transcription [5].

TLR9 is another endolysosomal sensor that recognizes viral and bacterial DNA, and can be artificially stimulated by unmethylated oligodeoxynucleotides CpG [1]. Contrary to TLR3, TLR9 recruit the adaptor myeloid differentiation factor-88 (MyD88) which recruits IL-1 receptor-associated kinases IRAK1 and IRAK2 in complex with TRAF6 and IRF-7 [6]. TRAF6

is then able to activate the NF-κB pathway and activated IRF-7 translocates to the nucleus to activate interferon-β gene transcription.

While the expression of TLRs is mostly limited to immune cells, intracellular PRRs are expressed more ubiquitously. Many cytoplasmic DNA sensors have been proposed, but the most well described pathway to date involves cyclic GMP-AMP (cGAMP) synthase (cGAS) [7]. Upon DNA binding, cGAS goes through a conformational change that activates its cGAMP synthase activity. This second messenger is sensed by stimulator of interferon genes (STING) which serves as an adaptor molecule for TBK1 and IRF-3 activation [8]. Activated IRF-3 is then able to induce the transcription of interferon-β.

Diverse roles of Type-I interferons in infections and chronic pathologies

Type-I interferons (IFN-I), of which interferon-β is a major member, are a class of cytokines that signal in an autocrine and paracrine fashion. While these molecules were first described regarding their antiviral activity [9], their deleterious role in bacterial infections were later investigated (reviewed in [10]). IFN-I has been shown to enhance the antiviral cellular response through multiple mechanisms. Type I interferons bind to a unique heterodimeric receptor complex, interferon alpha receptor 1 and 2 (IFNAR1/2). Receptor engagement leads to signaling through a JAK/STAT pathway [11]. Activated STAT homo/heterodimers translocate to the nucleus where they activate interferon stimulated genes (ISG) by binding to interferon-stimulated response element (ISRE) or gamma-activated sequences (GAS) promoter sequences [11]. Beyond its anti-viral effects, IFN-I has also been associated with anti-tumoral effects by acting directly on tumor cells (reviewed in [12]).

Type-I interferons also play a role in regulating the antigen-specific, adaptive immune response. IFN-I are crucial for the drastic expansion of CD8 T-cells in response to viral infection [13]. They can induce the production of cytokines such as IL-15 which enhances survival and proliferation of memory CD8 T-cells [14]. Type I interferons are also able to promote the proliferation of antigen specific CD8 T-cells by providing a third activation signal [15]. At the same time, they can curtail the proliferation of bystander, non-antigen-specific cells through differential STAT signaling [16]. IFN-I signaling can alter the differentiation of CD4 helper T-cells depending on the stage of infection, therefore regulating the kind of help available to other immune cells such as CD8 T-cells and B-cells [17]. Type-I interferons also enhance antigen cross-presentation, or the ability of dendritic cells (DC) to present extra-cellular peptides on the major histocompatibility complex-I (MHC-I) [18], [19].

During chronic diseases such as cancer and long-term viral infections, IFN-I are thought to have a negative effect on the immune response by promoting immunosuppression [17]. In a model of SIV infection, a strong but transient IFN-I response is associated with better control than a persistent IFN-I production [20]. They can skew the adaptive response by altering the differentiation of naïve CD4 T-cells [21]. PD-1 ligand 1 (PD-L1), an inhibitory receptor involved in T-cell inactivation, has its expression enhanced by IFN-I [22]. During chronic viral infection, IFN-I blockade facilitates viral clearance through a CD4 T-cell dependent mechanism [23].

Recent findings highlight that for an effective immune response to be provoked, a fine balance in the strength and timing of the type-I interferon response needs to be reached. In Chapter 2, we investigate IFN-I regulating genes in the Herpes Simples virus type 1 (HSV-1) virus. This pathogen has been used as an oncolytic vector for immunotherapy [24]. By gaining better insight

into the ways the virus regulates the host interferon response, we hope to develop new viral strains with improved immunogenicity. Our results describe novel immunoregulatory viral proteins and detail the mechanism by which one of them, the viral polymerase processivity factor UL42, is able to reduce interferon-β production and signaling.

Listeria monocytogenes as a vector of immunotherapy

Listeria monocytogenes (Lm) is a facultative intracellular gram-positive bacterium that has long been used as a tool to study CD8 T-cell cytotoxic response for its ability to induce strong anti-specific proliferation of those cells [25]. Upon infection, Lm is present in a vacuole in the cytoplasm of the infected cell. It is able to escape from that vacuole by secreting the virulence factor listeriolysin O (LLO). In the cytoplasm, it can proliferate and spread to neighboring cells using actin-assembly-inducing protein (ActA) to polymerase actin comet tails. This part of the life cycle being completely intracellular, Lm is shielded from antibody-mediated immune response, which skews the adaptive response to a cytotoxic phenotype. Interestingly, despite this intracellular life-cycle that could be compared to that of viruses, type-I interferon has been associated with reduced resistance to this pathogen [26]. Lm induces interferon-β through activation of the STING pathway. Mice deficient for that pathway showed no defect in Lm immunity. They also had higher levels of antigen-specific CD8 T-cells when infected with ActA-deficient Lm in conjunction with a STING activator [27]. Interestingly, STING has recently been shown to be deleterious during T-cell induction, which could explain that later result [28].

The ability of attenuated Lm strains to induce strong cytotoxic T-cell responses is being investigated in the context of cancer immunotherapy [29]. In Chapter 3, we investigate the use of

attenuated Lm as a vector for immunotherapy against tumor neoantigens. While some cancers are caused by viruses (HPV, EBV, HCV) and therefore provide good targets for immunotherapy, many tumors arise from somatic mutations. Thankfully, many cancers have elevated mutation rate that increase the chance of amino acid changes in cytotoxic T-cell specific peptides [30]. These present a good opportunity to search for those newly formed neo-antigens through tumor sequencing and in silico peptide prediction [31]. Our results show that this strategy is feasible and promising *in vitro*, although we were not able to obtain *in vivo* efficacy due to technical issues with our construct. Other groups have been more successful and such constructs are now being investigated in clinical trials [32].

T-cell receptor repertoire production and selection

T-cells and B-cells are the only cell type able to rearrange their DNA to produce novel receptors. This process takes place in the thymus for developing T-cells or thymocytes. Gene fragments (Variable V, diversity D, junction J, and constant C) are semi-randomly rearranged while nucleotides are randomly removed and added at each V-D, D-J, and J-C junction. This process, which happens for the α and β chains of the receptor, gives rise to a unique complementary determining region (CDR) that defines the binding selectivity of the newly formed T-cell receptor (TCR). The cells are then selected in the thymus to delete or inhibit auto-reactive clones, and the remainder cells exit to the periphery. Between cells that fail to produce a functional TCR and those that are self-reactive, it is estimated that over 99% of thymocytes are deleted during their differentiation into naïve T-cells as measured by the potential TCR diversity and that effectively observed in the repertoire [33].

The human circulating TCR repertoire is estimated to be composed of a few million different clones [33]. Out of these, only a small percentage is able to recognize tumor antigens or neoantigens. In the context of vaccine design and immunotherapy, it is crucial that the best clones be selected from the available repertoire. The breadth of the selected cells, or how diverse they are, can also improve the ability of the immune response to adapt to antigen mutations. For a T-cell to be activated, it must be presented its cognate antigen on the proper MHC molecule. The chances of that interaction leads to T-cell activation depends on multiple factors including the affinity of the TCR for its MHC-peptide complex [34], [35], the amount of antigen presented, and the strength of the co-stimulatory signals available to the T-cell [36].

Lines of evidence exist to show that different innate immune signals might alter the ability of a T-cell to get activated. On the one hand, our laboratory showed that different TLR ligands can induce different responses in dendritic cells [37]. One the other hand, T-cells are able to sense TLR ligands at rest or following activation [38], [39]. Previous works investigating the influence of innate immune signals into TCR repertoire selection have found that CD4 T-cells could select for TCR clones containing different, yet defined, amino acid sequence characteristics [40]. Another group found contradictory results in CD8 T-cells by using whole pathogens as innate stimuli [41]. We believe that these models have failed to identify the effect of individual innate immune pathways because they have used either complex adjuvants or whole pathogens. We hypothesized that a simpler model - using a single antigen and adjuvant at a time - should produce more definitive results.

In Chapter 4, we set to determine whether using a TLR3 agonist – polyI:C – or a TLR9 agonist – CpG – would result in the selection of TCR repertoires with different characteristics.

We set up a challenging *in vivo* model to study this question, using microparticle containing the chicken ovalbumin classical antigen and either TLR ligand. Although preliminary results were encouraging, technical difficulties rising from the choice of such a model and the TCR sequencing technique prevented us from obtaining a conclusive answer. We believe that future studies should focus on using a more controlled *in vitro* model, with a known input repertoire (possibly of recombinant clones) and purified dendritic cells.

Conclusion and future perspectives

This work combines different strategies we used to gain a better understanding of how innate immune stimuli regulate the adaptive immune response, or design ways to use those stimuli to improve adaptive responses. Through furthering our understanding of these interactions, we hope that future therapies can be engineered to provoke efficient immune responses against cancer, or improve vaccine designs.

REFERENCES

[1] T. Kawai and S. Akira, “The role of pattern-recognition receptors in innate immunity: update on Toll-like receptors,” *Nat. Immunol.*, vol. 11, no. 5, pp. 373–384, May 2010.

[2] N. W. Palm and R. Medzhitov, “Pattern recognition receptors and control of adaptive immunity,” *Immunol. Rev.*, vol. 227, no. 1, pp. 221–233, Jan. 2009.

[3] T. Kawai and S. Akira, “Toll-like receptors and their crosstalk with other innate receptors in infection and immunity,” *Immunity*, vol. 34, no. 5, pp. 637–650, May 2011.

[4] G. Oganesyan *et al.*, “Critical role of TRAF3 in the Toll-like receptor-dependent and -independent antiviral response,” *Nature*, vol. 439, no. 7073, pp. 208–211, Jan. 2006.

[5] H. Häcker and M. Karin, “Regulation and function of IKK and IKK-related kinases,” *Sci. STKE Signal Transduct. Knowl. Environ.*, vol. 2006, no. 357, p. re13, Oct. 2006.

[6] S. Akira, S. Uematsu, and O. Takeuchi, “Pathogen recognition and innate immunity,” *Cell*, vol. 124, no. 4, pp. 783–801, Feb. 2006.

[7] L. Unterholzner, “The interferon response to intracellular DNA: why so many receptors?,” *Immunobiology*, vol. 218, no. 11, pp. 1312–1321, Nov. 2013.

[8] Q. Chen, L. Sun, and Z. J. Chen, “Regulation and function of the cGAS-STING pathway of cytosolic DNA sensing,” *Nat. Immunol.*, vol. 17, no. 10, pp. 1142–1149, 20 2016.

[9] A. Isaacs and J. Lindenmann, “Virus interference. I. The interferon,” *Proc. R. Soc. Lond. B Biol. Sci.*, vol. 147, no. 927, pp. 258–267, Sep. 1957.

[10] G. M. Boxx and G. Cheng, “The Roles of Type I Interferon in Bacterial Infection,” *Cell Host Microbe*, vol. 19, no. 6, pp. 760–769, Jun. 2016.

[11] L. B. Ivashkiv and L. T. Donlin, “Regulation of type I interferon responses,” *Nat. Rev. Immunol.*, vol. 14, no. 1, pp. 36–49, Jan. 2014.

[12] L. Zitvogel, L. Galluzzi, O. Kepp, M. J. Smyth, and G. Kroemer, "Type I interferons in anticancer immunity," *Nat. Rev. Immunol.*, vol. 15, no. 7, pp. 405–414, Jul. 2015.

[13] G. A. Kolumam, S. Thomas, L. J. Thompson, J. Sprent, and K. Murali-Krishna, "Type I interferons act directly on CD8 T cells to allow clonal expansion and memory formation in response to viral infection," *J. Exp. Med.*, vol. 202, no. 5, pp. 637–650, Sep. 2005.

[14] D. B. Stetson and R. Medzhitov, "Type I interferons in host defense," *Immunity*, vol. 25, no. 3, pp. 373–381, Sep. 2006.

[15] J. M. Curtsinger, J. O. Valenzuela, P. Agarwal, D. Lins, and M. F. Mescher, "Type I IFNs provide a third signal to CD8 T cells to stimulate clonal expansion and differentiation," *J. Immunol. Baltim. Md 1950*, vol. 174, no. 8, pp. 4465–4469, Apr. 2005.

[16] M. P. Gil, R. Salomon, J. Louten, and C. A. Biron, "Modulation of STAT1 protein levels: a mechanism shaping CD8 T-cell responses in vivo," *Blood*, vol. 107, no. 3, pp. 987–993, Feb. 2006.

[17] L. M. Snell, T. L. McGaha, and D. G. Brooks, "Type I Interferon in Chronic Virus Infection and Cancer," *Trends Immunol.*, vol. 38, no. 8, pp. 542–557, Aug. 2017.

[18] M. S. Diamond *et al.*, "Type I interferon is selectively required by dendritic cells for immune rejection of tumors," *J. Exp. Med.*, vol. 208, no. 10, pp. 1989–2003, Sep. 2011.

[19] M. B. Fuertes *et al.*, "Host type I IFN signals are required for antitumor CD8+ T cell responses through CD8{alpha}+ dendritic cells," *J. Exp. Med.*, vol. 208, no. 10, pp. 2005–2016, Sep. 2011.

[20] L. D. Harris *et al.*, "Downregulation of robust acute type I interferon responses distinguishes nonpathogenic simian immunodeficiency virus (SIV) infection of natural hosts from pathogenic SIV infection of rhesus macaques," *J. Virol.*, vol. 84, no. 15, pp. 7886–7891, Aug.

2010.

[21] I. Osokine *et al.*, "Type I interferon suppresses de novo virus-specific CD4 Th1 immunity during an established persistent viral infection," *Proc. Natl. Acad. Sci. U. S. A.*, vol. 111, no. 20, pp. 7409–7414, May 2014.

[22] H.-Y. Cho, S.-W. Lee, S.-K. Seo, I.-W. Choi, I. Choi, and S.-W. Lee, "Interferon-sensitive response element (ISRE) is mainly responsible for IFN-alpha-induced upregulation of programmed death-1 (PD-1) in macrophages," *Biochim. Biophys. Acta*, vol. 1779, no. 12, pp. 811–819, Dec. 2008.

[23] E. B. Wilson *et al.*, "Blockade of chronic type I interferon signaling to control persistent LCMV infection," *Science*, vol. 340, no. 6129, pp. 202–207, Apr. 2013.

[24] B. L. Liu *et al.*, "ICP34.5 deleted herpes simplex virus with enhanced oncolytic, immune stimulating, and anti-tumour properties," *Gene Ther.*, vol. 10, no. 4, pp. 292–303, Feb. 2003.

[25] E. G. Pamer, "Immune responses to Listeria monocytogenes," *Nat. Rev. Immunol.*, vol. 4, no. 10, pp. 812–823, Oct. 2004.

[26] V. Auerbuch, D. G. Brockstedt, N. Meyer-Morse, M. O'Riordan, and D. A. Portnoy, "Mice lacking the type I interferon receptor are resistant to Listeria monocytogenes," *J. Exp. Med.*, vol. 200, no. 4, pp. 527–533, Aug. 2004.

[27] K. A. Archer, J. Durack, and D. A. Portnoy, "STING-dependent type I IFN production inhibits cell-mediated immunity to Listeria monocytogenes," *PLoS Pathog.*, vol. 10, no. 1, p. e1003861, Jan. 2014.

[28] B. Larkin, V. Ilyukha, M. Sorokin, A. Buzdin, E. Vannier, and A. Poltorak, "Cutting Edge: Activation of STING in T Cells Induces Type I IFN Responses and Cell Death," *J. Immunol.*,

vol. 199, no. 2, pp. 397–402, Jul. 2017.

[29] J. Rothman and Y. Paterson, "Live-attenuated Listeria-based immunotherapy," *Expert Rev. Vaccines*, vol. 12, no. 5, pp. 493–504, May 2013.

[30] L. B. Alexandrov *et al.*, "Signatures of mutational processes in human cancer," *Nature*, vol. 500, no. 7463, pp. 415–421, Aug. 2013.

[31] P. F. Robbins *et al.*, "Mining exomic sequencing data to identify mutated antigens recognized by adoptively transferred tumor-reactive T cells," *Nat. Med.*, vol. 19, no. 6, pp. 747–752, Jun. 2013.

[32] "Expressing Personalized Tumor Antigens Study" [Online]. Available: https://clinicaltrials.gov/ct2/show/NCT03265080. [Accessed: 20-May-2018].

[33] H. S. Robins *et al.*, "Comprehensive assessment of T-cell receptor β-chain diversity in αβ T cells," *Blood*, vol. 114, no. 19, pp. 4099–4107, Nov. 2009.

[34] H. D. Moreau *et al.*, "Dynamic in situ cytometry uncovers T cell receptor signaling during immunological synapses and kinapses in vivo," *Immunity*, vol. 37, no. 2, pp. 351–363, Aug. 2012.

[35] D. Skokos *et al.*, "Peptide-MHC potency governs dynamic interactions between T cells and dendritic cells in lymph nodes," *Nat. Immunol.*, vol. 8, no. 8, pp. 835–844, Aug. 2007.

[36] J.-L. Chen *et al.*, "Ca2+ release from the endoplasmic reticulum of NY-ESO-1-specific T cells is modulated by the affinity of TCR and by the use of the CD8 coreceptor," *J. Immunol. Baltim. Md 1950*, vol. 184, no. 4, pp. 1829–1839, Feb. 2010.

[37] S. E. Doyle *et al.*, "Toll-like receptors induce a phagocytic gene program through p38," *J. Exp. Med.*, vol. 199, no. 1, pp. 81–90, Jan. 2004.

[38] A. E. Gelman, J. Zhang, Y. Choi, and L. A. Turka, "Toll-like receptor ligands

directly promote activated CD4+ T cell survival," *J. Immunol. Baltim. Md 1950*, vol. 172, no. 10, pp. 6065–6073, May 2004.

[39] M. J. Richer, J. C. Nolz, and J. T. Harty, "Pathogen-specific inflammatory milieux tune the antigen sensitivity of CD8(+) T cells by enhancing T cell receptor signaling," *Immunity*, vol. 38, no. 1, pp. 140–152, Jan. 2013.

[40] L. Malherbe, L. Mark, N. Fazilleau, L. J. McHeyzer-Williams, and M. G. McHeyzer-Williams, "Vaccine adjuvants alter TCR-based selection thresholds," *Immunity*, vol. 28, no. 5, pp. 698–709, May 2008.

[41] B. D. Rudd, V. Venturi, M. J. Smithey, S. S. Way, M. P. Davenport, and J. Nikolich-Zugich, "Diversity of the CD8+ T cell repertoire elicited against an immunodominant epitope does not depend on the context of infection," *J. Immunol. Baltim. Md 1950*, vol. 184, no. 6, pp. 2958–2965, Mar. 2010.

CHAPTER 2

The major HSV-1 immunoregulatory protein UL42 inhibits type-1 interferon induction and signaling

ABSTRACT

HSV-1 is the most common alpha-herpesviridae infection and one of the major causes of cold sores and genital herpes. The viral genome is encoded by a 152kbp genome containing over 80 genes. HSV-1 is particularly apt at inhibiting the type-I interferon response, and many of the viral proteins carry out such activity. In this study, we created a viral mutant library by randomly inserting a disruptive 1.2kbp transposon into the genome. We then subjected the viral library to serial passaging in the presence or absence of type-I interferon selective pressure. We found that previously reported interferon regulating viral genes did not present the strongest selective phenotype. We report that the viral polymerase processivity factor UL42 can inhibit the interferon-β gene transcription, and that this activity is dependent on its interaction with the transcription factor IRF-3. This study represents a proof of concept for the use of high-throughput screening on the HSV-1 genome to gain a better insight into its biology and offers new targets for antiviral therapy and oncolytic vector design.

INTRODUCTION

The type-I interferon (IFN-I) response is one of the most common immune responses in our body, with most cells being able to produce interferon-β in response to pathogenic stimulation [1]. Cells detect the presence of pathogen associated molecular patterns (PAMP) through their binding to pattern recognition receptors (PRR) which lead to the activation of multiple signalization pathways [2]. Cytosolic viral DNA can be recognized by the cytosolic sensor cyclic GMP-AMP (cGAMP) synthase (cGAS) [3] which, following a conformational change, produces the second messenger cGAMP [4]. The adaptor molecule stimulator of interferon genes (STING) senses that signals and recruits TANK-binding kinase 1 (TBK1) which in turns activates the transcription factor IFN regulatory factor 3 (IRF-3) [5]. Activated IRF-3 translocates to the nucleus where it stimulates the transcription of interferon-β. Interferon-β production leads to transcriptional changes in an autocrine and paracrine manner that increases cells sensitivity to viral infections and leads to the production of numerous antiviral factors (reviewed in [1]). As such, many viruses have evolved means to regulate the IFN-I response, whether by blocking interferon production, its downstream signaling, or specific interferon stimulated genes (ISG) (reviewed in [6], [7]).

Herpes virus simplex type 1 (HSV-1) is the most common alpha-herpesviridae infecting humans with up to 90% of the population infected depending on age and location [8]. It is transmitted by contact and infects epithelial cells before migrating through neuronal axons to the nearest sensory neuron nucleus where it usually goes into a state of latency [9]. Viral reactivation usually takes place at several months interval, and generally does not lead to complications. As such a common pathogen, it has been the focus of years of investigation into its biology (reviewed in

[10]). Its large dsDNA genome contains over 80 open reading frames (ORF). Many of these proteins have been identified as regulators of the IFN-I response [11], including some targeting the cGAS/STING/TBK1/IRF-3 pathway [12], [13].

To date, most of the investigation into HSV-1 biology has been carried out by creating viral strains lacking a specific ORF. While highly successful, this method can present disadvantages such as lower speed, difficulty to assess multifunctional proteins, and lack of insight into intergenic regions. We chose to use a method that has proven successful in the study of other viral [14] and bacterial genomes [15]. We created a viral mutant library covering the entire HSV-1 genome and used differential selective pressure to identify novel IFN-I regulating viral proteins. We found that one of the major such regulatory protein is UL42. In addition to previously reported effect on NF-κB signaling [16], we found that UL42 is able to target IRF-3 and prevent interferon-β transcriptional induction. We also report that UL42 can reduce the activation of the ISRE promoter following interferon-β stimulation. Our study introduces a new tool to study the HSV-1 genome and identifies a novel mechanism by which this virus is able to prevent IFN-I activation and signaling.

RESULTS

Generation of a comprehensive HSV-1 mutant library

Herpes Simplex Viruses have been studied extensively over the years, usually through targeted mutations. A possible drawback of such strategy is the difficulty to assess the relative strength of two mutants sharing a similar phenotype. In order to interrogate the viral genome in an unbiased fashion, we generated a viral mutant library. We modified a MuA-based transposon system by inserting a BpuEI IIS restriction enzyme site at the final nucleotide of the inverted terminal repeat. This provides us with the ability to sequence 16nt on each end of the transposon insertion by digesting the viral genome with BpuEI. We then used the MuA transposase to randomly insert the 1.2kb transposon into a bacterial artificial chromosome containing the HSV-1 genome (BAC HSV-1) (Figure 2.1a). We transformed the library into *E. coli* bacteria and collected around 8000 clones to generate a mutant library with an insertion every 20 base pair on average. As expected, no clones were isolated with an insertion in the BAC maintenance genes, those being unable to maintain in *E. coli* (Figure 2.1b). Regions containing short repeats, while covered by the BAC library, do not provide enough diversity to align to the reference genome with sufficient confidence and are therefore not included in our analysis. Resequencing of the wild type BAC HSV-1 revealed it to be most closely related to the ZW6 strain (GenBank: KX424525.1) with the addition of the BAC and firefly luciferase reporter cassettes, and a deletion of oriL. Alignment of the library to this wild type reference genome was consistently superior to 90% of the processed reads (workflow described in Methods).

Library selection in wild-type cells reveals Unique Short genes as more dispensable

The BAC HSV-1 library was transfected in HEK 293T cells and expanded in Vero cells to generate our Input viral library. By comparing the BAC HSV-1 library to the Input library, we noticed the strongest reduction in transposon coverage was located at the viral OriS located in the Repeat Short fragment. In contrast to ZW6, our strain contains a deletion of the OriL origin of replication. Indeed, while wild type (WT) HSV-1 can replicate with a single origin of replication [17], a deletion of OriS in an OriL-deficient strain is not viable.

In order to generate a comprehensive map of essential genes of HSV-1 and confirm the soundness of our screening method, we subjected the library to five consecutive rounds of selection in wild-type cell lines. The trend initiated in the first generation of virus was confirmed after five successive passages in African green monkey kidney Vero cells, and HEK 293T embryonic kidney cells (Figure 2.1c, d).

The strongest selection occurred in HEK 293T cells, consistent with these being the least permissive of the two as determined by their respective viral growth curve (Figure S2.1a). Only three genes were differentially selected between Vero and HEK 293T cells: US9, US11, and US12 (Figure S2.1b). US11 and US12 disruption was better supported in Vero cells than in HEK293T cells. US9 was non-essential in both cell types but a very stringent competition in HEK 293T led up US9 mutants to represent up to 15% of the final passage library.

Most genes that have previously been reported to be essential for viral growth saw a reduction in their relative amount between the BAC library and the final passage viral libraries. Interestingly, WT virus, represented by insertions in proteins unrelated to the viral life cycle (green fluorescent protein, firefly luciferase, chloramphenicol resistance gene, hygromycin B resistance

gene) did not appear the fittest in these in vitro conditions. Indeed, viruses with insertions in several unique short (US) coding sequences saw their relative amount increased more significantly. Overall, insertions in the terminal repeats or the US sequences grew better as shown in Figure 2.1c and d where most positive fold changes are shifted to the right of the genome. In fact, many genes considered non-essential in the 3' end of the unique long (UL) fragment seem to be necessary for proper fitness in a population screening strategy. Indeed, insertions in genes such as UL39, UL41, or UL53 were deleterious to those mutants.

Library selection in WT vs IFNAR1$^{-/-}$ A549 cells reveals strong immunomodulatory candidates

To investigate the ways by which HSV-1 suppresses the type-I interferon (IFN-I) response, we passaged the viral library in A549 wild type and A549 IFNAR$^{-/-}$ cells (Figure 2.2a, b, respectively). Consistent with a defect in antiviral immunity, the viral titers collected during passages were superior in IFNAR1$^{-/-}$ cells (Figure S2.2).

We then compared the selective pressure in the two different cell lines, looking for genes that are non-essential in IFNAR1$^{-/-}$ cells but negatively selected in WT cells. We used TnSeqDiff to calculate the respective enrichment for each open reading frame of HSV-1 (Figure 2.2c). Importantly, the wild-type viruses, with insertions located in genes not related to HSV-1 biology – green circles on Figure 2.2c – do not show differential growth between the WT and IFNAR1$^{-/-}$ cell lines. Most genes are biased towards lesser selection in IFNAR1$^{-/-}$ cells, which is consistent with a reduced selective pressure. Proteins previously described to alter interferon production (US3, VP24) or signaling (ICP27) are biased towards better growth in IFNAR1$^{-/-}$ but do not show the

strongest phenotype. Indeed, the 3 most strongly biased genes have not previously been described to inhibit interferon activity in HSV-1.

To determine whether these candidates acted directly on interferon-β activation and to choose the top candidate to study further, we cloned these genes in a eukaryotic expression vector. We then expressed these proteins with an interferon-β luciferase reporter and determined that both US1 and UL42 are able to inhibit STING-dependent interferon-β activation, but UL44 is not (Figure 2.2d). UL42 having the strongest phenotype of the three, we decided to investigate its mechanism of action further.

UL42 inhibits interferon beta production and interacts with IRF3

The DNA polymerase processivity factor encoded by UL42 is an essential protein that, with the DNA polymerase catalytic subunit UL30, forms the viral DNA polymerase responsible for genome replication. Previous studies have characterized UL42 as a nuclear DNA binding protein with no sequence specificity [18]. Interestingly, early studies showed that about half of the UL42 protein was bound to UL30, while the other half was free from this complex, consistent with functions beyond DNA replication [19]. Another group previously reporter the ability of UL42 to inhibit TNF-α stimulated NF-κB activation, and the ability of UL42 to bind NF-κB subunits [16]. We were able to confirm this result using an NF-κB-luciferase reporter and TRAF6 overexpression (Figure S2.3a).

Further characterization of UL42 indicated a very strong effect on the IFN-I response as UL42 overexpression was sufficient to block IFN-β-Luc reporter activity induced by STING, TBK1, or IRF3 overexpression (Figure 2.3a, b, c).

BDNA transfection is able to recapitulate the effect of foreign DNA being present in the cell cytoplasm. This leads to cGAS activation and production of cyclic di-nucleotide second messengers that activate STING [4]. STING then migrates from the endoplasmic reticulum to the Golgi where it serves as a scaffolding protein for TBK1 and IRF3. TBK1 phosphorylates IRF3 which translocated to the nucleus and activates IFN-β transcription [5]. A20 is an inhibitor of TBK1 mediated activation of IRF3 [20]. Following BDNA stimulation, UL42 was able to suppress transcriptional activation of IFN-β and of its downstream interferon stimulated gene (ISG) ISG54 (Figure 2.3d, e).

As the previously reported NF-κB effect seemed unlikely to have such a potent effect on IFN-β activation, and IRF3 overexpression could not recapitulate IFN-β-Luc activation, we investigated whether UL42 could act directly on IRF3. Using co-immunoprecipitation, we found that UL42 is able to interact with IRF3 when both proteins are overexpressed (Figure 2.3f). A common mechanism of inhibition of transcription factor activity is to prevent the translocation of their active form to the nucleus. To investigate whether UL42 has an effect on IRF3 translocation, we co-transfected UL42-flag with HA-TBK1 and stained for endogenous IRF3. We observed that IRF3 translocation is dependent on TBK1 signal strength, but that UL42 is not able to prevent IRF3 nuclear translocation (Figure 2.3g). This was not dependent on the amount of UL42 co-transfected (data not shown).

The interferon enhanceosome is composed of four binding sites for three transcription factors: NF-κB, IRFs, and AP-1. Having established that UL42 can act on the first two components, we set to check whether it could also inhibit AP-1 activation using a luciferase

reporter. Under PMA stimulation, we found UL42 overexpression to have no effect on AP-1 activation (Figure S2.3b).

A non-DNA binding mutant of UL42 is unable to interact with IRF3 and has impaired IFN-β inhibition ability

Earlier studies determined the DNA binding surface of UL42 to be a positively charged area of the protein orthogonally located to its UL30 binding domain [21] (Figure 2.4a, blue). Arginine to alanine mutations on this surface were sufficient to hinder the ability of UL42 to bind DNA and perform its activity as polymerase processivity factor [22]. Additionally, mutations in this domain reduced the ability of UL42 to inhibit NF-κB signaling [16]. We therefore investigated whether mutating arginines 279 and 280 to alanines would have an effect on UL42's ability to reduce IFN-β activation. Similar to previous reports, the double mutant protein was not able to suppress IFN-β activation in the context of TBK1 overexpression, while a mutant truncated of its canonical NLS only showed an intermediate phenotype (Figure 2.4b). Additionally, the double mutant had reduced inhibition of BDNA induced activation of IFN-β and ISG54 transcript (Figure 2.4c, d).

While this R279-280A mutant has been described to be unable to bind DNA, we wanted to determine whether it maintained its ability to bind IRF3. We therefore overexpressed the WT or mutant flag-tagged UL42 with HA-IRF3 and immunoprecipitated IRF3. While WT UL42 is able to bind IRF3, the mutant is not (Figure 2.4e). This indicates that in addition to losing its ability to interact with DNA, the double mutant also loses its ability to bind IRF3, which is consistent with the loss of IFN-β transcriptional regulation activity.

UL42 inhibits IFN-β signaling and is not a non-specific transcriptional inhibitor

While UL42 did not inhibit IFN-β transcriptional activation as strongly as A20, it was able to suppress downstream genes such as ISG54 in the same amount (Figure 2.3d, e). To investigate whether UL42 is able to target IFN-β signaling on top of its transcriptional activation, we overexpressed UL42 in the presence of an interferon-sensitive response element (ISRE) luciferase reporter. We then treated the cells with recombinant IFN-β. Indeed, WT UL42, but not the R279-280A mutant, was able to suppress ISRE activity following IFN-β stimulation (Figure 2.5a). This indicates that UL42 is able to suppress both type-I interferon activation by inhibiting NF-κB and IRF3 signaling, and type-I interferon signaling by inhibiting the ISRE promoter activation.

To confirm that the UL42-driven effects did not result from a general transcriptional inhibition, we tested the effect of UL42 overexpression on the cAMP response element (CRE). We found that UL42 had no effect on Forskolyn driven activation of a CRE-luciferase reporter (Figure 2.5b). Furthermore, overexpression of UL42 had no effect on the level of housekeeping gene transcript as measured by RT-qPCR (Figure 2.5c).

DISCUSSION

Numerous studies have helped define the role of individual HSV-1 proteins [10]. The majority of these studies relied on the construction of strains knocked-out for one or more loci. This method has proven very effective but comes with multiple drawbacks including having to construct a mutant for every open reading frame, limited granularity in the analysis, and not examining intergenic regions. Having a limited genome, many viruses have evolved multifunctional

proteins. The major phenotype associated with knocking-out such proteins can make it difficult to recognize their secondary functions.

In this study, we decided to use an unbiased technique that has proven effective in the study of other viruses [14] and bacteria [15] but had never been used before in HSV-1. We created a library of mutants containing a disruptive 1.2kb insertion every 20 base pairs on average, with each mutant containing a single insertion. The coverage of the genome was complete, making this library an effective tool to interrogate every region of the viral genome, provided the proper selective environment exists. We show that sequential passaging of the library *in vitro* leads to the negative selection of genes that have been described as essential while disruption of non-essential genes is generally not deleterious to the virus. Interestingly, the viruses that were the fittest in this first screen were those that contained insertions in some non-essential genes and not the wild-type viruses (in which the insertion is in a gene not related to HSV-1 biology). This seems to indicate that in these in vitro conditions, some genes such as US9 are not simply non-essential but actually limit the growth of the virus. Indeed, US9 has been reported to be important for anterograde transport in neural axons, which could explain why its expression is dispensable in our system [23]. Importantly, our strain of HSV-1 does not contain mutations preventing expression of US9 which are present in the KOS strain [24] which would have made insertions in that ORF theoretically ineffectual.

Gaining a better understanding of the ways by which HSV-1 regulates the innate immune response has helped designing novel immunotherapies [25] and could also provide insight into antiviral therapies. By selecting our library in WT or IFNAR1$^{-/-}$ cells, we found that most previously described interferon regulating proteins were biased towards better growth in interferon

signaling deficient cells. Surprisingly, the most drastically selected ORFs had not been described as being involved in regulating this pathway before. HSV-2 US1 has been described as inhibiting type-I interferon activation by blocking IRF3 from binding its promoter [26]. In that study however, the HSV-1 US1 was not able to recapitulate that phenotype by luciferase assay. In that regard, our results are contradicting as we were able to confirm the ability of HSV-1 US1 to block STING-induced IFN-β luciferase reporter activation, whether the protein contained a C-terminal, N-terminal, or no tag (data not shown). It is possible that the viral strains our two laboratories used contain different sequences for the US1 gene that could explain this discrepancy. We showed that UL44 does not affect IFN-β activation. It is important to remember that by screening IFNAR1$^{-/-}$ cells, we are effectively looking at cells that have reduced type-I interferon production as well as reduced interferon stimulated gene production. Further studies could explore whether UL44 has an effect on type-I interferon signaling or an effect on particular ISGs.

We showed that UL42 is able to suppress production of IFN-β following BDNA stimulation or signaling intermediate overexpression. We showed that UL42 is able to interact with IRF3 and that this interaction is necessary for its inhibitory activity. While the two proteins interact, we found no evidence that UL42 prevents IRF3 translocation to the nucleus following its activation. This is consistent with UL42 being a nuclear protein, although other have reported that it can prevent nuclear translocation of NF-κB subunits [16]. UL42 is a subunit of the viral DNA polymerase responsible for viral DNA replication (the other being UL30). It carries out that function by stabilizing the catalytic subunit on the DNA strand [19]. It is therefore possible to imagine that UL42 prevents binding of IRF3 to its target sequence. We also confirm that UL42 is able to inhibit NF-κB activation after TRAF6 overexpression in our hands and suggest that it is

also able to inhibit type-I interferon signaling by inhibiting ISRE-luc activity following IFN-β treatment.

The major function of UL42 being its involvement in viral genome replication, viruses which are knocked-out for UL42 are non-replicative. We believe that by having a relatively high multiplicity of infection during our selection process (MOI 0.15) as well as collecting samples after more than one replicative cycle, there is a chance for mutants to be rescued by neighboring viruses carrying a different mutation. The main concern that arises with this possibility is whether the phenotype we observe can be attributed to a particular ORF, or whether it is a combinatorial phenotype from another mutant infecting the same cell. This is a strength of the high throughput mutation strategy. Indeed, for each ORF analyzed, there are dozens of mutants in the library. Additionally, each infection cycle was done at about 30x coverage (300,000pfu used per biological replicate for a library of 8-10,000 mutants). We believe that the odds of a randomly occurring combinatorial phenotype to repeat over 5 passages to provide a significant effect on library selection are sufficiently low to reject this hypothesis. This is supported by our results that confirm that UL42 expression is sufficient to inhibit type-I interferon activation and signaling.

To summarize, we have described a novel tool to study HSV-1 biology that allows to screen the entirety of its genome. We used this strategy to identify novel viral proteins that regulate the activation and signaling of type-I interferon and identified the mechanism by which one of these proteins carries out that function. We believe that this strategy could be used to study the HSV-1 genome in more detail, as the granularity of the library allows to analyze sub-100nt windows of the genome. It could also be used to better understand the role of intergenic regions. A better

understanding of how HSV-1 regulates the type-I interferon response provides novel antiviral targets and could help in the design of oncolytic vectors.

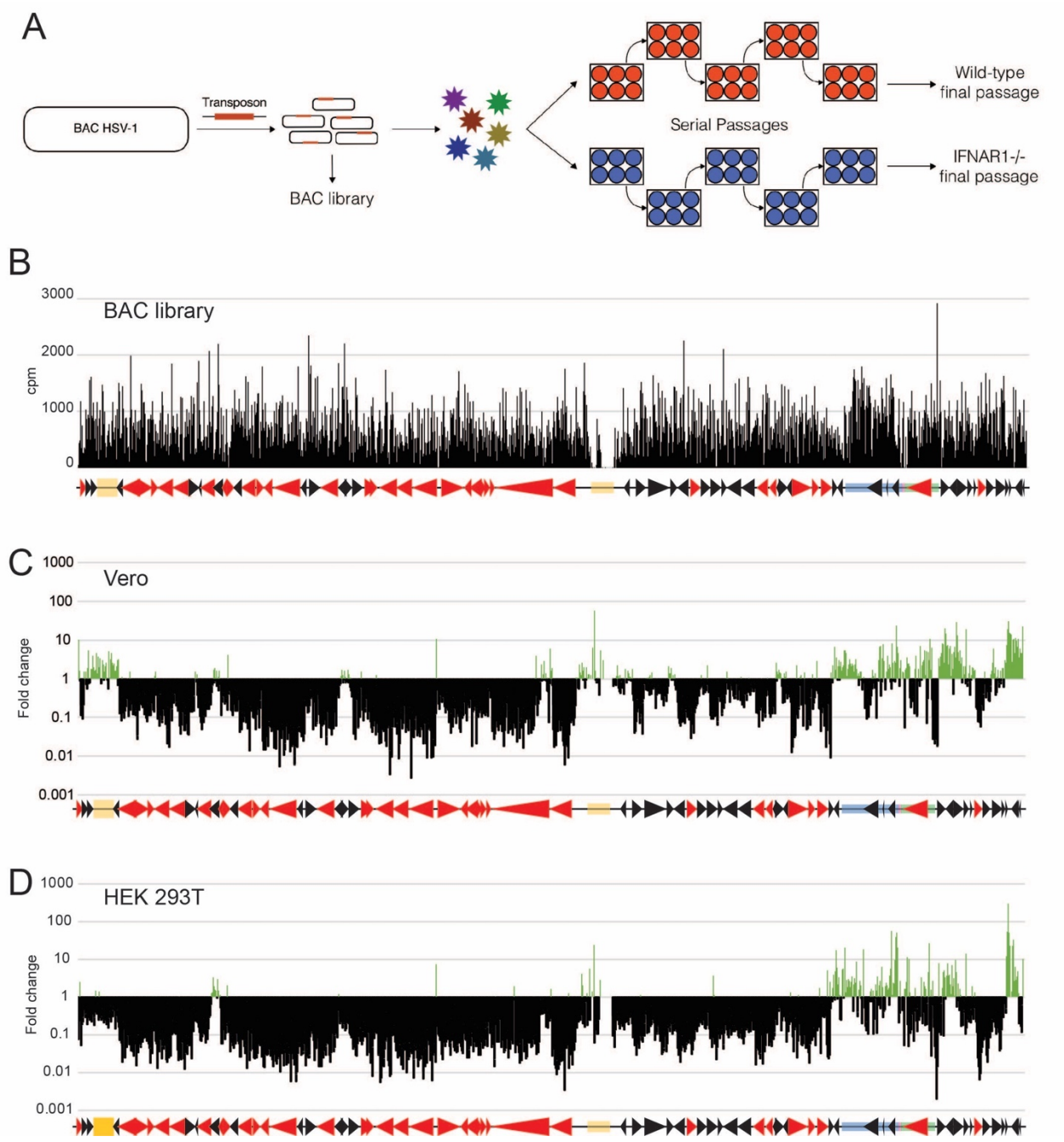
A
BAC HSV-1
Transposon
BAC library
Serial Passages
Wild-type
final passage
IFNAR1-/-
final passage
B
BAC library
3000
2000
1000
0
cpm
C
Vero
1000
100
10
1
0.1
0.01
0.001
Fold change
D
HEK 293T
1000
100
10
1
0.1
0.01
0.001
Fold change

Figure 2.1

Figure 2.1: Contruction of a comprehensive HSV-1 mutant library

A. A 1.2kb transposon containing BpuEI IIS restriction enzyme sites at each end was randomly inserted into a bacterial artificial chromosome containing the entire HSV-1 genome. The BAC library was amplified in E. coli and 8,000-10,000 clones were isolated. It was then transfected into HEK 293T cells. The viral library was expanded in Vero cells and serially passaged in different cell types. The viral mutants were collected, sequenced, and their relative amount was compared to the BAC library to determine viral fitness. B. BAC mutant library coverage. Yellow boxes represent BAC cassettes unrelated to the viral life cycle. Black arrows represent non-essential genes while red arrows represent essential genes. The blue and green box represents the long and short terminal repeats, respectively. Each bar represents a 100bp window of the viral genome. C. Fold change between the BAC library and the final passage in Vero cells. D. Fold change between the BAC library and the final passage in HEK 293T cells.

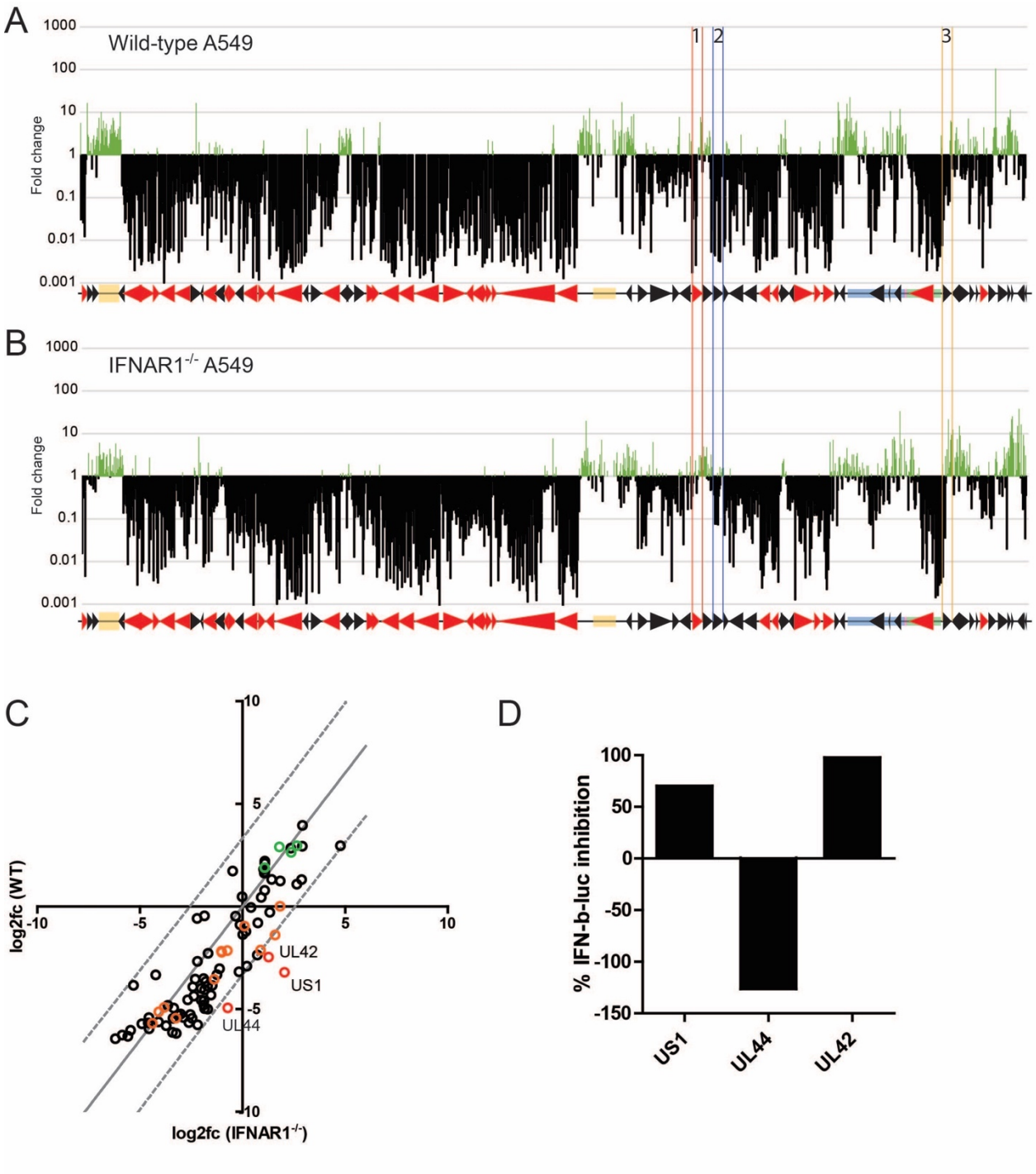
A
Wild-type A549
1
2
3
Fold change
1000
100
10
1
0.1
0.01
0.001
B
IFNAR1-/- A549
Fold change
C
log2fc (WT)
log2fc (IFNAR1-/-)
UL42
US1
UL44
D
% IFN-b-luc inhibition
100
50
0
-50
-100
-150
US1
UL44
UL42

Figure 2.2

Figure 2.2: Viral library selection with or without type-I interferon pressure reveals novel immunomodulatory candidates

A. Fold change between BAC library and final passage in wild-type A549 cells. Genes marked 1, 2, and 3 indicate UL42, UL44, and US1, respectively. B. Fold change between BAC library and final passage in IFNAR1-/- A549 cells. C. Comparison of the log2(fold change) in WT and IFNAR1-/- A549 cells. Green circles represent transposon insertions in genes not related to the viral life cycle, i.e. WT virus. Orange circles represent genes previously identified as viral regulators of the IFN-I response. Red circles highlight novel immunomodulatory candidates. D. Percent of interferon-β-luciferase reporter activity inhibition following HEK293T co-transfection of UL42, UL44, or US1 with or without STING.

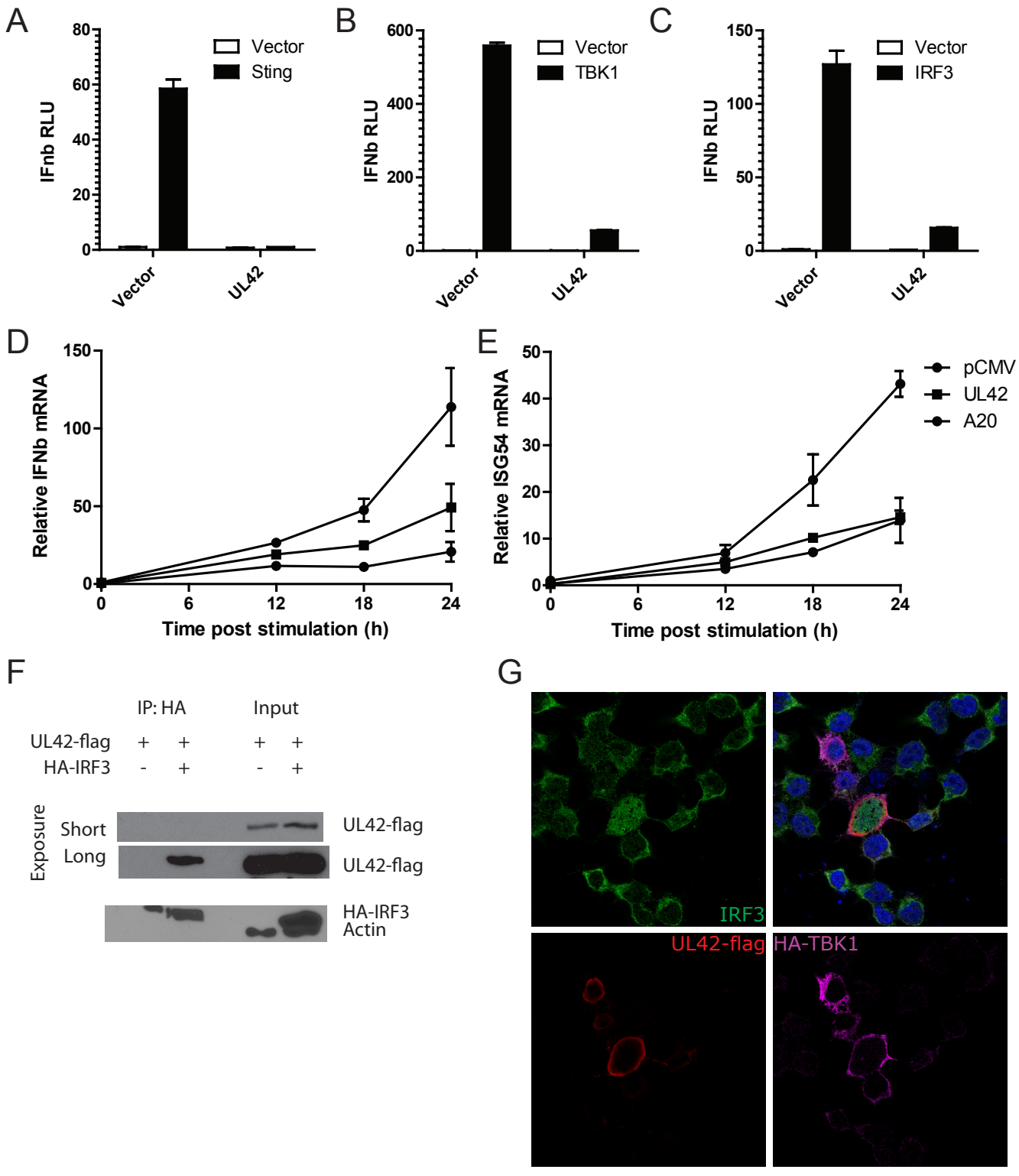
A
IFnb RLU
80
60
40
20
0
Vector
Sting
Vector
UL42
B
IFNb RLU
600
400
200
0
Vector
TBK1
Vector
UL42
C
IFNb RLU
150
100
50
0
Vector
IRF3
Vector
UL42
D
Relative IFNb mRNA
150
100
50
0
0
6
12
18
24
Time post stimulation (h)
E
Relative ISG54 mRNA
50
40
30
20
10
0
pCMV
UL42
A20
0
6
12
18
24
Time post stimulation (h)
F
IP: HA
Input
UL42-flag + + + +
HA-IRF3 - + - +
Exposure
Short
Long
UL42-flag
UL42-flag
HA-IRF3
Actin
G
IRF3
UL42-flag
HA-TBK1

Figure 2.3

Figure 2.3: UL42 inhibits interferon-β transcriptional activation and interacts with IRF3

Interferon-β-luciferase activity following overexpression of UL42 and STING (A), TBK1 (B), or IRF-3 (C) in HEK 293T cells. Induction of interferon-β (D) and ISG54 (E) mRNA following BDNA transfection in HEK 293T cells expressing UL42, A20, or pCDNA empty vector. F. Co-immunoprecipitation followed by western blotting of UL42-flag and HA-IRF3 in HEK 293T cells. G. Confocal microscopy of UL42-flag, HA-TBK1, and IRF-3 in HEK 293T cells. DNA is stained with DAPI and shown in blue.

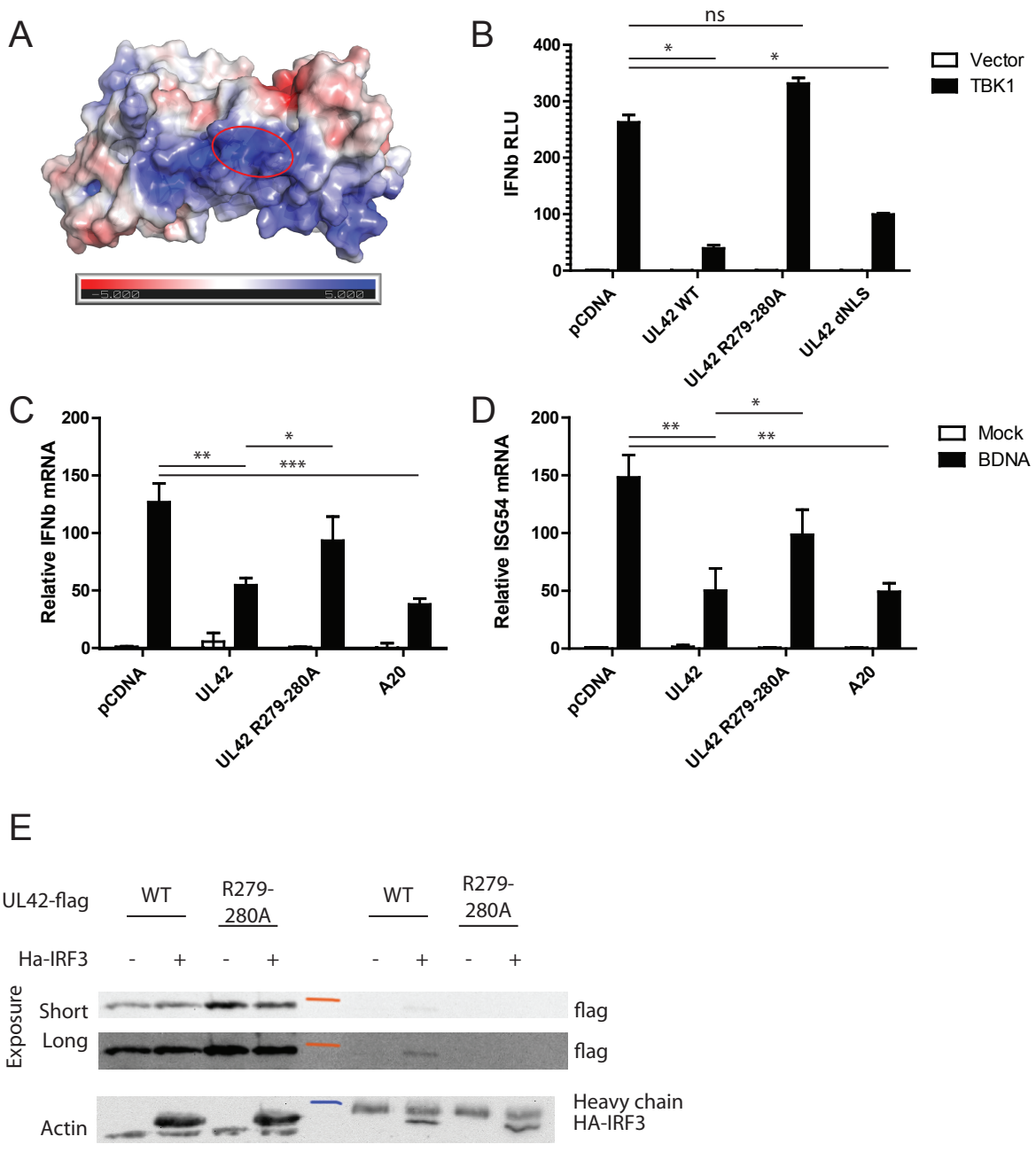
A
B
ns
*
*
400
300
200
100
0
IFNb RLU
Vector
TBK1
pCDNA
UL42 WT
UL42 R279-280A
UL42 dNLS
C
200
150
100
50
0
Relative IFNb mRNA
**
*
***
pCDNA
UL42
UL42 R279-280A
A20
D
200
150
100
50
0
Relative ISG54 mRNA
**
*
**
Mock
BDNA
pCDNA
UL42
UL42 R279-280A
A20
E
UL42-flag
WT
R279-280A
WT
R279-280A
Ha-IRF3
- + - + - + - +
Exposure
Short
Long
flag
flag
Actin
Heavy chain
HA-IRF3

Figure 2.4

Figure 2.4: Mutation to DNA binding domain of UL42 prevents IRF-3 interaction and interferon-β inhibition

A. DNA-binding positively-charged surface of UL42 (blue). Circled are the two arginines targeted by alanine mutation in other panels. Surface charge of UL42 calculated by PyMol using crystal structure from [21]. B. TBK1-induced interferon-β-luciferase activation in HEK 293T cells expressing WT UL42, UL42 R279-280A, UL42 dNLS, or pCDNA empty control. Interferon-β (C) and ISG54 (D) mRNA induction following BDNA transfection in HEK293T cells expressing WT UL42, UL42 R279-280A, A20, or pCDNA empty control. E. Co-immunoprecipitation and western blotting of HEK293T cells overexpressing WT UL42 or UL42 R279-280A with or without HA-IRF3.

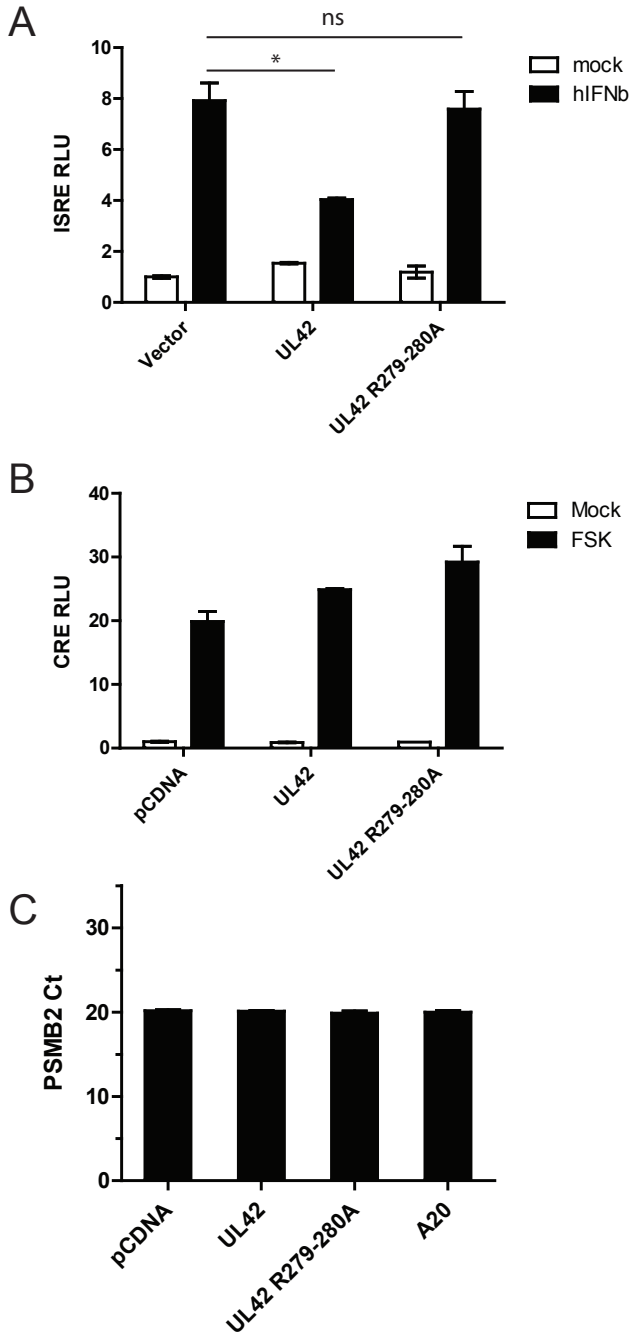
A
ns
*
mock
hIFNb
ISRE RLU
10
8
6
4
2
0
Vector
UL42
UL42 R279-280A
B
Mock
FSK
CRE RLU
40
30
20
10
0
pCDNA
UL42
UL42 R279-280A
C
PSMB2 Ct
30
20
10
0
pCDNA
UL42
UL42 R279-280A
A20

Figure 2.5

Figure 2.5: UL42 overexpression impairs IFN-β induced ISRE signaling

A. ISRE-luc reporter activation following interferon-β treatment in HEK 293T cells expressing WT UL42, UL42 R279-280A, or pCDNA empty control. B. cAMP Response Element luciferase activation following 5h Forskolyn treatment in HEK 293T cells expressing WT UL42, UL42 R279-280A, or pCDNA empty control. C. Cycle threshold of the housekeeping gene PSBM2 in HEK 293T cells expressing UL42 WT, UL42 R279-180A, A20, or pCDNA empty control.

Figure S2.1

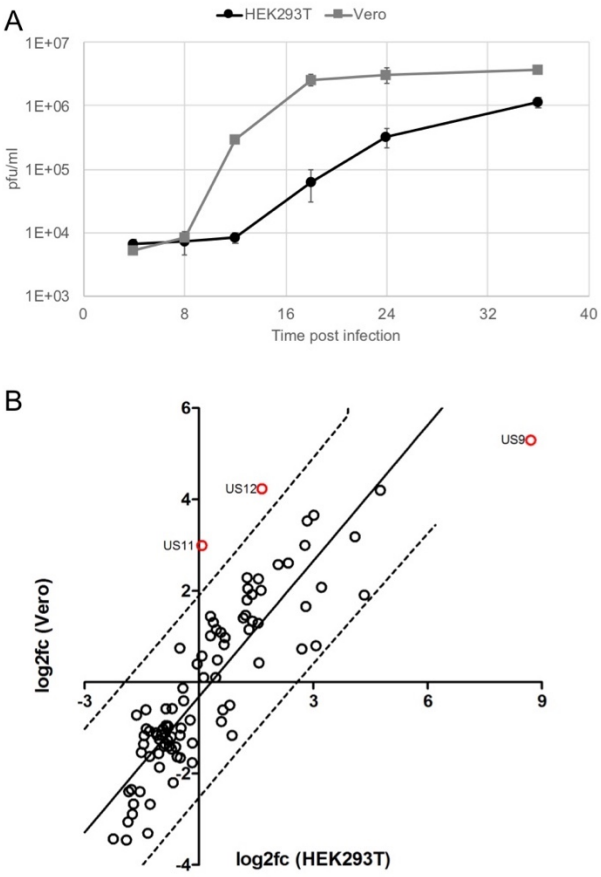
A
HEK293T
Vero
1E+07
1E+06
1E+05
1E+04
1E+03
pfu/ml
0
8
16
24
32
40
Time post infection
B
US9
US12
US11
6
4
2
-2
-4
-3
3
6
9
log2fc (Vero)
log2fc (HEK293T)

Figure S2.1: A. HSV-1 library growth curve in HEK 293T and Vero cells as determined by plaque assay. B. Log2(fold change) from BAC library to final passage comparison between HEK 293T and Vero cells.

Figure S2.2

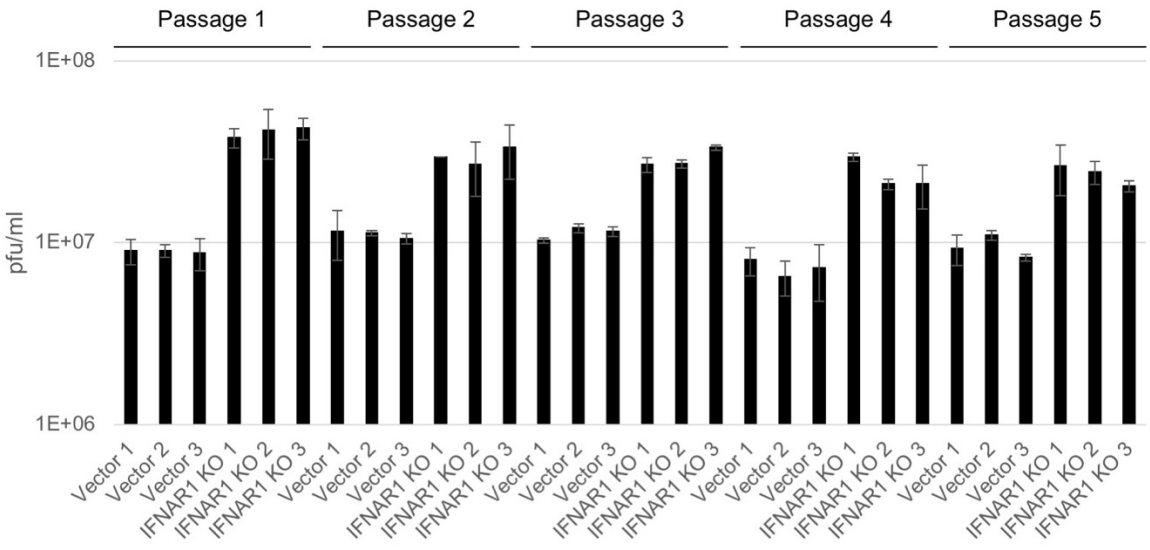
Passage 1
Passage 2
Passage 3
Passage 4
Passage 5
1E+08
1E+07
1E+06
pfu/ml
Vector 1
Vector 2
Vector 3
IFNAR1 KO 1
IFNAR1 KO 2
IFNAR1 KO 3

Figure S2.2: Viral titer at each passage during viral library selection in WT A549 and IFNAR1-/- A549 cells as determined by plaque assay.

Figure S2.3

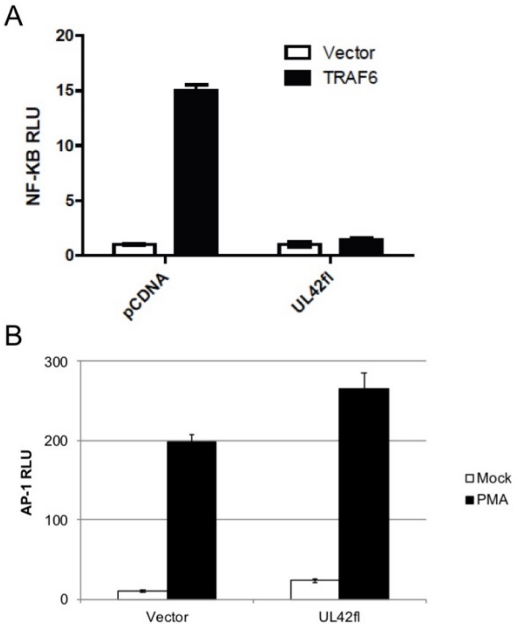
A
NF-KB RLU
20
15
10
5
0
Vector
TRAF6
pCDNA
UL42fl
B
AP-1 RLU
300
200
100
0
Vector
UL42fl
Mock
PMA

Figure S2.3: A. NF-KB-luc reporter activity in cells transfected with UL42 or pCDNA empty control. B. AP-1-luciferase reporter activation following PMA stimulation in cells expressing UL42 WT or pCDNA empty vector.

MATERIAL AND METHODS

Cells and recombinant HSV-1

African green monkey kidney Vero cells, and Human embryonic kidney HEK 293T cells were procured from ATCC. IFNAR1$^{-/-}$ A549 and their respective control were kindly provided by collaborator. A bacterial artificial chromosome containing the HSV-1 genome was a gift of Pr Zheng, [27].

Library construction

A pEntranceposon-kan vector (Thermo Fisher) was modified by PCR to insert BpuEI and KasI restriction enzyme sites at the end of the R1 site of the transposon. The transposon sequence was excised using KasI and mixed with MuA (Thermo Fisher) transposase for the transposition reaction. The transposition complex was mixed with purified BAC-HSV-1 and the reaction was carried out as described by the manufacturer. The resulting DNA was electroporated in DH10B high efficiency *E. coli* (Invitrogen) and plated on chloramphenicol or chloramphenicol/kanamycin LB plates. This allowed to confirm that fewer than 70% of the BAC molecules contained a transposon insertion. Eight to ten thousand double resistant colonies were collected, mixed, and frozen in LB with 15% glycerol. For BAC preparation, one aliquot is thawed and plated on 15cm LB chloramphenicol/kanamycin plates. The resulting lawn is collected the next day for BAC preparation.

For viral preparation, xµg of DNA was transfected into X million HEK293T cells using lipofectamine 2000. The resulting virus was used to infect 200 million Vero cells at a MOI of 0.01 to prepare the viral input.

In vitro passaging

One million cells were infected in triplicates at a MOI of 0.15. Forty hours post infection, the cells and supernatant were collected and freeze/thawed three times before being tittered on Vero cells. The virus collected from passage one was used to infect the cells of passage two. This process was repeated four times while keeping all replicates independent throughout passaging.

Library sequencing and data analysis

Cell lysates were cleared from cell debris by centrifugation. The virus from 500-1000 µl of viral supernatant was concentrated by centrifugation at 20200g for 90min at 4C. The viral particles were treated with DNAse I at 37C for 30min to remove traces of plasmid and the viral genomes were then extracted using the Viral DNA/RNA genome extraction kit (Invitrogen). Purified viral genomes were digested with BpuEI and annealed oligonucleotides were ligated overnight at 16C using T4 Ligase (NEB). The sequencing library was constructed using a two-step nextera indexing protocol with primers specific for the transposon and the adapter oligo (Illumina). The resulting library was sequenced on a MiSeq instrument (Illumina).

Raw reads were processed by extracting the 14-18nt HSV-1 sequence using cutadapt [28]. These reads were then aligned to the reference HSV-1 genome using bowtie [29] with -m 2 --best --strata arguments. Bedtools [30] was used to extract the number of aligned reads per 100bp window in the reference genome. The resulting counts were used as input to the TnSeqDiff [31] tool to compute fold changes and significance.

HSV-1 genes wild type and mutant cloning

Wild-type sequences were cloned out of the BAC HSV-1 sequence into a pCDNA3.1-flag plasmid under CMV promoter. Mutants were generated by PCR amplification and InFusion cloning (Clontech). All sequences were confirmed by sanger sequencing. The primers used were:

US1-F: `TTAATTCAGATCTAGttctggatggccgacatttcc`

US1-R: `CCCGGGATCCTCTAGatcacggccggagaaacgtg`

UL44-F: `TTAATTCAGATCTAGgaggcgtcgggcatggc`

UL44-R: `CCCGGGATCCTCTAGagcgttaccgccgatgacg`

UL42-F: `TAGACTCGAGCggccGCatgacggattcccctggcg`

UL42-R: `GTAATCTAGAAagctggggaatccaaaaccagacgg`

UL42-R279-80A_F: `tgctcgcagcgctgcaggtcggcggggg`

UL42-R279-80A_R: `tgcagcgctgcgagcaccgcccgcatgctg`

Luciferase reporter assays

HEK 293T cells were transfected with the firefly luciferase gene under the control of the IFN-β, ISRE, NF-κB, AP-1, or CRE promoter in conjunction with the renilla luciferase gene under the control of TK. The cells were co-transfected with HSV-1 genes and stimulatory genes using PEI. 16-20h after transfection, the cells were lysed, and the luciferase activity was measured using a dual luciferase kit (Promega). Firefly luciferase signal was normalized to renilla luciferase signal for analysis.

Reverse transcription quantitative polymerase chain reaction

HEK293T cells were transfected with HSV-1 proteins using PEI. The next day, cells were stimulated with 100ng/ml BDNA using lipofectamine 2000 (Invitrogen). The following day, total RNA was collected and later extracted using Trizol reagent (Invitrogen). Identical amounts of total RNA from each sample was reverse transcribed using iScript (Bio-Rad). Relative expression was calculated using PSMB2 as a housekeeping gene reference. Primers used were:

PSMB2-F: `ATCCTCGACCGATACTACACAC`

PSMB2-R: `GAACACTGAAGGTTGGCAGAT`

hIFNb-F: `TGTGGCAATTGAATGGGAGGCTTGA`

hIFNb-R: `CGGCGTCCTCCTTCTGGAACT`

hISG54-F: `TGCAACCTACTGGCCTATCTA`

hISG54-R: `CAGGTGACCAGACTTCTGATT`

Immunofluorescence

HEK293T cells were co-transfected with UL42-flag and HA-TBK1 using PEI. The following day, cells were fixed with 2% PFA for 15 minutes at room temperature. Cells were then permeabilized with 0.3% Triton-X 100 in PBS and blocked with 10% Donkey serum for 45 minutes at room temperature. Primary antibodies against flag (Sigma F1804), HA (Santa-Cruz SC-805), and IRF-3 (Santa-Cruz) were incubated overnight in PBS 0.1% Triton-X 100 1% BSA. Secondary fluorescent antibodies Donkey anti Goat Alexa555 (Invitrogen), Donkey anti Rabbit DyLight488 (Biolegend) were incubated for one hour at room temperature. Anti-goat antibodies were saturated with 10% goat serum in PBS 0.1% Triton-X 100 for 15 minutes at room

temperature and Goat anti mouse DyLight649 (Biolegend) secondary antibody was incubated for one hour at room temperature. Coverslips were mounted on slides using Prolong gold DAPI (Invitrogen) and imaged on a Leica SP5 confocal microscope.

Immunoprecipitation

HEK293T cells were co-transfected with UL42-flag WT or mutant, and HA-IRF3. Sixteen to 24 hours later, cells were lysed in NP40 lysis buffer and HA-IRF3 was pulled down using a Rabbit anti-HA antibody (sc-805) and magnetic protein A beads (Bio-Rad). The beads were washed 3 times according to the manufacturer's instructions and the immunoprecipitated and input fractions were run on an SDS PAGE. Proteins were transferred onto PVDF membranes and probed for flag (F1804), HA (sc-805), and actin (Cell signaling).

REFERENCES

[1] F. McNab, K. Mayer-Barber, A. Sher, A. Wack, and A. O'Garra, "Type I interferons in infectious disease," *Nat. Rev. Immunol.*, vol. 15, no. 2, pp. 87–103, Feb. 2015.

[2] S. Akira, S. Uematsu, and O. Takeuchi, "Pathogen recognition and innate immunity," *Cell*, vol. 124, no. 4, pp. 783–801, Feb. 2006.

[3] L. Sun, J. Wu, F. Du, X. Chen, and Z. J. Chen, "Cyclic GMP-AMP synthase is a cytosolic DNA sensor that activates the type I interferon pathway," *Science*, vol. 339, no. 6121, pp. 786–791, Feb. 2013.

[4] X. Zhang *et al.*, "The cytosolic DNA sensor cGAS forms an oligomeric complex with DNA and undergoes switch-like conformational changes in the activation loop," *Cell Rep.*,

vol. 6, no. 3, pp. 421–430, Feb. 2014.

[5] Y. Tanaka and Z. J. Chen, “STING Specifies IRF3 Phosphorylation by TBK1 in the Cytosolic DNA Signaling Pathway,” *Sci Signal*, vol. 5, no. 214, pp. ra20–ra20, Mar. 2012.

[6] A. S. Devasthanam, “Mechanisms underlying the inhibition of interferon signaling by viruses,” *Virulence*, vol. 5, no. 2, pp. 270–277, Feb. 2014.

[7] K. E. Taylor and K. L. Mossman, “Recent advances in understanding viral evasion of type I interferon,” *Immunology*, vol. 138, no. 3, pp. 190–197, Mar. 2013.

[8] J. S. Smith and N. J. Robinson, “Age-specific prevalence of infection with herpes simplex virus types 2 and 1: a global review,” *J. Infect. Dis.*, vol. 186 Suppl 1, pp. S3-28, Oct. 2002.

[9] O. O. Koyuncu, I. B. Hogue, and L. W. Enquist, “Virus infections in the nervous system,” *Cell Host Microbe*, vol. 13, no. 4, pp. 379–393, Apr. 2013.

[10] R. D. Everett, “HSV-1 biology and life cycle,” *Methods Mol. Biol. Clifton NJ*, vol. 1144, pp. 1–17, 2014.

[11] C. Su, G. Zhan, and C. Zheng, “Evasion of host antiviral innate immunity by HSV-1, an update,” *Virol. J.*, vol. 13, p. 38, Mar. 2016.

[12] C. Su and C. Zheng, “Herpes Simplex Virus 1 Abrogates the cGAS/STING-Mediated Cytosolic DNA-Sensing Pathway via Its Virion Host Shutoff Protein, UL41,” *J. Virol.*, vol. 91, no. 6, 15 2017.

[13] M. H. Christensen *et al.*, “HSV-1 ICP27 targets the TBK1-activated STING signalsome to inhibit virus-induced type I IFN expression,” *EMBO J.*, vol. 35, no. 13, pp. 1385–1399, 01 2016.

[14] L. Wang *et al.*, “Generation of a Live Attenuated Influenza Vaccine that Elicits

Broad Protection in Mice and Ferrets," *Cell Host Microbe*, vol. 21, no. 3, pp. 334–343, Mar. 2017.

[15] T. van Opijnen, K. L. Bodi, and A. Camilli, "Tn-seq: high-throughput parallel sequencing for fitness and genetic interaction studies in microorganisms," *Nat. Methods*, vol. 6, no. 10, pp. 767–772, Oct. 2009.

[16] J. Zhang, S. Wang, K. Wang, and C. Zheng, "Herpes simplex virus 1 DNA polymerase processivity factor UL42 inhibits TNF-α-induced NF-κB activation by interacting with p65/RelA and p50/NF-κB1," *Med. Microbiol. Immunol. (Berl.)*, vol. 202, no. 4, pp. 313–325, Aug. 2013.

[17] M. Polvino-Bodnar, P. K. Orberg, and P. A. Schaffer, "Herpes simplex virus type 1 oriL is not required for virus replication or for the establishment and reactivation of latent infection in mice," *J. Virol.*, vol. 61, no. 11, pp. 3528–3535, Nov. 1987.

[18] J. C. Randell and D. M. Coen, "Linear diffusion on DNA despite high-affinity binding by a DNA polymerase processivity factor," *Mol. Cell*, vol. 8, no. 4, pp. 911–920, Oct. 2001.

[19] J. Gottlieb, A. I. Marcy, D. M. Coen, and M. D. Challberg, "The herpes simplex virus type 1 UL42 gene product: a subunit of DNA polymerase that functions to increase processivity," *J. Virol.*, vol. 64, no. 12, pp. 5976–5987, Dec. 1990.

[20] K. Parvatiyar, G. N. Barber, and E. W. Harhaj, "TAX1BP1 and A20 inhibit antiviral signaling by targeting TBK1-IKKi kinases," *J. Biol. Chem.*, vol. 285, no. 20, pp. 14999–15009, May 2010.

[21] H. J. Zuccola, D. J. Filman, D. M. Coen, and J. M. Hogle, "The crystal structure of an unusual processivity factor, herpes simplex virus UL42, bound to the C terminus of its cognate polymerase," *Mol. Cell*, vol. 5, no. 2, pp. 267–278, Feb. 2000.

[22] J. C. W. Randell, G. Komazin, C. Jiang, C. B. C. Hwang, and D. M. Coen, "Effects of substitutions of arginine residues on the basic surface of herpes simplex virus UL42 support a role for DNA binding in processive DNA synthesis," *J. Virol.*, vol. 79, no. 18, pp. 12025–12034, Sep. 2005.

[23] K. Polcicova, P. S. Biswas, K. Banerjee, T. W. Wisner, B. T. Rouse, and D. C. Johnson, "Herpes keratitis in the absence of anterograde transport of virus from sensory ganglia to the cornea," *Proc. Natl. Acad. Sci. U. S. A.*, vol. 102, no. 32, pp. 11462–11467, Aug. 2005.

[24] A. Negatsch, T. C. Mettenleiter, and W. Fuchs, "Herpes simplex virus type 1 strain KOS carries a defective US9 and a mutated US8A gene," *J. Gen. Virol.*, vol. 92, no. Pt 1, pp. 167–172, Jan. 2011.

[25] B. L. Liu *et al.*, "ICP34.5 deleted herpes simplex virus with enhanced oncolytic, immune stimulating, and anti-tumour properties," *Gene Ther.*, vol. 10, no. 4, pp. 292–303, Feb. 2003.

[26] M. Zhang *et al.*, "HSV-2 immediate-early protein US1 inhibits IFN-β production by suppressing association of IRF-3 with IFN-β promoter," *J. Immunol. Baltim. Md 1950*, vol. 194, no. 7, pp. 3102–3115, Apr. 2015.

[27] Y. Li, S. Wang, H. Zhu, and C. Zheng, "Cloning of the herpes simplex virus type 1 genome as a novel luciferase-tagged infectious bacterial artificial chromosome," *Arch. Virol.*, vol. 156, no. 12, pp. 2267–2272, Dec. 2011.

[28] M. Martin, "Cutadapt removes adapter sequences from high-throughput sequencing reads," *EMBnet.journal*, vol. 17, pp. 10–12, May 2011.

[29] B. Langmead, C. Trapnell, M. Pop, and S. L. Salzberg, "Ultrafast and memory-efficient alignment of short DNA sequences to the human genome," *Genome Biol.*, vol. 10, no. 3,

p. R25, 2009.

[30] A. R. Quinlan and I. M. Hall, "BEDTools: a flexible suite of utilities for comparing genomic features," *Bioinforma. Oxf. Engl.*, vol. 26, no. 6, pp. 841–842, Mar. 2010.

[31] L. Zhao, M. T. Anderson, W. Wu, H. L. T Mobley, and M. A. Bachman, "TnseqDiff: identification of conditionally essential genes in transposon sequencing studies," *BMC Bioinformatics*, vol. 18, no. 1, p. 326, Jul. 2017.

CHAPTER 3

Expression of tumor neoantigens by Listeria monocytogenes to generate an antitumoral immune response

ABSTRACT

Listeria monocytogenes (Lm) is a bacterium able to generate strong antigen-specific cytotoxic T-cell responses. This ability has been used to target tumor antigens and protect from disease progression in the past. Whether this pathogen is able to protect from tumor growth by expression a limited set of self, mutated antigens remains to be determined. We constructed an attenuated strain of *Listeria monocytogenes* expressing multiple naturally occurring mutant tumor antigens from the B16 melanoma, and the chicken ovalbumin (OVA) peptide SIINFEKL. This vaccinal strain was able to induce OVA-specific CD8 T-cell proliferation *in vitro* as efficiently as an OVA expressing Lm strain. This effect did not translate into an *in vivo* tumor model where the vaccinal strain failed to protect from tumor growth or elicit an OVA-specific T-cell response.

INTRODUCTION

The ability of pathogens to prevent cancer progression has been known since the late 1890s [1]. While the mechanism remained unclear for decades, it is now understood that the immune response to the pathogen is able to break tolerance to the tumor [2]. Such immunotherapeutic effects are typically associated with a strong cytotoxic T-cell response targeted towards antigens that are specific to the tumor cells [1]. Several strategies are currently being investigated to reproduce those effects, from checkpoint inhibitors [3], to recombinant T-cells adoptive transfer [4], to recombinant pathogens [5].

Listeria monocytogenes (Lm) is a particularly effective bacterium at producing strong cytotoxic T-cell responses, due to its ability to live and reproduce in the cytoplasm of infected cells [6]. Proteins produced by the pathogen are therefore presented to CD8 T-cells on the class-I major

histocompatibility complex (MHC-I) proteins [7]. Mutant, attenuated strains of the bacterium have been shown to be able to prevent tumor growth in animal models [8]. These Lm strains typically overexpress an antigen that is recognized as foreign by the immune system, such as viral proteins [9], or rare self proteins that are overexpressed in the tumor cells [10].

Not all tumors carry strong antigens to be targeted by immunotherapy strategies while preventing off-target effects. Newer strategies intend to use naturally occurring amino acid mutations that occur when most tumors grow [11]. While foreign antigen expressing, attenuated Lm strains are currently being investigated in the clinic, the ability of these vectors to elicit a protective immune response from a limited set of tumor mutant antigens (neoantigens) is unclear.

In this study, we aimed to determine whether expression of tumor mutant antigens by an attenuated strain of Lm could prevent tumor growth in a murine model of disease. We confirmed that Lm is able to protect from disease progression in a model of foreign antigen expressing tumor. We constructed a neoantigen expressing strain of attenuate Lm and determined that it was able to produce an antigen-specific response towards a CD8 T-cell epitope *in vitro* but failed to protect from tumor growth *in vivo*.

RESULTS

OVA secretion by *Listeria monocytogenes* protects from EG7-OVA tumor infection

Listeria monocytogenes is a facultative intracellular gram-positive bacterium that has long been used as a model to study CD8 T-cell responses. When infecting a cell, Lm is able to the endosome by secreting a listeriolysin O (LLO) [6]. Once in the cytoplasm of an infected cell, Lm

produces the actin assembly-inducing protein ActA which polymerizes actin and propels the bacterium onto the neighboring cell where it is internalized [6].

The ability of Lm to live, reproduce, and secrete proteins into the cytoplasm of its host cell is what makes it perfect to trigger a CD8 T-cell response. Indeed, cytoplasmic peptides are transported into the endoplasmic reticulum through the transporter associated with antigen processing to be loaded onto major histocompatibility complex 1 (MHC-I) proteins [7]. CD8 T-cells are greatly restricted to MHC-I peptide complexes for their activation.

We sought to examine the potential of this pathogen to trigger an anti-tumoral immune response. It is known that Lm can be used to treat foreign antigen expressing tumors [8]. These are typically virally induced tumors where the oncogene is a viral protein. We decided to start by establishing such a model in our laboratory. The E.G7-OVA cell line is a derivative of the EL4 T-cell lymphoma cell line collected from C57BL/6 mice that expresses the chicken ovalbumin (OVA) antigen.

We engrafted this tumor at day 0 and treated the mice at day 5 with 2 million colony forming units (cfu) of Lm deficient for ActA (Lm-ActA) or Lm deficient for ActA secreting OVA (Lm-OVA) intravenously (Figure 3.1). Mice that were treated with Lm-ActA developed larger tumors and at a faster rate than mice treated with Lm-OVA (Figure 3.2a). Accordingly, mice treated with Lm-OVA showed better survival than those treated with Lm-ActA (Figure 3.2b).

In C57BL/6 mice, the most strongly recognized CD8 T-cell OVA peptide is SIINFEKL. To determine whether the tumor suppressive phenotype we observed was associated with a CD8 T-cell response, we stained splenic cells with SIINFEKL pentamer. Lm-OVA treated mice

showed an increase in OVA-specific CD8 T-cells during tumor control, consistent with a role for T-cell activity in disease protection (Figure 3.2c).

Construction of a neoantigen Lm vector

While viral oncogenes provide obvious antigens for the immune system to attack, tumors arising from other mechanisms can also provide specific targets. This is because most tumors lose control of their DNA integrity, and their high rate of replication accumulates many novel mutations [12]. When those mutations happen to be nonsense, i.e. the nucleotide change induces an amino acid difference in the peptide sequence, a novel antigen peptide can be produced. These peptides, or proteins, are referred to as neoantigens.

Others have shown that the immune system is able to distinguish between self and neoantigens by producing antigen-specific T-cells that are able to target cancer cells with limited to no effect on the surrounding tissue [13]. We aimed to extend our study of Lm as a tumor antigen carrier to the expression of neoantigens. This would open the use of this kind of immunotherapy to types of cancers not caused by viral infections.

Another goal of this study was to make the production of personalized therapy easier. This kind of therapy is designed for each individual patient to suit their particular disease. In the context discussed here, this means that the neoantigens that would be expressed by the Lm vaccine would be tailored to the mutations present in the tumor of the patient receiving the treatment. To make this process easier to carry out, we decided to use a plasmid expression system to prevent having to create a stable Lm strain for each construct.

We chose to use a well described mouse tumor model to test this method. The B16 C57BL/6 melanoma cell line is able to produce melanoma-like tumors when injected subcutaneously and organ metastases when injected intravenously. Additionally, neoantigens have been identified by others that are able to be targeted by the immune system of C57Bl/6 mice [14]. We cloned the hly-LLO promoter-protein fusion from pEJ140 (a gift of by Pr Jeffrey Miller, UCLA) into the shuttle vector pAM401 (a gift from Pr Daniel Portnoy, UCB). We then inserted a synthetic construct containing the OVA peptide SIINFEKL fused to B16 neoantigens (pAM-vac), or a scrambled version of SIINFEKL fused to the wild-type version of the same B16 neoantigens (pAM-WT) (Figure 3.3).

In vitro characterization of pAM-vac-carrying *Listeria monocytogenes*

Because our vaccine construct carries the SIINFEKL peptide, we were able to test the ability of the vaccine to trigger an immune response using OVA-specific tools such as MHC-peptide fluorescent pentamers and OT-I OVA-specific TCR transgenic mice.

To determine whether the vaccine-carrying Lm strain was able to trigger an antigen specific immune response, we infected total splenocytes with increasing amounts of Lm carrying pAM-vac (Lm-vac), pAM-WT (Lm-WT), or the OVA-secreting Lm strain.

Flow cytometric analysis showed that B-cells proliferate in response to the infection in an antigen independent manner, as measured by CFSE dilution (Figure 3.4a). Indeed, the proliferation was comparable in cells infected with Lm-OVA or Lm-vac and in cells infected with Lm-WT. This is consistent with B-cells being stimulated by bacterial surface antigens, where the

lack of specificity of the B-cell receptor (BCR) is trumped by the close repetition of the target on a solid surface which can cluster the BCR sufficiently to activate the cell.

Contrary to B-cells, CD8 T-cells only showed proliferation when the cells were infected with foreign antigens (Figure 3.4b). Indeed, the percentage of T-cells having diluted CFSE was the same or inferior between the uninfected control and the Lm-WT infected samples, while there was an increase in proliferation in the samples infected with the highest quantity of Lm-OVA or Lm-vac.

These data indicate that *in vitro*, our vaccine construct is able to trigger an antigen-specific response with the same amplitude as the Lm-OVA strain.

Lm-vac does not protect from EG7 growth *in vivo*

We confirmed the ability of Lm-vac to trigger an antigen specific immune response *in vitro*, as determined by the ability of SIINFEKL + mutant peptides to drive CD8 T-cell proliferation while WT peptides + scrambled SIINFEKL did not. The next step was to study the ability of Lm-vac to protect C57BL/6 mice from the growth of E.G7-OVA tumors.

We are able to use this model thanks to the inclusion of SIINFEKL in our vaccine construct. Indeed, the E.G7-OVA tumor cells present this peptide, and a significant share of CD8 T-cells are able to recognize it following Lm-OVA infection (Figure 3.2c). We therefore inoculated E.G7-OVA cells subcutaneously in wild-type C57BL/6 mice before vaccinating them with 2 million cfu Lm-OVA, Lm-vac, Lm-WT, or Saline control intravenously at day 5.

Unfortunately, Lm-vac showed no difference to Lm-WT in protecting mice from the growth of E.G7-OVA tumors while Lm-OVA was protective (Figure 3.5a). Lm-OVA was able

to induce proliferation of OVA-specific CD8 T-cells but not our vaccine construct (Figure 3.5b). To determine whether there was a difference in the immune response triggered by the different strains of bacteria, we collected splenocytes at day 19 from mice treated with either strain and assayed their ability to release cytotoxic granules when exposed to E.G7 tumor cells for 6h. We used CD107a exposure as a readout of granule release [15].

While the cells were able to release granules as determined by anti-CD3 anti-CD28 antibody co-stimulation (Figure 3.5c, circles), the E.G7 cells were not able to stimulate activation of these same cells in these conditions (Figure 3.5c, bars). In the same experiment, the amount of dead target cells did not depend on the type of immunization received by the donor of the effector cells (Figure 3.5d).

We also tested whether exposure to the different strains of Lm used would be able to trigger antigen-specific proliferation of CD8 T-cells. As previously observed in vitro, B-cell proliferation was independent of the antigen specificity of the stimulating pathogen (Figure 3.5e). Surprisingly, CD8 T-cell proliferation was not dependent on previous exposure of the pathogen either (Figure 3.5f). It is unclear whether these data are representative of the state of the immune response at the time of collection or whether the manipulations associated with collecting and storing the cells prior to the assays had a negative effect on their reactivity.

DISCUSSION

Using the immune system to fight against cancer is not a novel idea [1]. The immune system is indeed able to recognize many types of tumor, defined as immunogenic. These immunogenic tumors classically express tumor antigens that are often self, rarely expressed proteins, overexpressed

in tumors [16]. Immunogenic tumors make good candidates for immune modulating therapies such as checkpoint inhibitors because they are already identified by the adaptive immune system [16].

But what of tumors that are not immunogenic? A seminal study of the mutation rate in different cancer types showed that most tumors do indeed carry mutations [12]. These tumors, while not expressing foreign or self, overexpressed antigens, can express mutated peptides, called neoantigens [11]. Because the adaptive immune system has not been trained to ignore those peptides during its development, neoantigens represent a potential target for immunotherapy.

Here, we wanted to determine whether a strong pathogenic stimulus would help the immune system recognize neoantigens and trigger an anti-tumoral response. *Listeria monocytogenes* has been used as a model pathogen to study cytotoxic T-cell responses [6]. Lm is able to trigger a strong proliferation of antigen specific CD8 T-cells. We started by setting up a model of Lm-triggered anti-tumor response (Figure 3.1). By using tumor cells that express OVA, and an attenuated Lm strain expressing the same antigen, we model tumors that express non-self antigens such as virally induced tumors. In this model, we showed that Lm is able to trigger a strong OVA-specific CD8 T-cell response that is associated with protection from tumor growth (Figure 3.2).

The major downside of this model is that it is quite artificial and might not translate well into human disease. To improve on this model, we decided to use a step-wise strategy by first reducing the amount of antigen in Lm from the complete OVA to one immunodominant epitope. Further, we planned to use the spontaneously isolated B16 C57BL/6 melanoma cell line by adding neoantigens identified in that cell line [14] to the vaccine construct. We therefore constructed an

expression vector using the hly promoter to drive the expression of a fusion protein containing the C-terminus of the Lm LLO and a concatenated polypeptide of our mutant targets (Figure 3.3).

We found that Lm expressing this vaccine construct were able to trigger proliferation of OVA-specific CD8 T-cells, while expression of a scrambled version of the peptide fused to wild type neoantigens had no effect on those cells (Figure 3.4b). This does not mean that the Lm-WT did not trigger an immune response at all. Indeed, B-cells proliferated as well independently of the antigen expressed (Figure 3.4a).

We then moved *in vivo* to determine the ability of Lm expressing our vaccine construct to prevent the growth of E.G7-OVA tumor cells. Unfortunately, the *in vitro* data did not translate into *in vivo* protection (Figure 3.5). The vaccine construct was unable to trigger proliferation of antigen specificCD8 T-cells. Further characterization of the construct showed that the polypeptide was not secreted by the bacteria once inside the infected cells (data not shown). This could potentially explain a reduced efficacy in triggering a response *in vivo*, however it did not prevent *in vitro* stimulation.

Going forward, ensuring that the vaccine polypeptide is properly secreted by the attenuated Lm strain could potentially enhance activity in this tumor model. Others have shown that the same peptides can be used to trigger an immune response by using a different method of immunization [17]. It remains to be determined whether *Listeria monocytogenes*, because it is so efficient at triggering a strong CD8 response, and because of its inherent innate immune system stimulation abilities, is superior or not to these strategies.

Figure 3.1

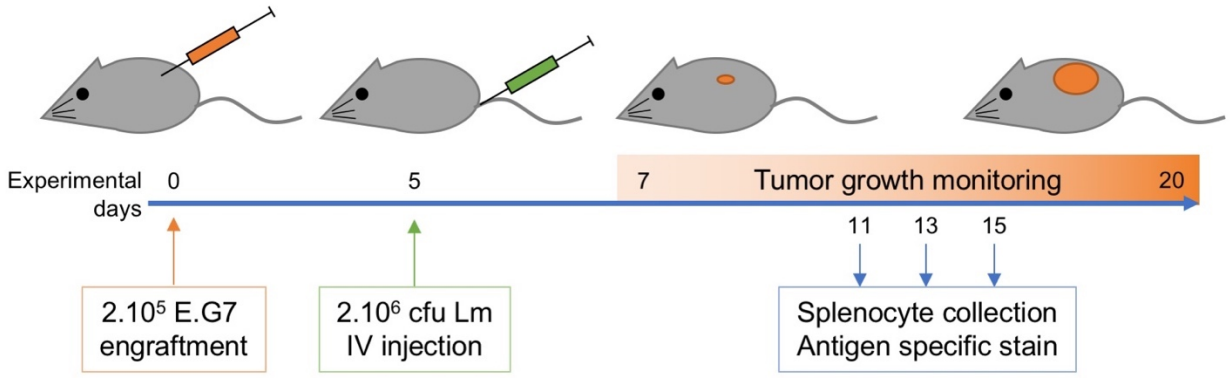
Experimental days
0
5
7
Tumor growth monitoring
20
11
13
15
2.10⁵ E.G7 engraftment
2.10⁶ cfu Lm IV injection
Splenocyte collection
Antigen specific stain

Figure 3.1: Experimental schedule

Wild-type C57BL/6 mice were inoculated with 200,000 E.G7-OVA cells subcutaneously at day 0. At day 5, 2 million cfu Lm-ActA or Lm-ActA-OVA were injected intra venously. Tumor growth was monitored every other day and groups of animals were sacrificed at day 11, 13, and 15. Their spleens were collected and splenocytes isolated for further experiments.

Figure 3.2

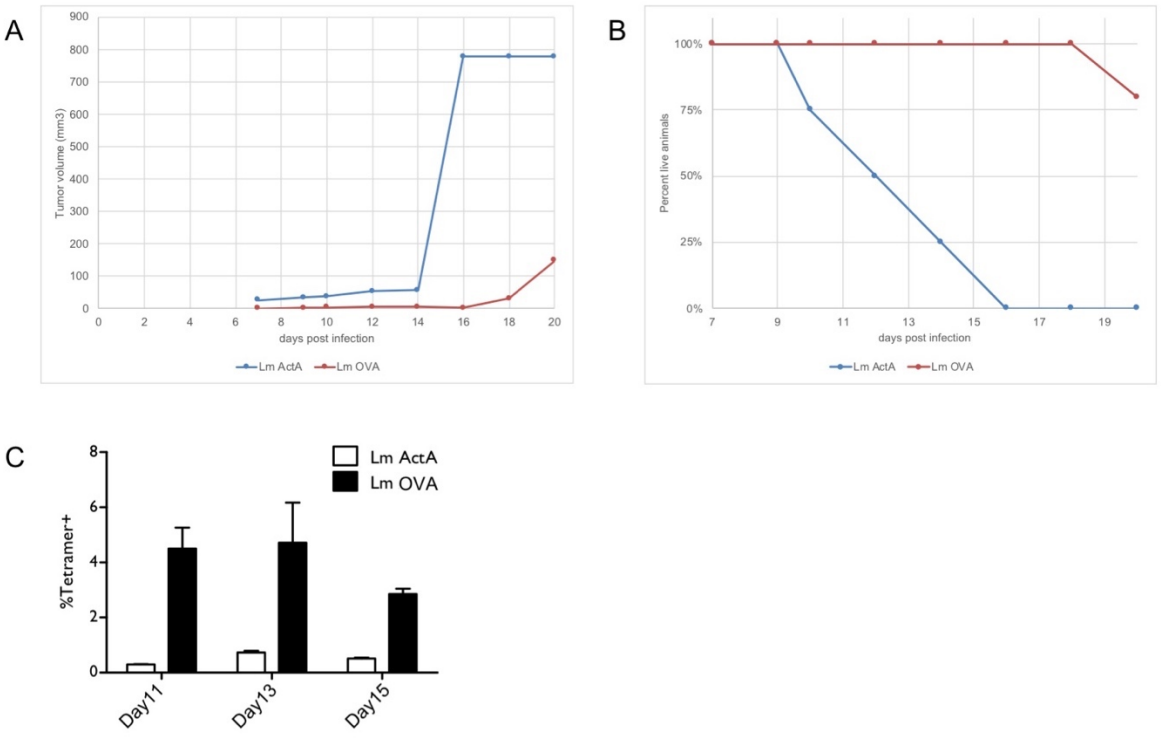
A
Tumor volume (mm3)
days post infection
Lm ActA
Lm OVA
B
Percent live animals
days post infection
Lm ActA
Lm OVA
C
%Tetramer+
Lm ActA
Lm OVA
Day11
Day13
Day15

Figure 3.2: Lm-OVA treatment protects from E.G7 tumor growth

A. Tumor volume of mice inoculated with E.G7 tumors and treated with Lm-ActA or Lm-ActA-OVA. B. Survival curve of mice inoculated with E.G7 tumors and treated with Lm-ActA or Lm-ActA-OVA. C. Percent of Kd-SIINFEKL positive CD8 T-cells in mice inoculated with E.G7 tumors and treated with Lm-ActA or Lm-ActA-OVA at days 11, 13, or 15 following inoculation.

Figure 3.3

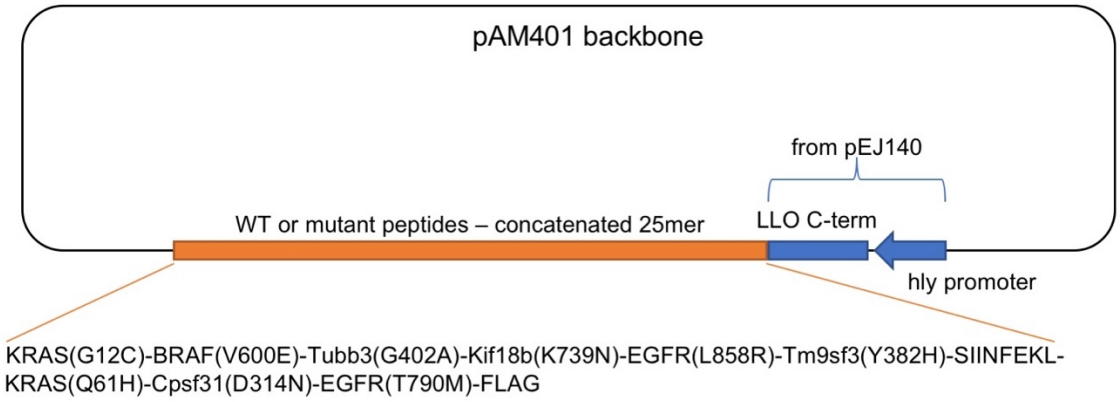

KRAS(G12C)-BRAF(V600E)-Tubb3(G402A)-Kif18b(K739N)-EGFR(L858R)-Tm9sf3(Y382H)-SIINFEKL-KRAS(Q61H)-Cpsf31(D314N)-EGFR(T790M)-FLAG

Figure 3.3: Neoantigen peptide Lm expression vector

The hly-LLO C-term promoter cassette was subcloned into a pAM401 shuttle vector. Wild-type or mutant peptide concatemers were inserted in frame with the LLO C-terminal peptide.

Figure 3.4

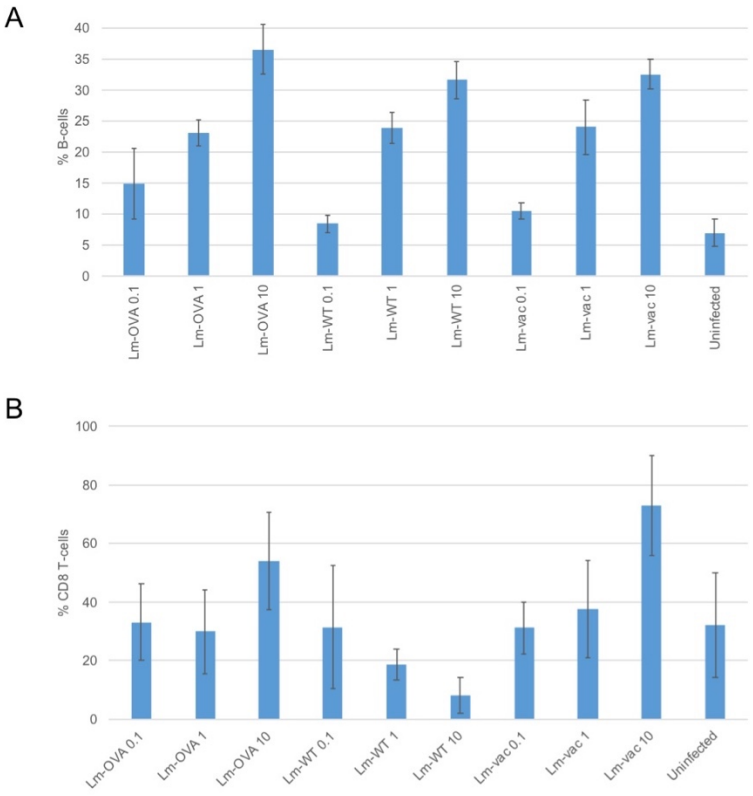
A
% B-cells
40
35
30
25
20
15
10
5
0
Lm-OVA 0.1
Lm-OVA 1
Lm-OVA 10
Lm-WT 0.1
Lm-WT 1
Lm-WT 10
Lm-vac 0.1
Lm-vac 1
Lm-vac 10
Uninfected
B
% CD8 T-cells
100
80
60
40
20
0
Lm-OVA 0.1
Lm-OVA 1
Lm-OVA 10
Lm-WT 0.1
Lm-WT 1
Lm-WT 10
Lm-vac 0.1
Lm-vac 1
Lm-vac 10
Uninfected

Figure 3.4: B-cells proliferate independently of peptides expressed by Lm while T-cells proliferate in an antigen-specific manner.

OT-I total splenocytes were plated in 96-U-well plates and infected with 0.1, 1, or 10 multiplicity of infection Lm-OVA, Lm-vac, or Lm-WT. Amount of cells having proliferated as a percentage of total B-cells (A) or T-cells (B) was measured by flow cytometry.

Figure 3.5

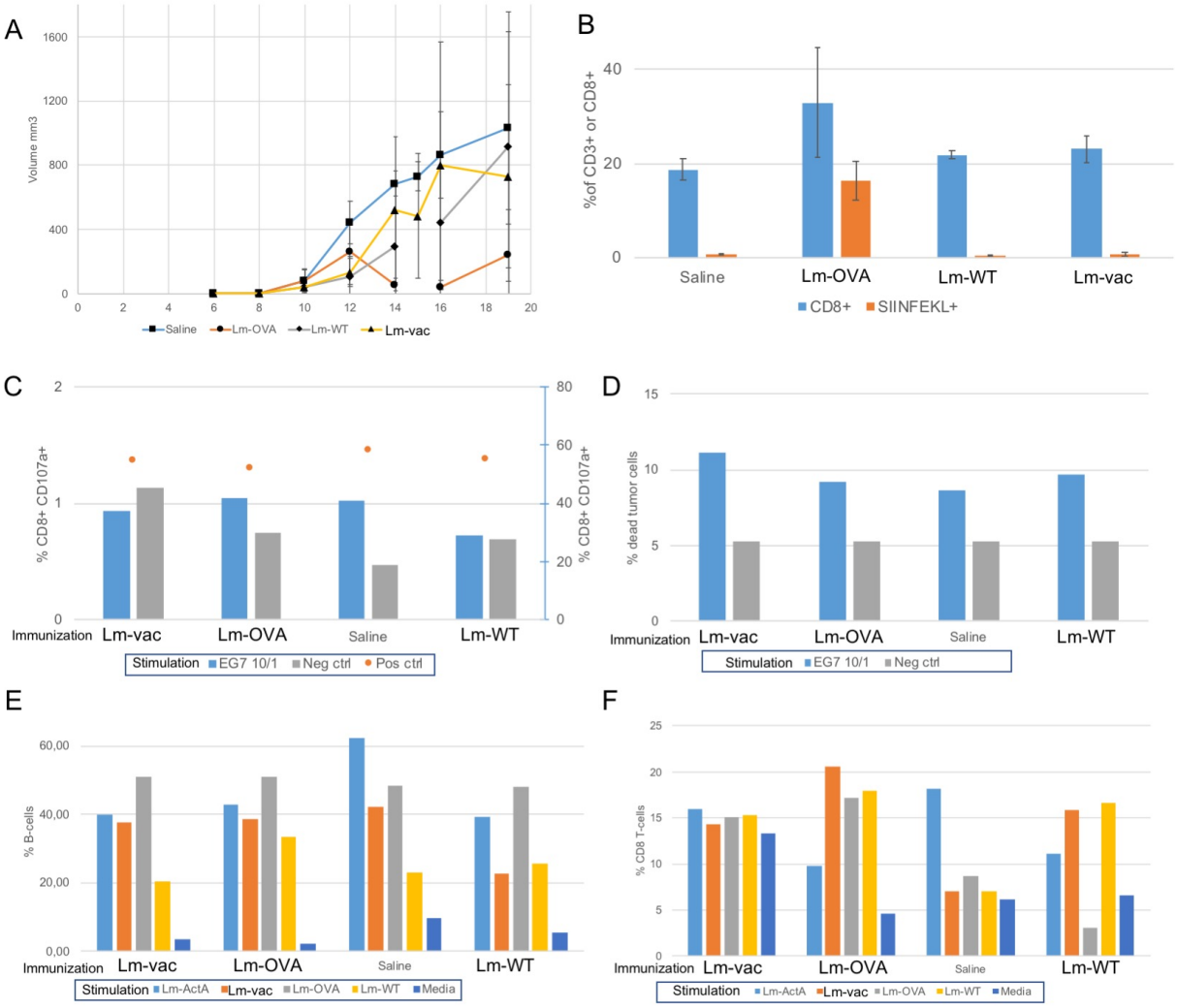
A
Volume mm3
Saline
Lm-OVA
Lm-WT
Lm-vac
B
%of CD3+ or CD8+
Saline
Lm-OVA
Lm-WT
Lm-vac
CD8+
SIINFEKL+
C
% CD8+ CD107a+
Immunization
Lm-vac
Lm-OVA
Saline
Lm-WT
Stimulation
EG7 10/1
Neg ctrl
Pos ctrl
D
% dead tumor cells
Immunization
Lm-vac
Lm-OVA
Saline
Lm-WT
Stimulation
EG7 10/1
Neg ctrl
E
% B-cells
Immunization
Lm-vac
Lm-OVA
Saline
Lm-WT
Stimulation
Lm-ActA
Lm-vac
Lm-OVA
Lm-WT
Media
F
% CD8 T-cells
Immunization
Lm-vac
Lm-OVA
Saline
Lm-WT
Stimulation
Lm-ActA
Lm-vac
Lm-OVA
Lm-WT
Media

Figure 3.5: Lm-vac does not protect from E.G7 tumor growth *in vivo*

A. Mice were inoculated as described in Figure 3.1 and treated with Lm-OVA, Lm-vac, or Lm-WT at day 5. Tumor volume was monitored every other day. Splenocytes isolated from mice immunized with Lm-OVA, Lm-vac, Lm-WT, or saline control were collected at day 19. The number of CD8+ CD3+ T-cells and of Kd-SIINFEKL+ CD8+ T-cells were measured by flow cytometry (B). The ability of the cytotoxic T-cells to degranulate in response to E.G7 cells was measured by CD107a exposure after 6h stimulation at a 10/1 effector/target ratio (C). The ability of splenocytes to kill E.G7 cells was measured in the same conditions (D). The same splenocytes were exposed to Lm-OVA, Lm-vac, Lm-WT, or saline control and the proliferation of B-cells (E) or CD8 T-cells (F) was measured by CFSE dilution.

MATERIAL AND METHODS

Mouse models

Wild-type C57Bl/6 mice were maintained in pathogen-free conditions. All experiments were approved by the UCLA IACUC. Six to twelve week old mice were engrafted under anesthesia with 200,000 E.G7 cells subcutaneously in the left flank. Five days later, mice were injected with 2,000,000 cfu of attenuated Lm strain or saline control intravenously. Tumor growth was monitored daily when measurable masses appeared (usually around day 7). Tumor volume was calculated every other day from caliper measurements using the formula:

$$Volume = Length\, x\, \frac{Width^2}{2}$$

Plasmid construction

Plasmids were cloned and maintained in *E. coli* K12 derivatives. The hly-LLO cassette was amplified out of pEJ140 using the polymerase chain reaction (PCR). Separately, the mutant peptides construct was amplified using PCR from a commercially synthesized construct (Genewiz) and both fragments were inserted into the linearized pAM401. The primers used were:

primer name	template	Primer sequence
pAM-pEJ_F	pEJ140	TGCGTCCGGCGTAGAGGATCtagagtgacttttatgttgaggc
pEJ-vac_R	pEJ140	ACTAGTTTATATTCCGTCATaggatccgatgcatcctttgc
pEJ-vac_F	peptide vaccine	caaaggatgcatcggatcctATGACGGAATATAAACTAGTAGTAG
vac-pAM_R	peptide vaccine	CCACACCCGTCCTGTGGATCCTATTTATCATCATCATCTTTATAATCTA

Mutant peptides sequence:

agctggatccATGACGGAATATAAACTAGTAGTAGTAGGTGCGTGTGGTGTA
GGTAAATCGGCGCTAACGATACAACTAATACTAACGGTAAAAATAGGTGATT
TTGGTCTAGCGACGGAAAAATCGCGTTGGTCGGGTTCGCATCAATTTGAAC
AACGTCGTAAAGCGTTTCTACATTGGTATACGGGTGAAGCGATGGATGAAA
TGGAATTTACGGAAGCGGAATCTAATTCGAAACCGTCGTTTCAAGAATTTGT
AGATTGGGAAAATGTATCGCCGGAACTAAATTCGACGGATCAACCGTTTAAA
ACGCCGCAACATGTAAAAATAACGGATTTTGGTCGTGCGAAACTACTAGGTG
CGGAAGAAAAAGAATATCATGGTACGGCGTTTTTTATAAATTTTATAGCGAT
ATATCATCATGCGTCGCGTGCGATACCGTTTGGTACGATGGTAGAAGTATCG
GGTCTAGAACAACTAGAATCGATAATAAATTTTGAAAAACTAACGGAATGGA
CGTCGTCGAATGTAGAAACGTGTCTACTAGATATACTAGATACGGCGGGTCA
TGAAGAATATTCGGCGATGCGTGATCAATATATGCGTTTTAAACATATAAAA
GCGTTTGATCGTACGTTTGCGAATAATCCGGGTCCGATGGTAGTATTTGCGA
CGCCGGGTCTAGGTATATGTCTAACGTCGACGGTACAACTAATAATGCAACT
AATGCCGTTTGGTTGTCTACTAGATTATGTAGATTATAAAGATGATGATGAT
AAATAGgaattcgcat

The wild-type peptides were amplified using PCR from a commercially synthesized construct (Genewiz) and cloned into a linearized pAM401-vac. The primers used were:

Name	Primer sequence
WT-pAM401-hly-5	agCAAAGGATGCATCGgatcctATGACGGAATATAAATTAGTTGTTGTAGGAGCTG
WT-pAM401-hly-3	ccacacccgtcctgtggatcCTATTTATCATCATCGTCTTTATAATCAACATAATCTAATAAAC

Wild-type peptides sequence:

agctggatccATGACGGAATATAAACTAGTAGTAGTAGGTGCGGGTGGTGTA
GGTAAATCGGCGCTAACGATACAACTAATACTAACGGTAAAAATAGGTGATT
TTGGTCTAGCGACGGTAAAATCGCGTTGGTCGGGTTCGCATCAATTTGAACA
ACGTCGTAAAGCGTTTCTACATTGGTATACGGGTGAAGGTATGGATGAAAT
GGAATTTACGGAAGCGGAATCTAATTCGAAACCGTCGTTTCAAGAATTTGTA
GATTGGGAAAAAGTATCGCCGGAACTAAATTCGACGGATCAACCGTTTAAAA
CGCCGCAACATGTAAAAATAACGGATTTTGGTCTAGCGAAACTACTAGGTGC
GGAAGAAAAAGAATATCATGGTACGGCGTTTTTTATAAATTTTATAGCGATA
TATTATCATGCGTCGCGTGCGATACCGTTTGGTACGATGGTAGAAGTATCG
GGTCTAGAACAACTAGAATCGATAATAAATTTTGAAAAACTAACGGAATGGA
CGTCGTCGAATGTAGAAACGTGTCTACTAGATATACTAGATACGGCGGGTCA
AGAAGAATATTCGGCGATGCGTGATCAATATATGCGTTTTAAACATATAAAA
GCGTTTGATCGTACGTTTGCGGATAATCCGGGTCCGATGGTAGTATTTGCG
ACGCCGGGTCTAGGTATATGTCTAACGTCGACGGTACAACTAATAACGCAAC
TAATGCCGTTTGGTTGTCTACTAGATTATGTAGATTATAAAGATGATGATGA
TAAATAGgaattcgcat

Listeria monocytogenes culture and conjugation

Listeria monocytogenes strain 10403S deficient for ActA was cultured in brain heart infusion (BHI). Colony forming units were determined by serial dilutions on BHI-Agar plates for each bacterial stock and confirmed after each *in vivo* inoculation. The pAM401 shuttle vector was transferred from *E. coli* to Lm strains using conjugation.

In vitro Lm stimulation assay

Splenocytes were collected from WT C57BL/6 naïve or Lm infected mice. Total splenocytes were loaded with CFSE as previously described [18]. Total splenocytes were plated in U-bottom wells and infected with increasing amounts of Lm (0.1 to 10 MOI) for 1h before being treated with gentamicin to prevent the bacteria overgrowing the cells. Seventy-two hours after infection, the cells were collected and analyzed on a flow cytometer (BD LSR II).

Flow cytometry reagents

Antibodies were purchased from Biolegend. Anti-CD3 A488 (#100212), anti-CD4 PerCP (#100431), anti-CD8 A700 (#100729), anti-CD19 APC (BD #550992), anti-CD107a BV421 (#121617) were used to stain total splenocytes. Kd-SIINFEKL pentamers were purchased from Proimmune to stain SIINFEKL-specific CD8 T-cells. Dead cells were stained with Zombie Aqua prior to fixation.

REFERENCES

[1] S. I. Grivennikov, F. R. Greten, and M. Karin, “Immunity, inflammation, and cancer,” *Cell*, vol. 140, no. 6, pp. 883–899, Mar. 2010.

[2] C. Maletzki, U. Klier, W. Obst, B. Kreikemeyer, and M. Linnebacher, “Reevaluating the Concept of Treating Experimental Tumors with a Mixed Bacterial Vaccine: Coley’s Toxin,” *Clin. Dev. Immunol.*, vol. 2012, 2012.

[3] S. L. Topalian, C. G. Drake, and D. M. Pardoll, “Immune checkpoint blockade: a common denominator approach to cancer therapy,” *Cancer Cell*, vol. 27, no. 4, pp. 450–461, Apr. 2015.

[4] S. Gill and C. H. June, “Going viral: chimeric antigen receptor T-cell therapy for hematological malignancies,” *Immunol. Rev.*, vol. 263, no. 1, pp. 68–89, Jan. 2015.

[5] V. Shahabi, P. C. Maciag, S. Rivera, and A. Wallecha, “Live, attenuated strains of Listeria and Salmonella as vaccine vectors in cancer treatment,” *Bioeng. Bugs*, vol. 1, no. 4, pp. 235–243, Aug. 2010.

[6] E. G. Pamer, “Immune responses to Listeria monocytogenes,” *Nat. Rev. Immunol.*, vol. 4, no. 10, pp. 812–823, Oct. 2004.

[7] D. A. Portnoy, V. Auerbuch, and I. J. Glomski, “The cell biology of Listeria monocytogenes infection: the intersection of bacterial pathogenesis and cell-mediated immunity,” *J. Cell Biol.*, vol. 158, no. 3, pp. 409–414, Aug. 2002.

[8] Z. K. Pan, G. Ikonomidis, A. Lazenby, D. Pardoll, and Y. Paterson, “A recombinant Listeria monocytogenes vaccine expressing a model tumour antigen protects mice against lethal tumour cell challenge and causes regression of established tumours,” *Nat. Med.*, vol. 1, no. 5, pp. 471–477, May 1995.

[9] N. C. Souders *et al.*, "Listeria-based vaccines can overcome tolerance by expanding low avidity CD8+ T cells capable of eradicating a solid tumor in a transgenic mouse model of cancer," *Cancer Immun. J. Acad. Cancer Immunol.*, vol. 7, Feb. 2007.

[10] D. T. Le *et al.*, "Safety and Survival With GVAX Pancreas Prime and Listeria Monocytogenes–Expressing Mesothelin (CRS-207) Boost Vaccines for Metastatic Pancreatic Cancer," *J. Clin. Oncol.*, vol. 33, no. 12, pp. 1325–1333, Apr. 2015.

[11] P. F. Robbins *et al.*, "Mining exomic sequencing data to identify mutated antigens recognized by adoptively transferred tumor-reactive T cells," *Nat. Med.*, vol. 19, no. 6, pp. 747–752, Jun. 2013.

[12] L. B. Alexandrov *et al.*, "Signatures of mutational processes in human cancer," *Nature*, vol. 500, no. 7463, pp. 415–421, Aug. 2013.

[13] C. J. Cohen *et al.*, "Isolation of neoantigen-specific T cells from tumor and peripheral lymphocytes," *J. Clin. Invest.*, vol. 125, no. 10, pp. 3981–3991, Oct. 2015.

[14] J. C. Castle *et al.*, "Exploiting the mutanome for tumor vaccination," *Cancer Res.*, vol. 72, no. 5, pp. 1081–1091, Mar. 2012.

[15] M. R. Betts *et al.*, "Sensitive and viable identification of antigen-specific CD8+ T cells by a flow cytometric assay for degranulation," *J. Immunol. Methods*, vol. 281, no. 1–2, pp. 65–78, Oct. 2003.

[16] D. Escors, "Tumour immunogenicity, antigen presentation and immunological barriers in cancer immunotherapy," *New J. Sci.*, vol. 2014, Jan. 2014.

[17] S. Kreiter *et al.*, "Mutant MHC class II epitopes drive therapeutic immune responses to cancer," *Nature*, vol. 520, no. 7549, pp. 692–696, Apr. 2015.

[18] B. J. C. Quah and C. R. Parish, "New and improved methods for measuring

lymphocyte proliferation in vitro and in vivo using CFSE-like fluorescent dyes," *J. Immunol. Methods*, vol. 379, no. 1–2, pp. 1–14, May 2012.

CHAPTER 4

Effect of innate immune signaling on the quality and diversity of the antigen-specific T-cell receptor repertoire

ABSTRACT

The adaptive immune system is characterized by its immense breadth of antigen recognition. Following stimulation, only a small subset of that repertoire is selected for expansion. The innate immune system is equipped with a more limited diversity caused by a small subset of receptors specific for broad molecular species. Innate immune stimuli generate differential gene regulation patterns based on the type of receptors that are engaged. It remains unclear what effect differential innate immune stimulations has on the selection of the adaptive immune repertoire. We tried to address this question by comparing the TCR repertoire following stimulation with a TLR3 or TLR9 agonist. Our preliminary findings are that while some differences in CDR length usage could be noticed, the breadth of the repertoire was not altered by differential TLR stimulation.

INTRODUCTION

During differentiation, T-cells pseudo-randomly construct their T-cell receptor (TCR) through DNA rearrangements. Cells that are able to express a non-self-reactive TCR are selected in the thymus and released in the periphery where they form a diverse repertoire. For a cell to be activated, it needs to be presented its target peptide by specialized cells providing the proper stimulation signals. Multiple reports indicate that the strength of the stimulation signal provided to the T-cell through its TCRs and co-stimulatory receptors needs to fall in a specific range for the cell to be activated [1]–[3]. This signal strength is the compound of all the TCR molecules individual strength and all the co-stimulatory signals individual strength.

Pathogenic stimulation results in the activation of the innate and adaptive immune system. T-cells that are specific to the invader's antigens receive proliferation signals and expand. The rules that regulate which cells are activated and which are not remain ill-defined. The innate immune signal is indispensable but the mechanism through which they regulate the T-cell repertoire selection are controversial [4], [5]. We have previously shown that diverse innate immune signals can differentially regulate receptor expression on dendritic cells [6]. Other have shown that T-cells are able to sense innate immune signals at rest or following activation [4], [7], [8].

In this work, we aimed to determine the differential effect of toll-like receptor (TLR) ligands on TCR repertoire selection. We stimulated wild-type mice with chicken ovalbumin and TLR3 or TLR9 ligands. We observed that different CDR lengths usages could be observed by spectratyping in animals having received one or the other regimen. More detailed analysis of the TCR repertoire in animals immunized with the differential regimen proved challenging. We report that the diversity of the repertoire did not seem to depend on the innate stimulus used during immunization, with the caveat that the sample size and depth of sequencing was small.

RESULTS

Effect of TRL3 vs TRL9 stimulation during OVA immunization as measured by quantitative spectratyping

Every natural immune stimulus is composed of a mixture of peptidic compounds and innate immune stimulating molecular patterns (be it pathogen-associated or damage-associated molecular patterns – PAMPs and DAMPs). The cells that are responsible for activating naïve T-cells are antigen presenting cells, classically dendritic cells (DCs). DCs are able to sense PAMPs through

the expression of pattern recognition receptors (PRR) specific for different PAMPs. In this study we chose to focus on two types of PAMPs and their associated PRRs. These are synthetic RNA poly-I:C (pIC) and synthetic unmethylated DNA CpG. They are recognized by the toll-like receptor (TLR) 3 and 9, respectively.

Our laboratory has shown that DCs will change expression of receptors depending on the type of TLR signal they receive [6]. Here we hypothesize that those differential gene regulation programs might have an effect on the expression of T-cell co-stimulatory molecules, antigen processing machinery, and antigen presentation machinery. These supposed changes triggered by TLR signals could lead to the strength of the TCR signal delivered to naïve T-cells to vary in strength. Others have shown that the strength of the TCR signal is important in regulating the level of activation of the antigen-specific T-cell [2].

To determine the effect of pIC versus CpG during an immunization against chicken ovalbumin (OVA), we immunized mice with either or no adjuvant, in addition to OVA, with DOTAP as a carrier. The animals received a boost immunization after 30 days, and their spleens were collected seven days later. Splenocyte RNA was extracted, cDNA synthesized, and the TCR repertoire was compared using quantitative spectratyping (Figure 4.1) [9].

The T-cell receptor gene is produced by each developing thymocyte through error-prone recombination during its development. Each TCR gene is assembled by joining a variable (V), diversity (D), and junction (J) segments to the constant (C) segment. Together, they form the complementarity-determining (CDR) region. During this process, nucleotides are pseudorandomly added or removed to/from the different segments. This results in a diverse population of cells with different CDR lengths. Spectratyping allows us to easily determine the

CDR length profile for each V family of the TCR alpha or beta chains. We chose to focus on TCR beta chain CDR length.

Following our stimulation regimen, the overall Vbeta usage was mostly not modified in control mice (DOTAP only) versus immunized mice (Figure 4.2a). There was a reduction in the Vb 31 usage for both CpG and pIC stimulated animals. In CpG immunized animals, there was an increase in Vb 14 usage. This was confirmed by looking in more details at the spectratype of this particular Vb family (Figure 4.2b). When comparing different animals immunized with the same regimen, we can see that CpG adjuvant lead to a stronger amplification of peaks in the Vb 14 and 16 families (Figure 4.2c). We can also see that different animals can share the same peak amplification.

By sequencing randomly selected TCR clones, we observed that certain sequences were shared between animals and stimulation (red, yellow, and green cells in Figure 4.2d). These clones are defined as public. Others were private, i.e. they only appear in a single animal, sometimes representing the majority of the population (Orange cells in C4M1).

Using PLGA microparticles to determine the effect of differential adjuvant stimulation

The data obtained using quantitative spectratyping confirmed the existence of public and private clones in our model. We hypothesized that different clones might arise from varied TCR signaling strength. In this context, public clones would be selected from a signal strength that can be triggered by either adjuvant, while CpG- or pIC-restricted public clones might need a specific signaling activation. To study this further, we decided to use polylactic-co-glycolic acid (PLGA) microparticles (Figure 4.3a). These water in oil in water emulsion particles contain a mixture of

OVA and adjuvant encapsulated in a biodegradable polymer. These particles can readily be absorbed by DCs, and their content presented [10].

We started by determining the best time to collect antigen-specific T-cells following the immunization protocol. Mice were immunized twice as previously described, and splenocytes were collected 2, 5, and 7 days following the second immunization. An OVA-secreting *Listeria monocytogenes* (Lm-OVA) strain was used as a positive control of CD8 T-cell activation. PLGA-OVA-CpG induced splenomegaly at later time points in some of the animals (Figure 4.3b). The activation marker CD69 was upregulated on CD4 and CD8 T-cells two days after the boost in CpG and pIC treated mice (Figure 4.3c and d, respectively). CD4 T-cells specific for an OVA peptide as determined by MHC-II tetramer stain were upregulated in some of the CpG and pIC mice (Figure 4.3e). CD8 T-cells specific to the MHC-I-SIINFEKL pentamer were upregulated in all conditions but more significantly in Lm-OVA treated mice (Figure 4.3f). It is interesting to note that although activation markers were not present on the T-cells purified from Lm-OVA immunized animals, these mice showed an impressive increase in anti-OVA CD8 T-cells (up to more than 20% of all CD8 T-cells).

Sequencing the TCR repertoire using massively parallel sequencing

To get an in-depth analysis of the TCR repertoire and obtain detailed access to the major public and private CDR sequences, we set up a TCR sequencing protocol using massively parallel sequencing. In contrast to spectratyping, we decided to amplify the TCRs using a single primer pair to reduce the risk of PCR bias in the analysis. A single reverse primer binding to the constant region of the TCR-beta chain was used to prime a 5' rapid amplification of cDNA ends (5'-RACE)

reaction. Briefly, the first strand synthesis continues along the mRNA all the way to the 5'-cap where 3 cytidines are added by the reverse transcriptase. A universal primer is then used to extend the second strand from the CCC stretch. All CDRs are then amplified using the constant forward primer added during RACE and a nested reverse primer [11].

We immunized mice with PLGA-OVA +/- CpG or pIC as described above. We then fluorescent activation cell sorted (FACS) OVA-specific CD8 T-cells from animals with more than 2% of CD8 T-cells positive for SIINFEKL and extracted mRNA (Figure 4.4a). CDR sequences were amplified and sequenced on an Illumina MiSeq platform. The clones were then assigned using MiTCR [12].

The numbers of SIINFEKL-specific clones varied between 5 and 80 per mouse (Figure 4.4b). This depended greatly on the number of cells collected (Figure 4.4c). If fewer than 20,000 cells were collected, the number of clones was reduced, while the number of clones did not increase linearly with more cells being sorted. The number of shared clones seemed to correlate with the total number of clones identified (Figure 4.4d).

Finally, we compared the diversity of the CpG or pIC stimulated TCR repertoires using Shannon's entropy. This relative unit measurement asses the diversity of a particular list of data, with the diversity increasing as the unit gets larger. There was no difference in the TCR diversity between mice immunized with CpG or pIC (Figure 4.4e). The variability of the measurement was great and additional data points would be necessary to provide a conclusive comparison.

DISCUSSION

In this work we tried to gain a better understanding of the possible regulatory effects of innate immune signals on the selection of the – adaptive immunity's – TCR repertoire. We hypothesized that different TLR signals, through their activating signals on APCs and T-cells, would lead to differential TCR signal strength. This was supported by work from our lab showing that DCs can differentially regulate their function based on the kind of TLR ligand they are exposed to [6]. Others had also shown that T-cells are able to sense TLR ligands, at rest or following activation, and that this had effects on downstream signaling pathways [4], [7], [8]. We predicted that the combination of those effects would lead to the selection of TCR repertoires with different avidity, breadth, or function.

Because of the predicted involvement of professional APCs and naïve T-cells, we decided to use an *in vivo* model, by fear that *in vitro* models would bias the selection to such extent that the predicted effect would be undetectable. We began by taking a high-level look at the repertoire by using quantitative spectratyping. This technique allows to detect Vb-fragment (TRBV) usage change as well as clonal amplification, without providing access to the CDR sequence. While there was no drastic change in the TRBV gene usage, we found that certain CDR peaks could be commonly amplified in different animals who shared the same immunization regimen (Figure 4.2a-c). This lead us to randomly sequence clones from one such TRBV family, which further confirmed that public clones were present in our dataset following immunization (Figure 4.2d). The existence of public clones has of course been described by others [13], but confirming their detectability in our experimental setup was encouraging as our ability to compare adjuvant regimens

relies on the capacity to functionally characterize TCRs. Public TCRs simplify this task by limiting the number of TCRs to study as well as making direct comparisons possible.

These preliminary data encouraged us to further pursue this question by massively sequencing the TCR repertoire of mice immunized with different TLR ligands. The preliminary experiment having given somewhat disappointing results in terms of strength of the response, we decided to change the carrier. PLGA microparticles are efficient at packaging different compounds together and at slowly releasing them [10]. The polymer is also effectively degraded in the lysosomes of dendritic cells, therefore liberating the antigen and adjuvant [10]. The size of the particles seemed to matter as sub-micron particles were able to trigger a stronger response than ~2μm diameter ones (Figure 4.4a vs figure 4.3, respectively). These particles were more efficient at triggering a response as soluble compounds as seen in Figure 4.4a. However, they never induced proliferation of CD8 T-cells as strongly as *Listeria monocytogenes* did (Figure 4.3f).

TCR receptor repertoire sequencing proved challenging. This was due to the limited number of cells sorted (as low as 1,000) which lead to small amounts of RNA purified, as well as to a suboptimal efficiency of 5' RACE compared to standard reverse transcription. We chose 5' RACE to limit the chances of PCR biasing the results during amplification of individual TRBV families. This is a stance that would benefit from a more detailed analysis of the drawbacks of each method. The analysis showed that the number of clones identified per sample was greatly limited by the quantity of cells sorted, if that number was inferior to 20,000 (Figure 4.4c). Similarly, the ability of identifying shared clones depended greatly on the number of clones identified in a specific sample (Figure 4.4d). Indeed, the fewer the clones, the more likely only the major clonotypes will be identified. While public clones can be the major clonotype in some individuals, they are usually

not always the same between individuals [13]. Finally, by comparing the diversity of the repertoires collected from mice stimulated with CpG or pIC, we found that there was no difference. The variability was also important and depended greatly on the number of clones identified.

While this project did not produce the results we expected, we believe it is still an important question to address. Differential signaling in response to innate signals has been described in many models [14]. The role of TCR signal strength on T-cell activation has also been described [1], [2]. In retrospect, we believe the best way to address this question would be, at least at first, in a well-controlled *in vitro* environment, for instance using clonal TCRs, mutated target peptides, and purified antigen presenting cells.

Figure 4.1

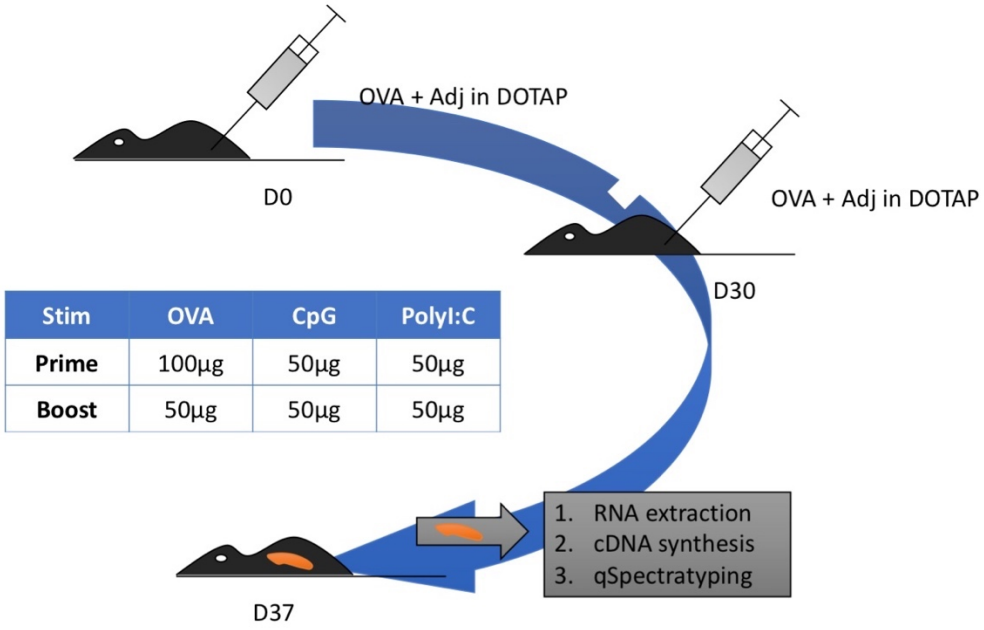

Stim	OVA	CpG	PolyI:C
Prime	100µg	50µg	50µg
Boost	50µg	50µg	50µg

Figure 4.1: Experimental schedule

Wild-type C57BL/6 mice were immunized with OVA + CpG, polyI:C, or saline control in a DOTAP emulsion (Prime). Thirty days later, the animals were immunized a second time (boost). Seven days following boost, the animals were sacrificed, their splenocytes purified, and the total RNA isolated with Trizol. Total RNA was then reverse transcribed and used for quantitative spectratyping.

Figure 4.2

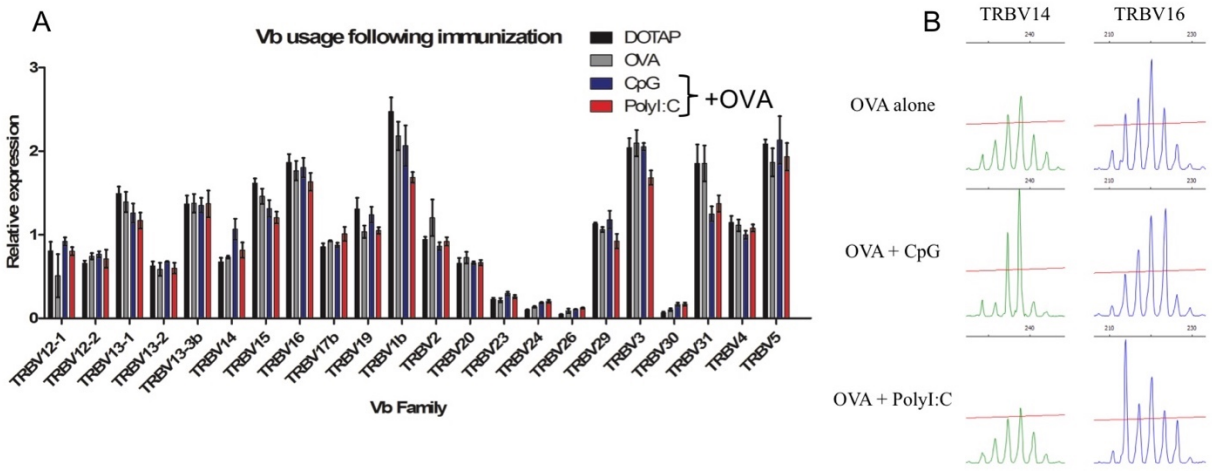

C

	OVA			OVA+CpG			OVA+PolyI:C		
Peak	C2M2	C3M3	C5M5	C4M1	C5M1	C5M2	C4M3	C5M3	C5M4
14 - 1	0	0	0	1	0	0	0	1	0
14 - 2	0	0	0	0	0	0	0	0	0
14 - 3	0	0	0	1	1	1	1	1	0
14 - 4	0	0	0	1	0	1	0	0	0
14 - 5	0	0	0	1	0	0	0	0	1
14 - 6	0	0	0	0	0	0	0	0	0
16 - 1	0	0	0	0	0	0	0	0	0
16 - 2	0	0	0	1	1	0	1	1	0
16 - 3	0	0	0	0	0	0	0	0	0
16 - 4	0	0	0	0	0	0	0	0	0
16 - 5	0	0	0	1	1	1	0	0	0
16 - 6	0	0	0	1	0	1	0	0	0
16 - 7	0	0	0	0	0		0	0	0

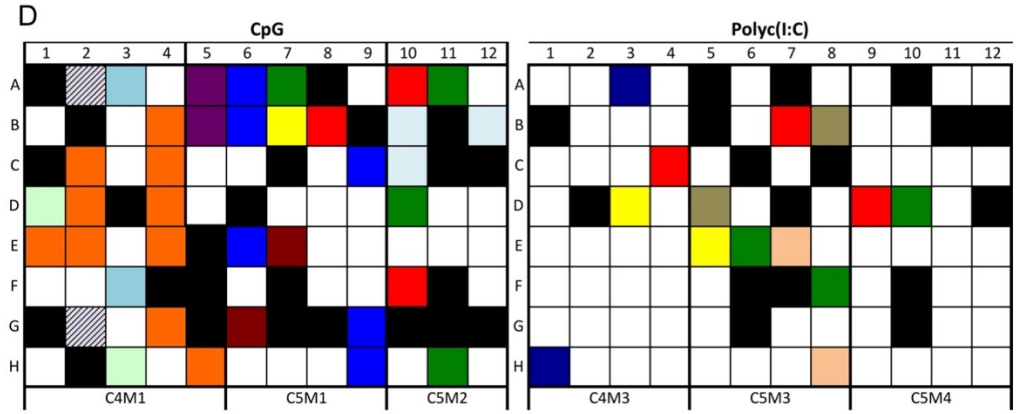

Figure 4.2: TLR3 versus TLR9 stimulation provokes mostly comparable TCR clone proliferation

The relative expression of every TCR V-beta (TRBV) family was measured by quantitative PCR (A). The CDR length profile obtained by spectratyping is shown for TRBV14 and TRBV16 (B), and the presence of clonal amplification for each peak in every animal is indicated in C. Proliferation was defined by an increase of the peak area over 4 standard deviation compared to the OVA only control. D. A random selection of TCR sequences were cloned from the TRBV14 family and sequenced by sanger sequencing. Identical clones are represented by identical colors. Black cells represent no sequence. White cells represent unique sequences.

Figure 4.3

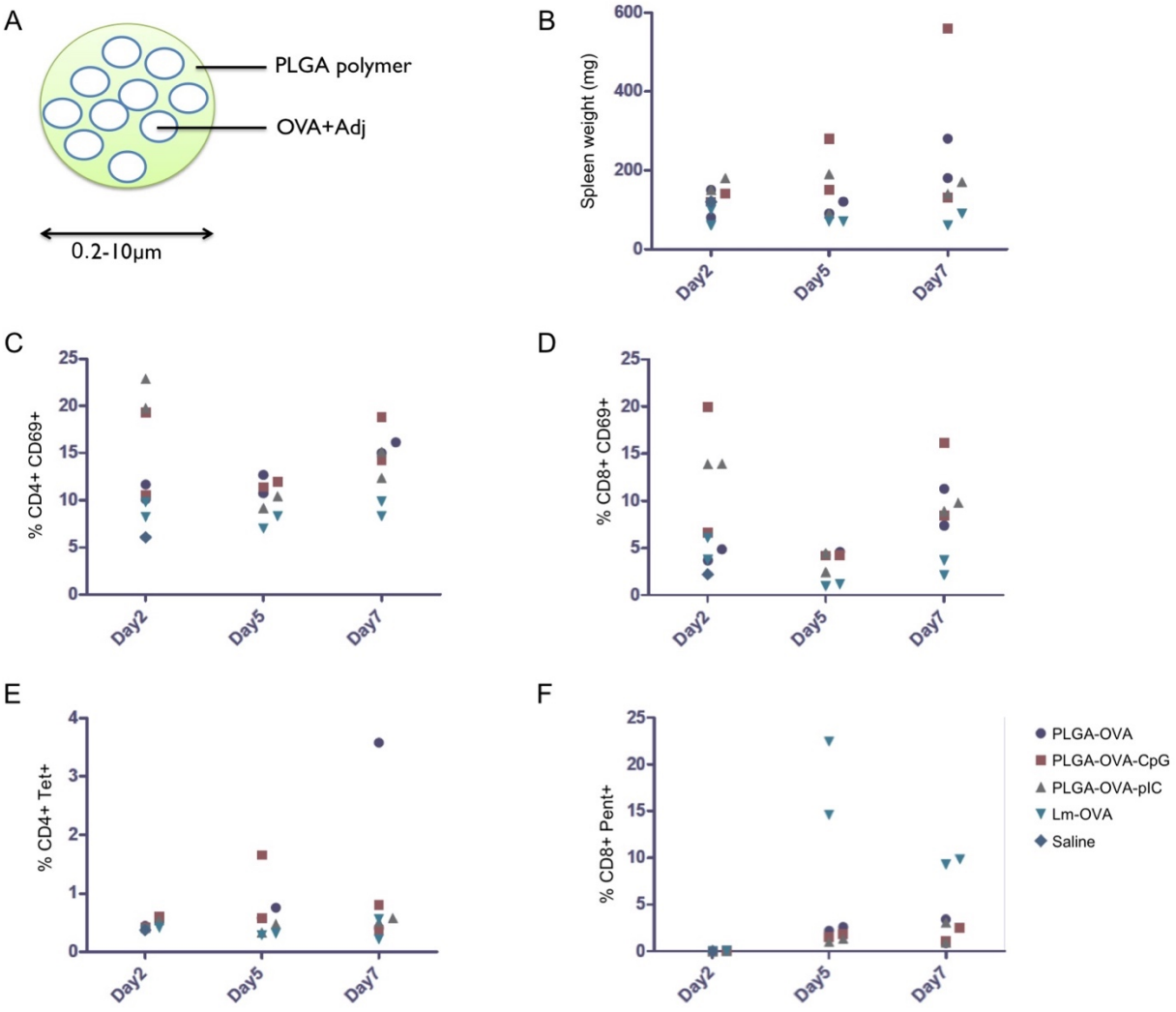
A
PLGA polymer
OVA+Adj
0.2-10μm
B
Spleen weight (mg)
600
400
200
0
Day2
Day5
Day7
C
% CD4+ CD69+
25
20
15
10
5
0
Day2
Day5
Day7
D
% CD8+ CD69+
25
20
15
10
5
0
Day2
Day5
Day7
E
% CD4+ Tet+
4
3
2
1
0
Day2
Day5
Day7
F
% CD8+ Pent+
25
20
15
10
5
0
Day2
Day5
Day7
PLGA-OVA
PLGA-OVA-CpG
PLGA-OVA-pIC
Lm-OVA
Saline

Figure 4.3: PLGA microparticles loaded with TLR ligands can induce T-cell activation

A. Schematic representation of a PLGA microparticle. Mice were immunized twice as in figure 4.1 with PLGA microparticles containing OVA alone or with CpG or polyI:C, or with saline as negative control or Lm-OVA as positive control. Two, five, and seven days following boost, two animals per group were sacrificed and their spleen weight measured (B). The percentage of activated CD4 (C) or CD8 (D) T-cells was measure as CD69 expression. The percentage of OVA-specific CD4 (E) or CD8 (F) T-cells was measured by MHC multimer staining.

Figure 4.4

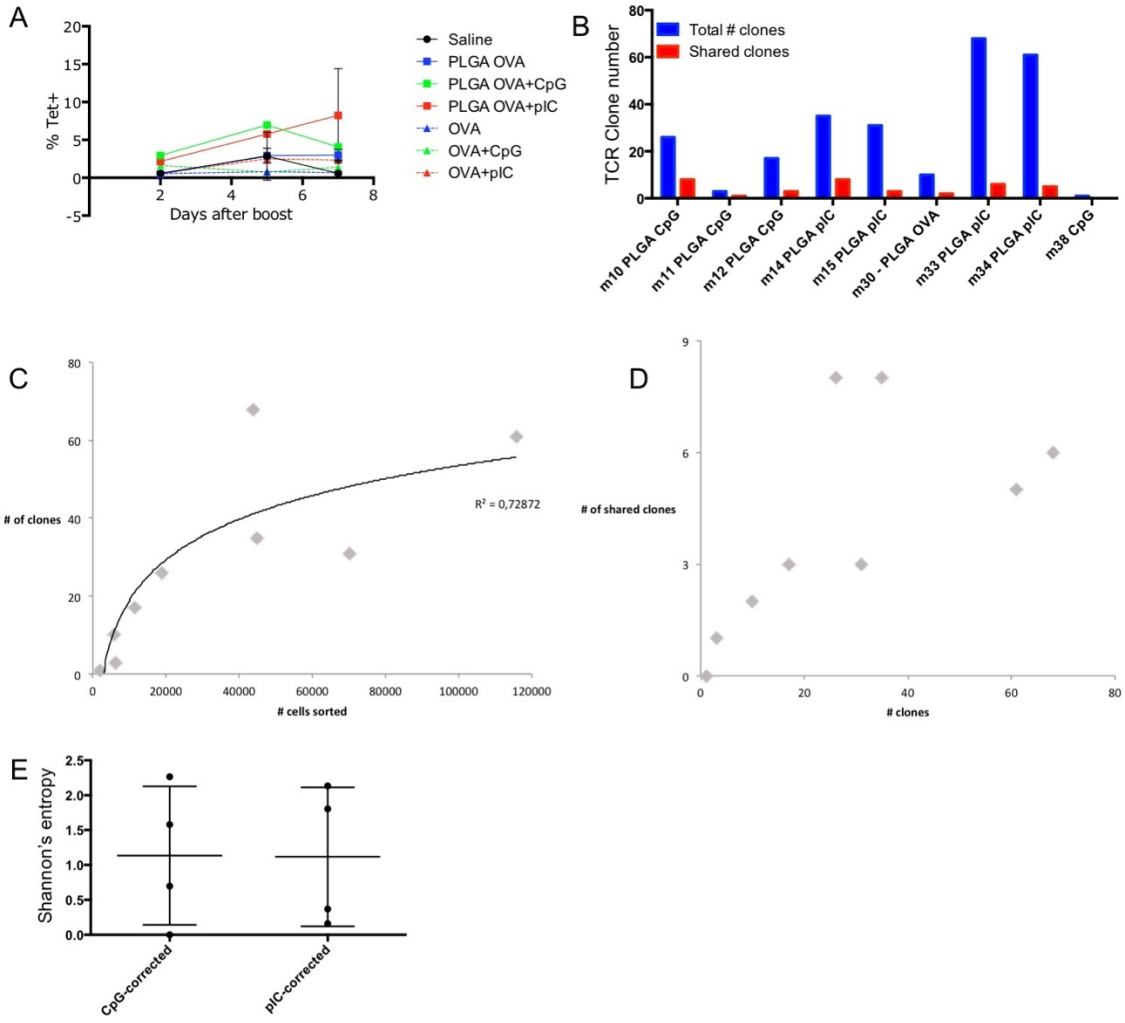
A
% Tet+
Days after boost
Saline
PLGA OVA
PLGA OVA+CpG
PLGA OVA+pIC
OVA
OVA+CpG
OVA+pIC
B
TCR Clone number
Total # clones
Shared clones
m10 PLGA CpG
m11 PLGA CpG
m12 PLGA CpG
m14 PLGA pIC
m15 PLGA pIC
m30 - PLGA OVA
m33 PLGA pIC
m34 PLGA pIC
m38 CpG
C
# of clones
# cells sorted
R² = 0,72872
D
# of shared clones
clones
E
Shannon's entropy
CpG-corrected
pIC-corrected

Figure 4.4: PLGA microparticle stimulation is more effective than soluble stimulation but differential TLR stimulation does not induce divergent TCR repertoires

Mice were immunized as in Figure 4.1 with Saline, PLGA particles containing OVA alone or combine with CpG or polyI:C, or with soluble OVA alone or with CpG or polyI:C. The percentage of OVA-specific CD8 T-cells was measured by pentamer staining (A). OVA specific CD8 T-cells were sorted by fluorescence activated cell sorting and their TCR was sequenced. The total number of clones identified in each animal, as well as the number of shared clones among them is displayed in B. The total number of clones is graphed against the total number of cells sorted in C (with exponential curve fit). The number of shared clones is graphed against the total number of clones in D. Shannon's entropy of the TCR repertoire from mice immunized with OVA+CpG or OVA+polyI:C is graphed in E (mean + SD).

MATERIAL AND METHODS

Mice and immunizations

Male and female WT C57BL/6 mice 6-12 weeks of age were used in all experiments. All experiments were approved by the institutional IACUC. Soluble model: mice were immunized intraperitoneally with 100µg OVA +/- 50µg CpG or pIC (adjuvants, Invivogen) with DOTAP (Roche) as a carrier. Immunization was repeated after 30 days with 50µg OVA and 50µg adjuvant. Mice were sacrificed seven days later, and their spleen collected for analysis. Microparticles model: mice were immunized intraperitoneally with PLGA-OVA +/- CpG or pIC containing 100µg OVA and 50µg adjuvant (in collaboration with Pr Aliasger K Salem, University of Iowa), 2.10^6 colony forming units Lm-OVA, or saline. Immunization was repeated two weeks later, and mice were sacrificed 2, 5, or 7 days following the second immunization. Spleens were collected for analysis.

Flow cytometry

All antibodies were purchased from Biolegend. K^d-SIINFEKL (OVA) pentamer were purchased from Proimmune. I-A^b-AAHAEINEA (OVA) tetramers were obtained from the NIH Tetramer Core Facility at Emory University. Anti-CD3 A488 (#100212), anti-CD4 PerCP (#100431), anti-CD8 A700 (#100729), anti-CD25 BV421 (#102033), anti-CD69 BV605 (#104529) and zombie aqua were used to stain splenocytes according to manufacturer's instructions. Cells were acquired on a BD LSR-II FACS analyzer or sorted on a BD FacsAria III at the UCLA Jonsson Comprehensive Cancer Center (JCCC) and Center for AIDS Research Flow Cytometry Core Facility. Analysis was done using FlowJo (Beckton Dickinson).

TCR quantitative spectratyping

Following total RNA extraction using Trizol reagent (Life technologies), cDNA was prepared using iScript (Bio-Rad) following the manufacturer's instructions. Quantitative spectratyping was carried out as previously described [9]. The mouse TCRB specific primers were (based on [15], [16]):

IMGT	Sequence	Currier & Robinson
TRBV1	ggtcactgatacggagctgag	MuBV2
TRBV2	CCTCAAGTCGCTTCCAACCTC	MuBV4
TRBV3	cactctgaaaatccaacccacag	MuBV16
TRBV4	CAAGTCTGTAGAGCCGGAGGA	MuBV10
TRBV5	AATGCCCAGACAGCTCCAAGC	MuBV1
TRBV12-1	AAGGTGGAGAGAGACAAAGGATTC	MuBV5.2
TRBV13-1	gTGCTGGCAACCTTCaAATAGGA	MuBV8.3
TRBV12-2	aacagactcaggggcaggaac	MuBV5.1
TRBV13-2	CATATGGTGCTGGCAGCACTG	MuBV8.2N
TRBV12-3	agAGAAAGGAAACCTGCCTGGTT	MuBV5.3
TRBV13-3	catatgtcgctgacagcacgg	MuBV8.1N
TRBV14	AGGCCTAAAGGAACTAACTCCACT	MuBV13N
TRBV15	GATGGTGGGGCTTTCAAGGATC	MuBV12
TRBV16	ACTCAACTCTGAAGATCCAGAGC	MuBV11
TRBV17	cagtcggcctaacaattctttctg	MuBV9
TRBV19	CTCTCACTGTGACATCTGCCC	MuBV6

TRBV20	CCATCAGTCATCCCAACTTATCC	MuBV15
TRBV21	ccCTGCTAAGAAACCATGTACCA	MuBV19
TRBV23	cTCTGCAGCCTGGGAATCAGA	MuBV20
TRBV24	agCTAAGTGTTCCTCGAACTCAC	MuBV17N
TRBV26	CCTTGCAGCCTAGAAATTCAGT	MuBV3.1
TRBV29	TACAGGGTCTCACGGAAGAAGC	MuBV7
TRBV30	GCCGGCCAAACCTAACATTCTC	MuBV18
TRBV31	gACGACCAATTCATCCTAAGCAC	MuBV14
TRBC	cAAGCACACGAGGGTAGCCT	MuTCB3C
TRBC Probe	AAGGAGACCTTGGGTGGAGTCACATTTCTC	MuTCB1-FAM

Massively parallel TCR sequencing

Following total RNA extraction using Nucleospin RNA Plus XS (Clontech), cDNA preparation was carried out using the SMARTer 5' RACE kit (Clontech) with the gene specific primer:

Race GSP	GGG AAG AAG CCC CTG GCC AAG CAC ACG

CDRs were amplified with primers containing Illumina Nextera adapters:

Nested primer	TCGTCGGCAGCGTCAGATGTGTATAAGAGACAGGGAGACC
	TTGGGTGGAGTCACATTTCTC
Nested reverse	GTCTCGTGGGCTCGGAGATGTGTATAAGAGACAGCAAGCA
	GTGGTATCAACGCAGAGT

Indexing was carried out using the Nextera indexing kit (Illumina), and the library was sequenced on a MiSeq sequencer at the UCLA Genoseq core facility. Raw reads were processed using MiTCR [12] to identify CDR sequences.

REFERENCES

[1] H. D. Moreau *et al.*, "Dynamic in situ cytometry uncovers T cell receptor signaling during immunological synapses and kinapses in vivo," *Immunity*, vol. 37, no. 2, pp. 351–363, Aug. 2012.

[2] D. Skokos *et al.*, "Peptide-MHC potency governs dynamic interactions between T cells and dendritic cells in lymph nodes," *Nat. Immunol.*, vol. 8, no. 8, pp. 835–844, Aug. 2007.

[3] J.-L. Chen *et al.*, "Ca2+ release from the endoplasmic reticulum of NY-ESO-1-specific T cells is modulated by the affinity of TCR and by the use of the CD8 coreceptor," *J. Immunol. Baltim. Md 1950*, vol. 184, no. 4, pp. 1829–1839, Feb. 2010.

[4] L. Malherbe, L. Mark, N. Fazilleau, L. J. McHeyzer-Williams, and M. G. McHeyzer-Williams, "Vaccine adjuvants alter TCR-based selection thresholds," *Immunity*, vol. 28, no. 5, pp. 698–709, May 2008.

[5] B. D. Rudd, V. Venturi, M. J. Smithey, S. S. Way, M. P. Davenport, and J. Nikolich-Zugich, "Diversity of the CD8+ T cell repertoire elicited against an immunodominant epitope does not depend on the context of infection," *J. Immunol. Baltim. Md 1950*, vol. 184, no. 6, pp. 2958–2965, Mar. 2010.

[6] S. E. Doyle *et al.*, "Toll-like receptors induce a phagocytic gene program through p38," *J. Exp. Med.*, vol. 199, no. 1, pp. 81–90, Jan. 2004.

[7] A. E. Gelman, J. Zhang, Y. Choi, and L. A. Turka, "Toll-like receptor ligands

directly promote activated CD4+ T cell survival," *J. Immunol. Baltim. Md 1950*, vol. 172, no. 10, pp. 6065–6073, May 2004.

[8] M. J. Richer, J. C. Nolz, and J. T. Harty, "Pathogen-specific inflammatory milieux tune the antigen sensitivity of CD8(+) T cells by enhancing T cell receptor signaling," *Immunity*, vol. 38, no. 1, pp. 140–152, Jan. 2013.

[9] A. Balamurugan, H. L. Ng, and O. O. Yang, "Rapid T cell receptor delineation reveals clonal expansion limitation of the magnitude of the HIV-1-specific CD8+ T cell response," *J. Immunol. Baltim. Md 1950*, vol. 185, no. 10, pp. 5935–5942, Nov. 2010.

[10] V. B. Joshi, S. M. Geary, and A. K. Salem, "Biodegradable particles as vaccine delivery systems: size matters," *AAPS J.*, vol. 15, no. 1, pp. 85–94, Jan. 2013.

[11] M. F. Quigley, J. R. Almeida, D. A. Price, and D. C. Douek, "Unbiased molecular analysis of T cell receptor expression using template-switch anchored RT-PCR," *Curr. Protoc. Immunol.*, vol. Chapter 10, p. Unit10.33, Aug. 2011.

[12] D. A. Bolotin *et al.*, "MiTCR: software for T-cell receptor sequencing data analysis," *Nat. Methods*, vol. 10, no. 9, pp. 813–814, Sep. 2013.

[13] V. Venturi *et al.*, "A mechanism for TCR sharing between T cell subsets and individuals revealed by pyrosequencing," *J. Immunol. Baltim. Md 1950*, vol. 186, no. 7, pp. 4285–4294, Apr. 2011.

[14] C. A. Thaiss, M. Levy, S. Itav, and E. Elinav, "Integration of Innate Immune Signaling," *Trends Immunol.*, vol. 37, no. 2, pp. 84–101, Feb. 2016.

[15] J. R. Currier and M. A. Robinson, "Spectratype/immunoscope analysis of the expressed TCR repertoire," *Curr. Protoc. Immunol.*, vol. Chapter 10, p. Unit 10.28, May 2001.

[16] V. Giudicelli, D. Chaume, and M.-P. Lefranc, "IMGT/GENE-DB: a comprehensive

database for human and mouse immunoglobulin and T cell receptor genes," *Nucleic Acids Res.*, vol. 33, no. Database issue, pp. D256-261, Jan. 2005.

CHAPTER 5

Conclusion and future perspectives

It has become apparent in the past 20 years that the immune system is involved to some extent in most long term human pathologies. This has set the stage for in depth studies of immune related signaling and cellular processes, and the emergence of therapies that utilize our understanding of the immune system to treat disease. Cancer immunotherapy has allowed for the treatment of advanced stage tumors in patients that did not respond to previous regimens, such as chemotherapy and radiotherapy. Still, our understanding of immunology remains incomplete, and a recent regain of interest in innate immunity is trying to integrate previously separate fields into a more complete picture. During this thesis work, my focus centered identifying ways to trigger efficient antigen-specific T-cell responses.

In Chapter 2, we focused on gaining a better understanding of how HSV-1 regulates the host innate immune response. The ability of Herpesviridae to infect many cell types and their large genome have made them good candidates for vectors of immunotherapy. Others have shown that by reducing the type-I interferon response, one can obtain better antitumor efficacy of an oncolytic HSV-1 vector [1]. On the other hand, type-I interferon is able to enhance the specificity of the T-cell response by suppressing proliferation of non-specific T-cells [2] and enhancing that of antigen-specific clones [3]. It is clear that regulating the type-I interferon response in this context will prove useful. The viral genome itself presents an opportunity as HSV-1 has evolved many strategies to suppress this response [4]. By creating a library of viral mutants that covers the entire genome, we were able to assess the effect of each viral protein in resisting the type-I interferon response. We found that three viral proteins possess a previously unreported function in suppressing the IFN-I response. Further characterization of one of them, the DNA polymerase processivity factor UL42, allowed us to identify that it is able to inhibit transcriptional activation of the interferon-β gene by

interacting with the transcription factor IRF-3. We also found that UL42 has a partial but consistent effect in inhibiting ISRE promoter activation following interferon-beta treatment. Further studies are necessary to characterize the other candidates from this screen. HSV-2 US1 has been shown to inhibit interferon-beta activation by inhibiting IRF-3 binding to its target DNA, in a fashion that reminds of UL42 [5]. It would be interesting to determine whether the mechanism of HSV-1 US1 is similar. UL44 is a membrane protein that does not affect interferon-β activation. It is possible that UL44 acts downstream of type-I interferon, either on its signaling or on specific ISGs. Further, the tool I created for this study could be used to decipher other viral protein functions, provided the proper selection condition exist. We are currently in the process of determining whether novel oncolytic mutations can be identified by screening the library in non-immortalized human cells and cancer cell lines.

In Chapter 3, we used a different pathogen to trigger a strong antigen-specific CD8 T-cell response. This model had previously been used by others to demonstrate its ability to protect from tumor growth when *Listeria monocytogenes* expressed model tumor antigens [6]. We were stricken in our experiments by the ability of Lm to induce up to 25% of total splenic CD8 T-cell to target a specific antigen. We decided to investigate whether this ability would make Lm a good candidate to produce immunity against more difficult targets, neoantigens. These are antigens that result from a self-protein becoming mutated as a result of tumorigenesis [7]. During development, the adaptive immune system is selected so that cells that recognize self-peptides or proteins are either deleted or rendered inactive. Since neoantigens often present a single amino acid change, we hypothesized that a complex innate stimulus such as Lm would help produce an immune response strong enough to brake a possible immune tolerance to those peptides. We constructed a strain of

Lm that expressed neoantigens from a syngeneic mouse tumor and characterized its ability to induce antigen-specific CD8 T-cell proliferation *in vitro*. Unfortunately, the engineered pathogen was unable to protect from tumor growth *in vivo*. Further characterization by our collaborators found that this particular construct was not secreted by the bacterium into the host cytoplasm. Further studies are currently being explored in the clinic by others using a similar strategy [8].

Finally, I set out to better understand the relationship between innate and adaptive immunity in Chapter 4. This was by far the most challenging project I undertook during my graduate work. Based on our lab's [9] and others works [10], [11], we hypothesized that differential regulation that happens in antigen presenting cells and T-cells when exposed to diverse PRR ligands would result in the selection of TCR repertoires with distinct characteristics. Assuming that the starting naïve repertoire of T-cell is identical, the PRR ligand might influence repertoire selection at two separate levels that regulate TCR signaling. On the one hand, gene regulation happening in the APC might modify the type of peptide that are presented (through regulation of the immunoproteasome expression), and the amount of co-stimulation that is provided through the expression of receptor ligands. On the other hand, induction or activation of signaling intermediates downstream of the TCR could change the avidity required to activate a T-cell. To test this hypothesis, I resorted to using an *in vivo* model by immunizing animals with a classical antigen (OVA) and one of two TLR ligand, CpG or polyI:C. The reasoning for this choice was that we were looking to detect such a sensitive process that any *ex vivo* manipulation might bias the result in such a way that we could not detect any difference. This was a mistake and eventually led us into technical difficulties that prevented us to definitely conclude as to our original

hypothesis. Further studies should focus on setting up a controlled environment where a pre-defined TCR repertoire (potentially artificial) is selected on purified APCs.

REFERENCES

[1] B. L. Liu *et al.*, "ICP34.5 deleted herpes simplex virus with enhanced oncolytic, immune stimulating, and anti-tumour properties," *Gene Ther.*, vol. 10, no. 4, pp. 292–303, Feb. 2003.

[2] M. P. Gil, R. Salomon, J. Louten, and C. A. Biron, "Modulation of STAT1 protein levels: a mechanism shaping CD8 T-cell responses in vivo," *Blood*, vol. 107, no. 3, pp. 987–993, Feb. 2006.

[3] J. M. Curtsinger, J. O. Valenzuela, P. Agarwal, D. Lins, and M. F. Mescher, "Type I IFNs provide a third signal to CD8 T cells to stimulate clonal expansion and differentiation," *J. Immunol. Baltim. Md 1950*, vol. 174, no. 8, pp. 4465–4469, Apr. 2005.

[4] C. Su, G. Zhan, and C. Zheng, "Evasion of host antiviral innate immunity by HSV-1, an update," *Virol. J.*, vol. 13, p. 38, Mar. 2016.

[5] M. Zhang *et al.*, "HSV-2 immediate-early protein US1 inhibits IFN-β production by suppressing association of IRF-3 with IFN-β promoter," *J. Immunol. Baltim. Md 1950*, vol. 194, no. 7, pp. 3102–3115, Apr. 2015.

[6] Z. K. Pan, G. Ikonomidis, A. Lazenby, D. Pardoll, and Y. Paterson, "A recombinant Listeria monocytogenes vaccine expressing a model tumour antigen protects mice against lethal tumour cell challenge and causes regression of established tumours," *Nat. Med.*, vol. 1, no. 5, pp. 471–477, May 1995.

[7] P. F. Robbins *et al.*, "Mining exomic sequencing data to identify mutated antigens

recognized by adoptively transferred tumor-reactive T cells," *Nat. Med.*, vol. 19, no. 6, pp. 747–752, Jun. 2013.

[8] "Expressing Personalized Tumor Antigens Study." [Online]. Available: https://clinicaltrials.gov/ct2/show/NCT03265080. [Accessed: 20-May-2018].

[9] S. E. Doyle *et al.*, "Toll-like receptors induce a phagocytic gene program through p38," *J. Exp. Med.*, vol. 199, no. 1, pp. 81–90, Jan. 2004.

[10] A. E. Gelman, J. Zhang, Y. Choi, and L. A. Turka, "Toll-like receptor ligands directly promote activated CD4+ T cell survival," *J. Immunol. Baltim. Md 1950*, vol. 172, no. 10, pp. 6065–6073, May 2004.

[11] M. J. Richer, J. C. Nolz, and J. T. Harty, "Pathogen-specific inflammatory milieux tune the antigen sensitivity of CD8(+) T cells by enhancing T cell receptor signaling," *Immunity*, vol. 38, no. 1, pp. 140–152, Jan. 2013.

APPENDIX A

Generation of a Live Attenuated Influenza Vaccine that Elicits Broad Protection in Mice and Ferrets

Cell Host & Microbe
Article

Generation of a Live Attenuated Influenza Vaccine that Elicits Broad Protection in Mice and Ferrets

Lulan Wang,[1,2,3,12] Su-Yang Liu,[3,12] Hsiang-Wen Chen,[3,4,12] Juan Xu,[1,2,12] Maxime Chapon,[3] Tao Zhang,[1,2] Fan Zhou,[5] Yao E. Wang,[3] Natalie Quanquin,[3] Guiqin Wang,[5] Xiaoli Tian,[6] Zhanlong He,[7] Longding Liu,[7] Wenhai Yu,[7] David Jesse Sanchez,[8] Yuying Liang,[9] Taijiao Jiang,[1,2] Robert Modlin,[3,10] Barry R. Bloom,[11] Qihan Li,[7] Jane C. Deng,[6] Paul Zhou,[5] F. Xiao-Feng Qin,[1,2,*] and Genhong Cheng[1,2,3,13,*]

[1]Center for Systems Medicine, Institute of Basic Medical Sciences, Chinese Academy of Medical Sciences and Peking Union Medical College, Beijing 100005, China
[2]Suzhou Institute of Systems Medicine, Suzhou 215123, China
[3]Department of Microbiology, Immunology, and Molecular Genetics, University of California, Los Angeles, Los Angeles, CA 90095, USA
[4]Department of Microbiology, Faculty of Medicine, Kaohsiung Medical University, Kaohsiung 807, Taiwan
[5]Unit of Anti-Viral Immunity and Genetic Therapy, Key Laboratory of Molecular Virology and Immunology, Institute Pasteur of Shanghai, Chinese Academy of Sciences, Shanghai 200025, China
[6]Division of Pulmonary and Critical Care Medicine, Department of Medicine, University of California, Los Angeles, Los Angeles, CA 90095, USA
[7]Institute of Medical Biology, Chinese Academy of Medical Science and Peking Union Medical College, Kunming 650106, China
[8]Department of Pharmaceutical Sciences, Western University of Health Sciences, Pomona, CA 91766, USA
[9]295K Animal Science/Veterinary Medicine, University of Minnesota, 1988 Fitch Avenue, St. Paul, MN 55108, USA
[10]Division of Dermatology, Department of Medicine, University of California, Los Angeles, Los Angeles, CA 90095, USA
[11]Harvard School of Public Health, Boston, MA 02115, USA
[12]Co-first author
[13]Lead Contact
*Correspondence: fqin1@foxmail.com (F.X.-F.Q.), gcheng@mednet.ucla.edu (G.C.)
http://dx.doi.org/10.1016/j.chom.2017.02.007

SUMMARY

New influenza vaccines that provide effective and broad protection are desperately needed. Live attenuated viruses are attractive vaccine candidates because they can elicit both humoral and cellular immune responses. However, recent formulations of live attenuated influenza vaccines (LAIVs) have not been protective. We combined high-coverage transposon mutagenesis of influenza virus with a rapid high-throughput screening for attenuation to generate W7-791, a live attenuated mutant virus strain. W7-791 produced only a transient asymptomatic infection in adult and neonatal mice even at doses 100-fold higher than the LD_{50} of the parent strain. A single administration of W7-791 conferred full protection to mice against lethal challenge with H1N1, H3N2, and H5N1 strains, and improved viral clearance in ferrets. Adoptive transfer of T cells from W7-791-immunized mice conferred heterologous protection, indicating a role for T cell-mediated immunity. These studies present an LAIV development strategy to rapidly generate and screen entire libraries of viral clones.

INTRODUCTION

Influenza A virus is a major public health problem. In a typical year, influenza infects as many as 500 million people worldwide and leads to more than 500,000 deaths. In the United States, 5%–10% of the population is infected by influenza virus in an average season, resulting in ~220,000 hospitalizations and ~36,000 deaths (WHO, 2003). However, significant mutations in the virus will bypass host immunity to previously exposed strains, leading to considerably greater mortality. The devastating "Spanish flu" pandemic of 1918 was one such example, where the virus itself or complications from secondary infections killed an estimated 40–50 million people worldwide. Vaccination has been the most effective way to prevent the spread of influenza and its complications. Live attenuated influenza vaccines (LAIVs) are known to be more immunogenic than inactivated vaccines, likely because they stimulate both humoral and cell-mediated immune responses (Belshe et al., 2007). Traditionally, attenuated vaccines such as the measles-mumps-rubella and influenza vaccines were made via a forward genetics approach, using random mutagenesis followed by rounds of selection in non-physiological conditions, a time-intensive process that produces few vaccine candidates (Lamb et al., 1981). Moreover, these vaccines need to be reformulated annually due to antigenic drift and poor cross-protection against emerging pandemic strains (Jang and Seong, 2012; Krammer and Palese, 2015). In addition to difficulties in producing and formulating the vaccine, recent findings suggest that the quadrivalent LAIVs used over the last 3 years have not been protective. The CDC has actually recommended against using the LAIV during the 2016-2017 season (Grohskopf et al., 2016). In a proof-of-principle study, we sought to use the reverse genetics system of influenza virus and a transposon mutagenesis system as tools toward the rapid, high-throughput generation and screening of viral clones with attenuated growth in vivo as candidate LAIVs.

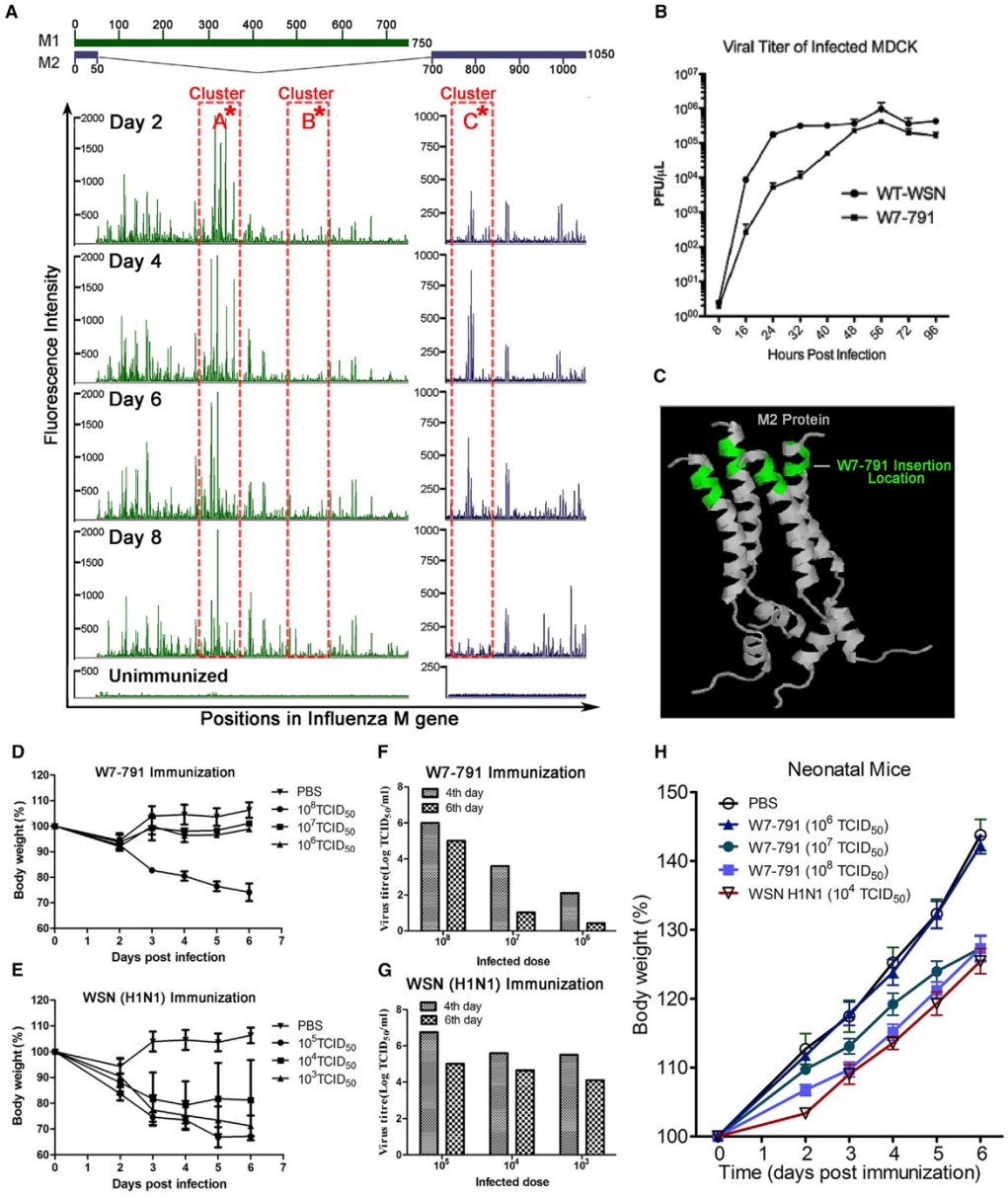

Figure 1. Generation of LAV W7-791 Using Genome-wide Mutagenesis and In Vivo Profiling

(A) Six- to eight-week-old C57BL/6 mice were infected with the M gene segment mutant population by i.t. injection (n = 8). Lungs were harvested at the indicated dpi and homogenized for genotyping. Peaks (M1 gene in green; M2 gene in blue) indicate the amount of viral RNA with insertions at that nucleotide position. Lung homogenates from PBS- or WT WSN-injected mice serve as negative controls. Clusters A*, B*, and C* are highlighted in red, representing the three types of observed growth profiles.

(legend continued on next page)

RESULTS

Generation of LAV W7-791 Using Genome-wide Mutagenesis and In Vivo Profiling

In contrast to the antigenic variability of the influenza hemagglutinin and neuraminidase genes, the matrix (M) gene segment encoding viral capsid protein (M1) and the proton-selective channel protein (M2) has evolved very slowly in all lineages of the virus and has been evaluated as a target for universal vaccine development (De Filette et al., 2005, 2008; Huleatt et al., 2008; Ilyinskii et al., 2008; Krammer and Palese, 2015; Neirynck et al., 1999; Schnell and Chou, 2008; Schotsaert et al., 2009; Tompkins et al., 2007; Wang et al., 2014). We created a mutant library comprised of $>10^5$ random insertions of a 15 nt sequence, 5′-NNNNNTGCGGCCGCA-3′, in the M gene of influenza A/WSN/1933 H1N1 (WSN), using a Mu-transposon mutagenesis method previously described (Arumugaswami et al., 2008). We then used the reverse genetics system of influenza to transfect the M gene mutant library with the seven complementary segments of wild-type (WT) WSN into HEK293T cells, creating a mutant virus library (Figures S1A–S1C). A primer based on the unique sequence contained within the insert was paired with different downstream primers along the length of the gene, generating a genotyping product of a specific length that could be used to extrapolate the position of the insertion. In this way, the mutation coverage of the entire viral pool could be visualized simultaneously. Analysis of this high-throughput genotyping data following in vitro infection of the mutant virus library (Figure S1D) shows that the majority of viable mutants (green peaks) are located in the non-conserved regions of the M1 and M2 proteins (Figures S1E and S1F).

In order to search for a potential LAIV, we monitored the in vivo growth profiles of the entire mutant virus population. Eight mice were given an intratracheal (i.t.) injection of the M gene mutant virus library, and cDNA was synthesized from the RNA recovered from lung homogenates collected 2, 4, 6, and 8 days post-infection (dpi). Through genotyping, we identified the location of each insertion in the pool of surviving mutant viruses at each time point. We observed three distinct growth profiles in these viruses (Figure 1A), possibly related to the mutations' effect on the replication, fitness, or host immune-related properties of the virus. Cluster A* represents an example of the fast-growing and likely disease-causing population. Cluster B* represents a slow-growing population, due either to intrinsically slow growth or suppression due to the host's immune response. By contrast, the viruses in cluster C* grew rapidly during the first 6 days, but were cleared between days 6 and 8. The advantages of this population are that these candidates persist long enough to trigger strong immune responses, but are too attenuated to cause significant disease in the host. We isolated 67 single mutant clones to screen as potential vaccine candidates (Figures S2A and S2B). We amplified three mutants in cluster C* (W7-757, W7-791, and W7-797) in Madin-Darby canine kidney (MDCK) cells and found that W7-791 grew to a high titer (Figure 1B) with a slightly lower cell toxicity (Figure S2C), causing less cell death as measured by LDH viability assay compared to the WT WSN virus. The mutant clone W7-791 had the insertion RHCGRI after the 26th amino acid of the M2 gene (Figure S2D), which is located on the cytoplasmic portion of the proton channel (Figure 1C) (Schnell and Chou, 2008). To ensure that W7-791 does not revert back to the WT WSN strain, we passaged W7-791 in vitro for multiple generations and found that the insertion remains unchanged in the genome (data not shown). To examine the in vivo stability of W7-791, we passaged the virus consecutively to groups of naive mice at 4 dpi (Figures S2E–S2G). We found that the W7-791 titer decreased after each passage, suggesting that the insertion mutation strain remained attenuated. Intranasal immunization of 6- to 8-week-old mice with different titrations of W7-791 showed no signs of weight loss even at 10^7 $TCID_{50}$ (50% tissue culture infection dose) per mouse, while significant weight loss was observed in mice infected with 10^3 $TCID_{50}$ of WSN (Figures 1D and 1E) or 10^4 $TCID_{50}$ of the H3 strain (Figure S3A). Similarly, the viral load in the lungs of W7-791-infected mice measured at 6 dpi was nearly 100-fold lower than in the WSN-infected group (Figures 1F and 1G) or the H3-infected group (Figure S3B). Lung samples collected at 4 dpi in both PBS and W7-791 groups showed no obvious pathology, whereas WT WSN mice, even at a much lower dose, showed severe tissue damage (Figure S3C). We further tested the safety of W7-791 in 15-day-old neonatal BALB/c mice by intranasal injection (10^6, 10^7, or 10^8 $TCID_{50}$) of W7-791 or 10^4 $TCID_{50}$ of WSN. The weight loss (Figure 1H) and lung findings (Figure S3D) suggest that W7-791 also exhibits significantly less pathology than WT WSN in neonatal mice. To test the extent of this particular insertion in causing viral attenuation, we inserted the same mutation into the matrix gene of influenza A/Puerto Rico/8 H1N1 (PR8), another mouse-adapted but heterologous H1 strain. We found that this mutant showed the same level of attenuation compared to its parent strain in vivo (Figure S4A). Taken together, we have established that the mutant W7-791 influenza strain is sufficiently attenuated to cause only a temporary infection and is safe at high titers in both adult and neonatal mice.

A Single Dose of W7-791 Can Elicit Protection against Lethal Homologous Influenza Virus Challenge

We next sought to determine whether vaccination with a single dose of W7-791 could protect mice against a lethal influenza virus challenge (Figure 2A). One month after i.t. inoculation with W7-791, mice were given a lethal dose of 4 MLD_{50} (50% mouse lethal dose) of WT WSN virus (Figures 2B and 2C). While the mock-vaccinated group all lost weight and died, all W7-791-vaccinated mice maintained a normal weight and survived. Interestingly, W7-791-vaccinated mice also survived without

(B) MDCK cells were infected at 0.25 MOI of WT WSN and W7-791 to determine the titer of virus at various time points. Data are mean ± SEM.
(C) The insertion position of W7-791 was mapped onto the known M2 crystal structure in green.
(D and E) Mouse body weight was monitored for 7 days post-inoculation with 10^6, 10^7, or 10^8 $TCID_{50}$ of W7-791 (D) or WT WSN (E). Data are mean body weight ± SEM.
(F and G) The viral titers from the W7-791 (F) or WT WSN (G) inoculation were evaluated on day 4 and day 6.
(H) The weight change of BALB/c pup mice (15 days of age) inoculated with the indicated titer of W7-791, WSN, or PBS. Data are mean body weight ± SEM.

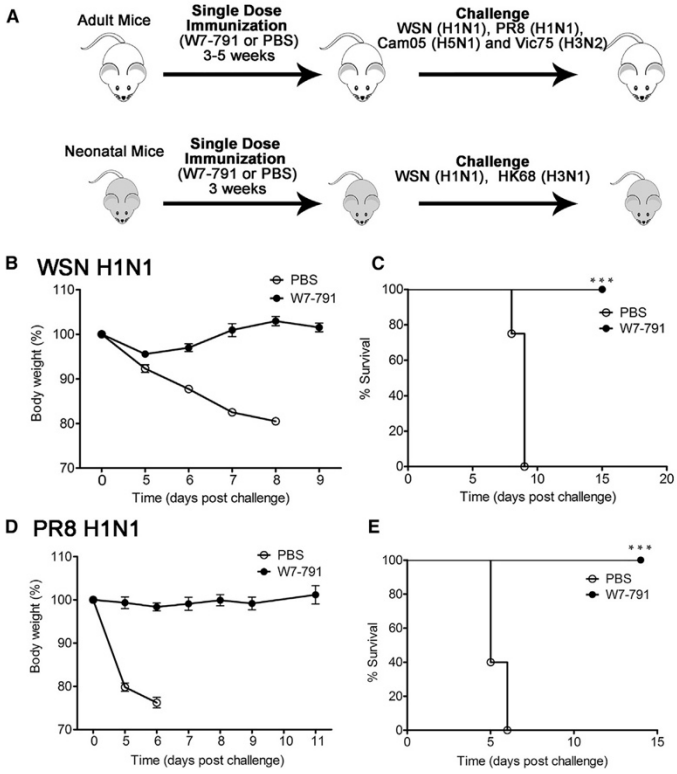

Figure 2. A Single Dose of W7-791 Can Elicit Protection against Lethal Homologous Influenza Virus Challenge

(A) Schematics of strategies used for mouse immunization and challenge.

(B and C) Mice were immunized intratracheally with 10^5 PFU of W7-791 (n = 5) or PBS (n = 5). One month after vaccination, mice were challenged with 4 MLD_{50} of WSN. Mouse weight (B) and survival (C) were measured at the indicated days after lethal challenge. Data are mean body weight ± SEM.

(D and E) Mice were immunized intratracheally with 10^5 PFU of W7-791 (n = 5) or PBS (n = 5). One month after vaccination, mice were challenged with 4 MLD_{50} of PR8. Mouse weight (D) and survival (E) were measured at the indicated days after lethal challenge. Data are mean body weight ± SEM. ***$p < 0.001$.

showing signs of illness or weight loss after challenge with 4 MLD_{50} of PR8 virus (Figures 2D and 2E).

A Single Dose of W7-791 Can Elicit Robust Cross-Protection against Lethal Heterologous Influenza Virus Challenge

We further explored whether W7-791 could cross-protect against heterologous highly pathogenic avian influenza (HPAI) A/Cambodia/P0322095/05 H5N1 (Cam/H5) (Figures 3A and 3B). Groups of BALB/c mice were inoculated intranasally (i.n.) with 10^6 plaque-forming units (PFU) of W7-791 and challenged 3 weeks later with 2 MLD_{50} of Cam/H5. All of the unvaccinated mice died, but the W7-791-vaccinated mice resisted the challenge without exhibiting significant weight loss. We extended our study to another phylogenetic influenza group, A/Victoria/3/75 H3N2 (Vic/H3) (Figures 3C and 3D). Mice were vaccinated with 10^5 PFU of W7-791, and then lethally challenged with 2 MLD_{50} after 4 weeks. Interestingly, W7-791-vaccinated mice only lost about 10% of their initial weight at 3–5 dpi with Vic/H3 before fully recovering, whereas the mock-vaccinated group succumbed to the H3N2 infection. Furthermore, we challenged W7-791-immunized mice against an escalated lethal dose of 5 MLD_{50} of WSN or HK68/H3 (Figure S4B). As before, all of the mice that were vaccinated with W7-791 survived the challenge, whereas PBS-immunized groups succumbed. Lastly, we tested whether W7-791 could cross-protect neonatal mice against lethal homologous and heterologous infections (Figures 3E and 3F). Fifteen-day-old BALB/c mice were immunized i.n. with 10^6 $TCID_{50}$ of W7-791 or PBS and then challenged with a lethal dose (10^5 or 10^6 $TCID_{50}$/mice) of WSN, or a lethal dose (10^6 or 10^7 $TCID_{50}$/mice) of A/Hong Kong/68 H3N1 (HK68/H3). Again, all vaccinated mice cleared the virus and survived the infection. Lastly, we compared our W7-791 strain with a quadrivalent LAIV used over the 2015-2016 season, FluMist. That LAIV contains attenuated viruses carrying antigens of two influenza B viruses, an H3N2 virus (Switzerland/9715293/2013), and an H1N1 strain (California/7/2009 pandemic virus). In vivo immunization and challenge with the same $TCID_{50}$ showed that W7-791 confers greater protection to mice against HK68/H3 (Figure S4C). All together, these results illustrate the capacity of our minimally modified mutant influenza strain to generate heterosubtypic protection against lethal virus challenge with a single immunization.

W7-791 Activates Both Humoral and Cell-Mediated Immune Responses

Live attenuated vaccines are thought to confer broad cross-protection against heterologous strains through activation of both humoral and cell-mediated immune responses. To determine the mechanisms responsible for the protective effects of W7-791, we immunized mice i.n. with W7-791, then challenged with WSN or PR8 viruses. We found that W7-791-vaccinated mice had significantly improved viral clearance against both viruses (Figure 4A). Surprisingly, W7-791-vaccinated mouse serum only showed hemagglutination inhibition (HAI) against WSN and not against heterologous strains PR8, HK68/H3,

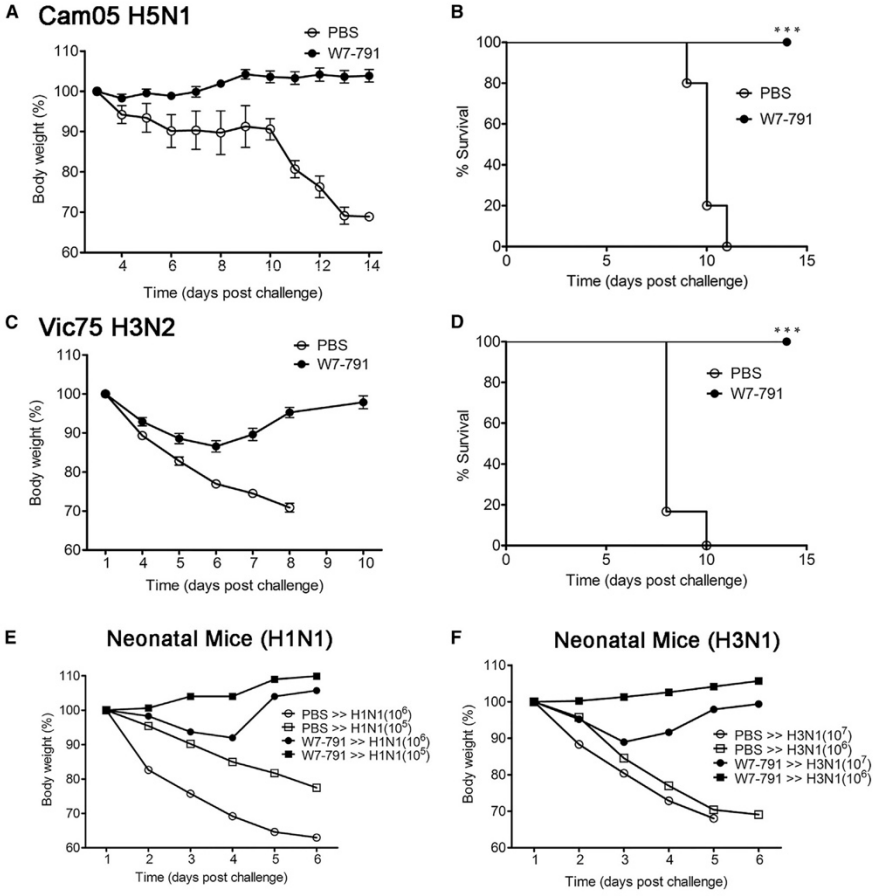

Figure 3. A Single Dose of W7-791 Can Elicit Robust Cross-Protection against Lethal Heterologous Influenza Virus Challenge

(A and B) Mice were immunized i.n. with 10^6 PFU of W7-791 (n = 6) or PBS (n = 5). Three weeks after vaccination, mice were challenged with 2 MLD_{50} of Cam/H5. Mouse weight (A) and survival (B) were measured at the indicated days after lethal challenge. Data are mean body weight ± SEM.

(C and D) Mice were immunized i.n. with 10^5 PFU of W7-791 (n = 9) or PBS (n = 6). One month after vaccination, mice were challenged with 2 MLD_{50} of Vic/H3. Mouse weight (C) and survival (D) were measured at the indicated days after lethal challenge. Data are mean body weight ± SEM.

(E and F) Weight change of neonatal mice lethally challenged with WSN (10^5 or 10^6 $TCID_{50}$) (E) or HK68/H3 (10^6 or 10^7 $TCID_{50}$) (F) 3 weeks after challenge. ***$p < 0.001$.

A/Wisconsin/2005 H3N2 (Wis/H3), or Cam/H5 pseudotype virus (Figures 4B and 4C). We further tested the serum using a microneutralization assay against WSN, PR8, and HK68/H3. Mice vaccinated with W7-791 showed a high neutralization titer against WSN and a lower level against PR8 and HK68/H3 (Figure 4D). These findings led us to believe that antibodies may not be the only source of protection mediated by W7-791.

To differentiate the cross-protective effect of cell-mediated and humoral responses, we immunized mice i.n. with 10^6 PFU of W7-791 or PBS, and collected serum and total T cells from spleens and lymph nodes 1 month later. We transferred these separately to naive mice and challenged them i.n. with a lethal dose of WSN or HK68/H3. The directly vaccinated (not transferred) group was used as a positive control and showed 100% protection. Adoptive transfer of serum from W7-791-immunized mice gave full protection against WSN, but not against HK68/H3 (Figure 4E). However, adoptive transfer of T cells from W7-791-immunized mice was able to partially or fully protect naive mice from HK68/H3 or WSN, respectively (Figure 4F). This demonstrates that W7-791 vaccination can generate a T cell-mediated immune response with a heterosubtypic protective ability. Furthermore, we evaluated CD8 T cell

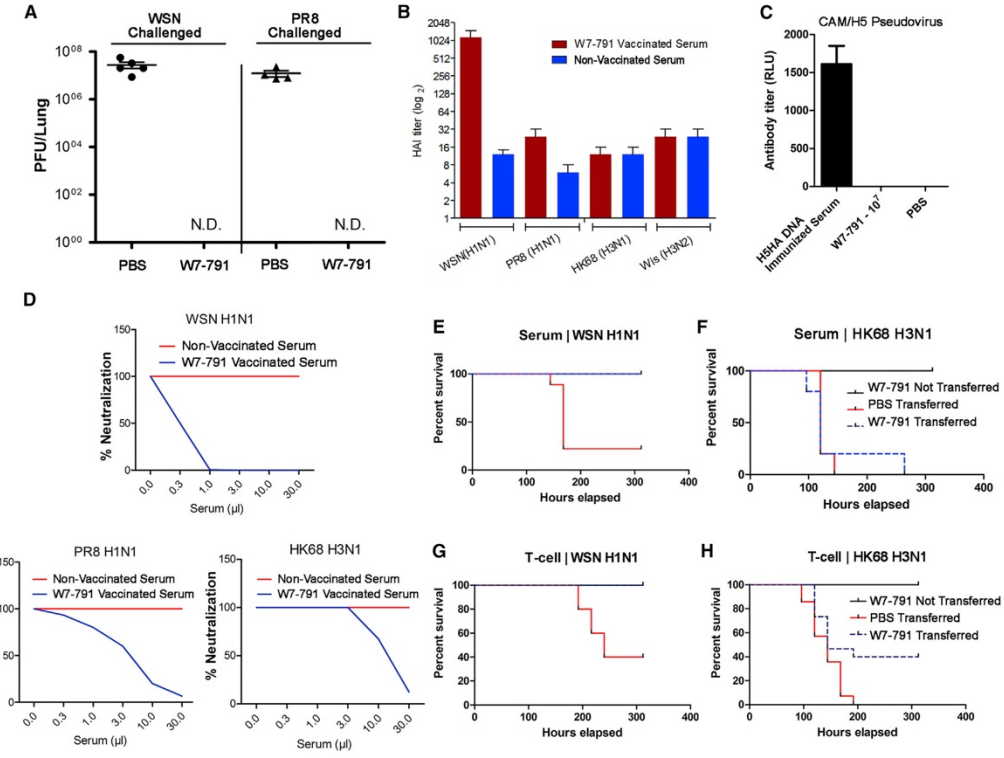

Figure 4. W7-791 Activates Both Humoral and Cell-Mediated Immune Responses

(A) Viral titers in lung homogenates of vaccinated and unvaccinated mice, challenged with lethal WSN or PR8, were quantified by plaque assay at the time of death or euthanasia.

(B) HAI assay of vaccinated and unvaccinated mouse serum against WSN, PR8, HK68/H3, and A/Wisconsin/05 H3N2. Mean ± SEM.

(C) The level of antibody in vaccinated and unvaccinated mouse serum was measured using Cam/H5 pseudovirus neutralization. Measurements are in relative light units (RLU). Mean ± SEM.

(D) Microneutralization assay of W7-791 vaccinated or unvaccinated mouse serum against WSN, PR8, and HK68/H3.

(E and F) Survival of mice receiving serum from W7-791- (n = 14) or PBS-vaccinated mice (n = 10). Mice were challenged 24 hr later with a lethal dose of WSN (E) or HK68/H3 (F).

(G and H) Survival curve of mice receiving T cells from W7-791- (n = 20) or PBS-immunized mice (n = 19), subsequently challenged with a lethal dose of WSN (G) or HK68/H3 (H). W7-791-vaccinated, but not transferred, mice were used as a control (n = 10).

epitopes in the W7-791-vaccinated mice (data not shown). We found that a large proportion of lung CD8+ T cells in W7-791-immunized mice were specific to H-2^{Db}-ASNENMETM (NP) 7 days after an H3N1 challenge. These data, combined with our adoptive T cell transfer experiment (shown in Figures 3F and 3H), has led us to believe that W7-791 immunization elicits cross-protective CD8+ T cell responses in our mouse model.

A Single Dose of W7-791 Elicits Heterologous Protection in the Ferret Model

To further explore the efficacy of W7-791 as an LAIV strain, we selected the ferret model, which resembles the pathophysiology of human influenza infection more closely than the mouse (Maher and DeStefano, 2004; Matsuoka et al., 2009). To evaluate the clinical response, we inoculated ferrets with 10^6, 10^7, and 10^8 $TCID_{50}$ of W7-791. We observed no significant changes in temperature (Figure 5A) or clinical symptoms (Figure 5B) after inoculation with 10^8 $TCID_{50}$ of W7-791. W7-791-vaccinated ferrets showed a significant increase in serum antibody titer (Figure 5C), but HAI assay confirmed that these antibodies bind to only the HA from WSN, and not HK68/H3 (Figures 5D) or H5N1 (Figure S5A). To examine protection against heterologous viruses, we challenged the ferrets 4 weeks post-immunization with either 10^6 $TCID_{50}$ of WSN, 10^6 $TCID_{50}$ of HK68/H3, or PBS. Ferrets that had been immunized with 10^3 and $10^{4.7}$ $TCID_{50}$ of W7-791 showed significant reduction in shedding of the challenge virus

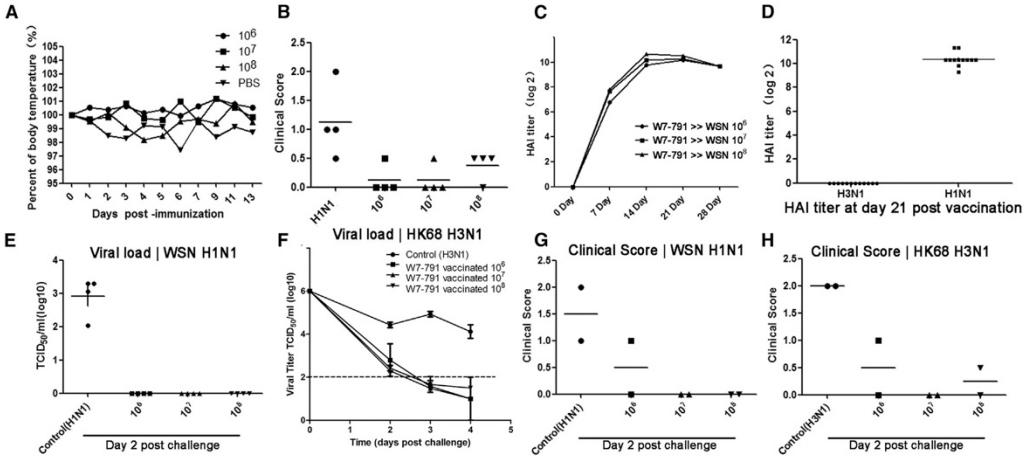

Figure 5. A Single Dose of W7-791 Elicits Heterologous Protection in the Ferret Model

(A) Temperature curve of ferrets inoculated i.n. with 10^6, 10^7, or 10^8 $TCID_{50}$ of W7-791 or PBS.

(B) Clinical scores of the ferrets 2 and 3 days post-inoculation with indicated doses of W7-791 or 10^6 $TCID_{50}$ of WSN. Clinical signs were evaluated as previously described (Reuman et al., 1989).

(C) HAI assay showing the increase of anti-W7-791 HA antibody titer from W7-791 inoculated ferrets after vaccination.

(D) HAI assay showing the titer of anti-H1HA or H3HA antibody 21 days post-inoculation.

(E–H) The viral titers (E and F) and the clinical scores (G and H) of the immunized and non-immunized ferrets challenged with 10^6 $TCID_{50}$ of WSN or HK68/H3. Data are mean body weight ± SEM.

within 2 dpi, compared to the unvaccinated group (control WSN or HK68/H3, respectively) (Figures 5E, 5F, and S5B). The vaccinated ferrets displayed an undetectable WSN or HK68/H3 viral load at 2 or 4 dpi, respectively. The vaccinated ferrets also showed improved clinical symptoms compared to non-vaccinated ferrets (Figures 5G and 5H). These data suggest that a single dose of W7-791 is safe in ferrets and can also elicit heterologous subtypic protection.

DISCUSSION

We have taken the approach of combining genome-wide mutagenesis and in vivo growth profile screening for the rapid and high-throughput development of LAIVs. As proof of principle, we used this method to uncover a promising LAIV, W7-791, that is over 100-fold more attenuated than the parent H1N1 virus, and is even tolerated in neonatal mice with no observable lung pathology. This strain could also confer complete cross-protection against heterologous H3 and H5 subtype influenza strains in mice. We further demonstrated that the insertion could be broadly applicable to attenuate other clades of influenza virus. The knockout or modified influenza M2 has been previously described as a potential LAIV candidate (Hatta et al., 2011; Watanabe et al., 2009). This present study explored the untapped potential of the M protein in generating LAIVs. The quadrivalent LAIV (FluMist) that was administered in the United States over the previous three seasons was shown to be ineffective compared to the inactivated vaccine. Our own comparison between the 2015-2016 FluMist formulation and W7-791 showed that our mutant H1 strain could confer greater protection in mice against challenge with an H3 virus than FluMist, which itself contains an H3 strain component. One possible explanation is that the primary method of protection in this case was not via H3-specific epitopes that were otherwise present in the quadrivalent LAIV, but rather through conserved epitopes still present in our H1 mutant strain. It is also plausible that W7-791, which is derived from a mouse-adapted strain, stimulated the immune system more efficiently through active replication in mice, and whether it can outperform FluMist in primates remains to be investigated. Although the reason for the failure of the FluMist over the last three seasons is under investigation, it was observed that this failure came at a time when the formulation was changed to having four viral components. While the inactive quadrivalent vaccine formulation is still effective, it is possible that including too many live influenza strains in the vaccine causes growth competition and reduced infectivity. Therefore, our strain may simply have been more effective because it was a single-component vaccine. The failure of FluMist is unfortunate, as live attenuated vaccines induce cell-mediated responses that are thought to target the more conserved parts of the virus, giving them the greatest potential for inducing broad protection against a multitude of strains. This would not only bypass the need to adjust our vaccines each year to account for antigenic drift variants, but could also protect us from highly pathogenic avian strains and novel reassortment viruses that could become the next influenza pandemic. W7-791 has shown great promise in its ability to confer protection against lethal heterologous influenza H1, H3, and H5 strains in mice (including

neonates) and ferrets. We demonstrated that even a single dose of W7-791 in mice could induce protection, without the need for prime-boost strategies or adjuvants. However, we acknowledge that the current extent of our LAIV characterization is limited. Future studies could include transferring the insertion to a master donor strain used for LAIVs, and expanding the range of the challenge doses to further evaluate the potential of this candidate vaccine. It also remains to be seen whether W7-791 will be successful in animals that have been previously exposed to influenza virus. In short, the development of a better influenza vaccine will require much more investigation, and the present work is only an initial step.

Our study also advances our understanding of the roles of antibody and T cell responses in influenza infection. Furthermore, we hypothesize that our strategy of screening for a growth phenotype that permits limited replication in the host and can elicit both cell-mediated and humoral immune responses without causing illness may be applicable to finding attenuated vaccines for other viruses. It would also be interesting to compare how the innate and adaptive immune systems communicate in response to influenza infection, an LAIV, or an inactivated vaccine.

This work presents an LAIV development strategy that can rapidly generate and screen entire libraries of viral clones for attenuation. We associated a particular viral growth profile in mice with the ability to elicit both cell-mediated and humoral immune responses without causing significant disease. From a cluster of viruses showing this ideal level of attenuation, we identified a promising LAIV candidate. This approach could potentially be implemented to discover attenuated mutants for other RNA and DNA viruses. It would require no working knowledge of specific genes or their functions in the virus, but could be used to establish a comprehensive profiling of the entire genome in vitro and in vivo. This system would also be ideal for expediting the design of live attenuated vaccines against less understood or emergent viruses.

EXPERIMENTAL PROCEDURES

Cell Culture

HEK293T cells were cultured in DMEM supplemented with 5% heat-inactivated fetal bovine serum (FBS). MDCK cells were maintained in DMEM containing 5% FBS, penicillin/streptomycin (100 U/mL and 50 μg/mL, respectively), and 1 mM sodium pyruvate at 37°C with 5% CO_2.

Generation of M Gene Segment Mutant Plasmid Library and Functional Profiling

To create the mutant plasmid library of the M gene segment of influenza A virus A/WSN/1933, a 15-nt sequence (5′-NNNNNTGCGGCCGCA-3′; N = duplicated 5 nucleotides from target DNA) was randomly inserted by Mu-transposon-mediated mutagenesis (MGS kit, Finnzymes) according to the manufacturer's instructions. The M gene mixed mutant pool was transformed into *E. coli* DH10B by electroporation at 2.0 kV, 200 Ω, 25 μF (ElectroMax DH10B, Invitrogen). The mutant M gene plasmid and seven remaining WT plasmids were transfected concomitantly into HEK293T cells for virus generation. Three days after transfection, the supernatant was collected and transferred to MDCK cells for propagation. Virus was collected after 48 hr, then either stored or used for further propagation for up to four passages. RNA was isolated with the TRIzol reagent (Invitrogen) after each generation. RT-PCR was carried out with the iScript cDNA Synthesis kit (Bio-Rad) to create cDNA. Three gene-specific forward primers approximately 400 bp apart in the M-gene segment (5′-AGCAAAAGCAGGTAGATATT-3′, 5′-GGGGCCAAAGAAATAGCACT-3′, and 5′-TCCTAGCTCCAGTGCTGGTC-3′) and a Vic-labeled insertion-specific mini-primer (5′-TGCGGCCGCA-3′) were used to amplify fragments containing the 15 nt insert using KOD Hot-Start polymerase (Novagen). The PCR conditions were set to 95°C for 10 min (1 cycle); 95°C for 45 s, 52°C for 30 s, and 72°C for 90 s (30 cycles); and 72°C for 10 min (1 cycle). The fluorescent-labeled PCR products were analyzed in duplicate with a Liz-500 size standard (Applied Biosystems) using a 96-capillary genotyper (3730xl DNA Analyzer, Applied Biosystems) at the UCLA GenoSeq Core facility. Sequencing data were analyzed for clarity using ABI software, with the following criteria: (1) all data passed the standard default detection level; (2) the first 70 bp were removed due to non-specific background noise; (3) all data were aligned to the nearest base pair in the influenza A WSN matrix gene; and (4) all genotyping experimental data were normalized with WT WSN-infected cells, non-transfected cells, and a different gene library as controls. This eliminated non-specific data from the PCR, primers, and the DNA Analyzer. For infection in vivo, the mutant virus pool was titered, concentrated by ultra-centrifugation and re-titered, and used for mouse injection. Two dpi, the lungs were harvested, homogenized, and resuspended in TRIzol for RNA isolation, followed by the same procedures as described above. PBS or WSN-infected mice served as controls.

Virus Strains

We used the influenza A/WSN/1933 reverse genetics system to generate seasonal A/H1N1 virus (Hoffmann et al., 2000). This strain is a mouse-adapted influenza virus and has been used as the parental strain to generate potential LAIVs using transposon mutagenesis. The eight plasmids containing the cDNA of A/WSN/33 (gift from Dr. Yuying Liang at Emory University) were transfected into HEK293T cells using TransIT LT-1 (Panvera) by the manufacturer's protocol. The virus was serially passaged three times in MDCK cells to a final titer of $10^{7.4}$ PFU/mL. Influenza virus A/Puerto Rico/8/1934 (seasonal A/H1N1 virus) was a gift from Dr. Yuying Liang. The virus was serially passaged three times in MDCK cells to a titer of $10^{7.5}$ PFU/mL. The MLD_{50} of both strains was determined in C57BL/6 mice.

Influenza virus A/Victoria/3/75 (seasonal A/H3N2 virus), A/Wisconsin/65/05 (seasonal A/H3N2 virus), and A/Hongkong/68 (seasonal A/H3N1 virus) were gifts from Dr. Ioanna Skountzou at Emory University. These viruses were amplified using MDCK cells for two to three passages to a final titer of $10^{5.5}$ PFU/mL, $10^{5.4}$ PFU/mL, and 10^{7} PFU/mL, respectively. The MLD_{50} was determined in C57BL/6 and BALB/c mice.

Influenza virus A/Cambodia/P0322095/05 (highly pathogenic avian influenza H5N1 virus) was originally isolated from human patients at the Pasteur Institute in Cambodia (Buchy et al., 2007). Virus was propagated in MDCK cells and virus-containing supernatants were pooled, clarified by centrifugation, and stored at −80°C. The $TCID_{50}$ and the MLD_{50} of the viruses were determined in MDCK cells and in BALB/c mice, respectively, and were calculated as described previously (Ding et al., 2011).

Virus Titrations

The concentration of infectious viruses was determined by plaque assay and end-point titrations. Plaque assays were performed in MDCK cells and calculated as PFU/μL of supernatant. The viral samples were serially diluted in dilution buffer (PBS with 10% BSA, $CaCl_2$, 1% DEAE-dextran, and $MgCl_2$). Diluents were added to a monolayer of MDCK cells in 6-well plates for 1 hr at 37°C, and then covered with growth medium containing 1% low-melting agarose and TPCK-treated trypsin (0.7 μg/mL). Infected cells were stained after 48 hr (1% crystal violet, 20% ethanol, in PBS) to visualize the plaques. Virus titrations were performed by end-point titration in MDCK cells. MDCK cells were inoculated with 10-fold serial dilutions of the virus, then washed with PBS once 1 hr after inoculation, and cultured in DMEM for 48 hr to visualize cell viability. The viral titer was determined by luminescence assay or by plaque assay. To measure the growth of individual mutants in vitro (Figure S2B), an influenza virus-responsive *Gaussia* luciferase (gLuc) reporter system was used. Briefly, the gLuc coding region was inserted in the reverse-sense orientation between a human RNA polymerase I promoter and a murine RNA polymerase I terminator. The gLuc coding sequence was flanked by the UTRs from the PA segment of influenza virus A/WSN/33 strain so that gLuc expression is dependent on influenza virus infection. The gLuc reporter was transfected into HEK293Ts for 24 hr before the supernatants containing mutant or WT influenza

viruses were added. Upon active infection, gLuc is released into the supernatant and can be quantified with *Renilla* luciferase substrate (Promega).

Animals

Adult Mice

Female C57BL/6 mice, 6–8 weeks old, were purchased from the Jackson Laboratory. All animals were housed in pathogen-free conditions within the UCLA animal facilities.

Neonatal Mice

Fifteen-day-old BALB/c mice (Vital River Beijing) weighing 6–9 g were inoculated i.n. with PBS, 10^4 $TCID_{50}$ of WSN virus, or dilutions of W7-791. For the dose-dependent experiment, mice were inoculated i.n. with 10^6, 10^7, and 10^8 $TCID_{50}$ of W7-791. Sixteen days post-treatment, mice were challenged i.n. with a lethal dose (10^5 or 10^6 $TCID_{50}$/mouse) of WSN or (10^6 or 10^7 $TCID_{50}$/mouse) A/Hong Kong/68 H3N1 (HK68/H3) in a 30 μL volume. Randomly selected mice from each group were sacrificed for pathological examinations of the lung at 4 and 6 dpi. Then the lungs were homogenized to measure viral titer using end-point-dilution assays.

Ferrets

Healthy young adult outbred female ferrets (Mustela putorius furo; between 4 and 5 months of age) were purchased from a commercial breeder (Wuxi) and confirmed to be seronegative by HAI assay to A/WSN/1933 (H1N1), A/Victoria/3/75 (H3N2), HK68 (H3N1), and W7-791(H1N1). A minimum of three independently housed ferrets were inoculated i.n. with 0.5 mL (0.25 mL per nostril) of 10^6, 10^7, or 10^8 $TCID_{50}$ of W7-791 or PBS. Anesthesia was performed on the quadriceps muscles of the left hind leg with a total volume of 0.02 mL Lumianning (Hua Mu Animal Care). Serum samples were collected at days 0, 7, 14, 21, and 28 post-immunization for HAI studies. Nasal washes were collected 0–7 days after immunization. Four weeks after immunization, the ferrets were challenged i.n. with 10^6 $TCID_{50}$ of WSN (H1N1) or HK68 (H3N1). Weights and temperatures were monitored daily for 7 days after inoculation. Nasal washes were collected 0–7 days after the challenge. Clinical signs were evaluated 3 days prior to vaccination, then 9, 11, 13, and 15 dpi, and 2 days prior to challenge and 1–7 dpi. The clinical signs were scored as previously described (Reuman et al., 1989). All animal studies were performed according to the guidelines of the UCLA Animal Research Committee.

Mouse Immunization and Challenge

Female C57BL/6 and BALB/c mice were randomly divided into groups of five or six mice. Groups were inoculated i.n. or intratracheally with either PBS or W7-791 in a volume of 50 μL. Intratracheal injection was performed by anesthetizing mice intraperitoneally with a ketamine/xylazine mixture, then surgically exposing the trachea for direct injection of 30 μL of solution with a sterile 27G needle (Shahangian et al., 2009). Four weeks after immunization, all mice were challenged i.n. or intratracheally with an influenza strain in a 50 μL volume: A/WSN/1933 (H1N1) at 4 MLD_{50}, A/Puerto Rico/8/1934 (H1N1) at 4 MLD_{50}, A/Cambodia/P0322095/05 (HPAI-H5N1) at 2 MLD_{50}, or A/Victoria/3/75 (H3N2) at 2 MLD_{50}. Mice were monitored and recorded daily for signs of illness, such as lethargy, ruffled hair, and weight loss. When mice lost 30% or more of their original weight, they were euthanized and counted as dead. For the adoptive transfer experiment, female C57BL/6 mice were randomly divided into two sets of vaccinated or unvaccinated groups. Unvaccinated mice were sham immunized, whereas the vaccinated group received a single dose of W7-791 at 10^6 PFU/mouse. One set from each group was used to harvest cells for the transfer experiment 4 weeks post-vaccination, while the other set was used as a vaccinated, but not transferred, control. Total CD4+ and CD8+ T cells were isolated from the spleens of the vaccinated and the unvaccinated mice using the Mouse Pan T Cell Isolation Kit and MS columns (Miltenyi Biotec). On the same day, the cells from the same group were pooled, and $\sim 10^{6.3}$ T cells/mouse were injected via the retro-orbital route to a new set of naive female C57BL/6 mice. Likewise, sera were isolated from either the vaccinated or unvaccinated groups and matching groups were pooled, then 100 μL/mouse of serum was administered retro-orbitally to a new set of naive female C57BL/6 mice. The mice in all groups were challenged i.n. at 24 hr post-adoptive transfer with 2 MLD_{50} of WSN or 2 MLD_{50} of HK68/H3.

In Vivo Challenge Using HPAI Virus H5N1

All animal protocols were approved by the Institutional Animal Care and Use Committee at the Pasteur Institute of Cambodia. Female BALB/c mice (*Mus musculus*) at the age of 6–8 weeks were purchased from Charles River Laboratories and housed in microisolator cages ventilated under negative pressure with HEPA-filtered air and a 12/12 hr light/dark cycle. Virus challenge studies were conducted in BSL3 facilities at the Pasteur Institute of Cambodia. Before each inoculation or euthanasia procedure, the mice were anesthetized by intraperitoneal (i.p.) injection of pentobarbital sodium (75 mg/kg; Sigma).

Ethical Statement

All animal experiments were carried out at biosafety level 3 (BSL3) containment facilities complying with the Ethics Committee regulations of the Institut Pasteur, in accordance with EC directive 86/609/CEE and were approved by the Animal Ethics Committee of the Institut Pasteur in Cambodia (permit number VD100820). Before each inoculation or euthanasia procedure, the mice were anesthetized by i.p. injection of pentobarbital sodium, and all efforts were made to minimize suffering.

Lung Homogenization

After animals were sacrificed, lungs were perfused by injecting 1 mL PBS containing 5 mM EDTA into the right ventricle. Whole lungs were removed and the lymph nodes were dissected away. The lungs were homogenized with 1 mL PBS containing a proteinase inhibitor cocktail (Roche Applied Science), and virus titers in lungs were evaluated by plaque assay. After homogenates were centrifuged at 10,000 × *g* for 10 min, the supernatant was collected for genotyping.

Sequence Comparisons

Influenza A Matrix 1 and Matrix 2 protein sequences from ~300 previously reported strains from 1918 to 2014 were compared and aligned using the NCBI influenza database (https://www.ncbi.nlm.nih.gov/genomes/FLU/about database.html).

Structure Analysis

Conserved and viable mutations in the M gene were mapped onto the crystal structure of the monomeric M1 gene (PDB: 2Z16) and the tetrameric M2 gene (PDB: 2L0J), which were obtained from PDB. The structure labeling was performed using PyMOL v.1.0.

In Vitro Assays

Cell Viability Assay

Cell viability was measured by CytoTox 96 Non-Radioactive Cytotoxicity Assay (Promega) according to the manufacturer's instructions.

HAI Assay

Viruses A/WSN/1933, A/Puerto Rico/8/1934, A/Wisconsin/65/05, and A/Hong Kong/68 were diluted to 4 HA units and incubated with an equal volume of serially diluted sera for 30 min at room temperature. An equal volume of 1% chicken red blood cells was added to the wells and incubation continued on a gently rocking plate for 30 min at room temperature. Button formation was scored as evidence of HAI. Assays were performed in triplicate.

Microneutralization Assay

MDCK cells (5×10^5 cells per well) were seeded onto a 12-well culture plate in complete DMEM overnight. To test the neutralization activity of immune sera, serial 3-fold dilutions of sera were incubated with $10^{6.5}$ PFU/mL, $10^{4.4}$ PFU/mL, and $10^{4.2}$ PFU/mL of viruses A/WSN/1933, A/Hongkong/68, and A/Puerto Rico/8/1934 at the final volume of 100 μL at room temperature for 1 hr. After the incubation, the mixture was added onto a monolayer of MDCK cells and was incubated for 1 hr at 37°C and then covered with growth medium containing 1% low-melting-point agarose and TPCK-treated trypsin (0.7 μg/mL). Infected cells were stained after 48 hr (1% crystal violet, 20% ethanol, in PBS) to visualize the plaques. Assays were performed in triplicate.

Pseudovirus Neutralization Assay

H5N1 pseudotype virus expressing the H5HA derived from A/Cambodia/P0322095/05 (GenBank: ADM95463), the N1NA (GenBank: AY555151) derived from A/Thailand/1(KAN-1)/2004, and a luciferase reporter gene were used in this experiment. The ferret sera were diluted in 2-fold serial dilutions from 1/20 to 1/1,280 and the mouse sera were diluted from 1/10 to 1/1,280. Sera from mice immunized by injection of H5HA DNA (GenBank: AAS65615) from A/Thailand/1(KAN-1)/2004 were used as a positive control. IC_{50} values were defined as the dilution of a given immune serum that resulted in 50% reduction of RLA. The assay was performed in triplicate.

SUPPLEMENTAL INFORMATION

Supplemental Information includes five figures and can be found with this article online at http://dx.doi.org/10.1016/j.chom.2017.02.007.

AUTHOR CONTRIBUTIONS

Conceptualization, G.C.; Methodology, L.W., S.-Y.L., and H.-W.C.; Investigation, L.W., S.-Y.L., H.-W.C., J.X., M.C., T.Z., F.Z., Y.E.W., N.Q., and G.W.; Writing – Original Draft, S.-Y.L. and L.W.; Writing – Review & Editing, L.W., M.C., and N.Q.; Resources, X.T., Z.H., L.L., W.Y., D.J.S., and Y.L.; Supervision, T.J., R.M., B.R.B., Q.L., J.C.D., P.Z., F.X.-F.Q., and G.C.

ACKNOWLEDGMENTS

We would like to thank Drs. Yuying Liang and David Sanchez for providing the influenza 8-plasmid reverse genetics system. We would like to thank Dr. Ren Sun for his help in the mutagenesis assay. This work was supported by grants from the Chinese Academy of Medical Sciences, including CAMS Initiative for Innovative Medicine (2016-I2M-1-005), the institutional research fund for Thousand Talents Program at the CAMS, the national special research fund for public welfare industry at the CAMS, and PUMC Youth Fund (3332015124); grants from the National Natural Science Foundation of China (91542201, 81590765, and 81501351); the Ministry of Health of China grant (201302018); Ministry of Science and Technology of China grant (2013CB911103); the national key scientific and technological special project of China for the development of major innovative drug (2015ZX09102023); the national special research fund for public welfare industry from the Ministry of Health and Family Planning of China (201302018); and NIH grants AI069120, AI056154, AI078389, and T32 AI089398.

Received: October 24, 2016
Revised: January 5, 2017
Accepted: February 6, 2017
Published: March 8, 2017

REFERENCES

Arumugaswami, V., Remenyi, R., Kanagavel, V., Sue, E.Y., Ngoc Ho, T., Liu, C., Fontanes, V., Dasgupta, A., and Sun, R. (2008). High-resolution functional profiling of hepatitis C virus genome. PLoS Pathog. *4*, e1000182.

Belshe, R.B., Edwards, K.M., Vesikari, T., Black, S.V., Walker, R.E., Hultquist, M., Kemble, G., and Connor, E.M.; CAIV-T Comparative Efficacy Study Group (2007). Live attenuated versus inactivated influenza vaccine in infants and young children. N. Engl. J. Med. *356*, 685–696.

Buchy, P., Mardy, S., Vong, S., Toyoda, T., Aubin, J.T., Miller, M., Touch, S., Sovann, L., Dufourcq, J.B., Richner, B., et al. (2007). Influenza A/H5N1 virus infection in humans in Cambodia. J. Clin. Virol. *39*, 164–168.

De Filette, M., Min Jou, W., Birkett, A., Lyons, K., Schultz, B., Tonkyro, A., Resch, S., and Fiers, W. (2005). Universal influenza A vaccine: optimization of M2-based constructs. Virology *337*, 149–161.

De Filette, M., Martens, W., Roose, K., Deroo, T., Vervalle, F., Bentahir, M., Vandekerckhove, J., Fiers, W., and Saelens, X. (2008). An influenza A vaccine based on tetrameric ectodomain of matrix protein 2. J. Biol. Chem. *283*, 11382–11387.

Ding, H., Tsai, C., Gutiérrez, R.A., Zhou, F., Buchy, P., Deubel, V., and Zhou, P. (2011). Superior neutralizing antibody response and protection in mice vaccinated with heterologous DNA prime and virus like particle boost against HPAI H5N1 virus. PLoS ONE *6*, e16563.

Grohskopf, L.A., Sokolow, L.Z., Broder, K.R., Olsen, S.J., Karron, R.A., Jernigan, D.B., and Bresee, J.S. (2016). Prevention and control of seasonal influenza with vaccines. MMWR Recomm. Rep. *65*, 1–54.

Hatta, Y., Hatta, M., Bilsel, P., Neumann, G., and Kawaoka, Y. (2011). An M2 cytoplasmic tail mutant as a live attenuated influenza vaccine against pandemic (H1N1) 2009 influenza virus. Vaccine *29*, 2308–2312.

Hoffmann, E., Neumann, G., Kawaoka, Y., Hobom, G., and Webster, R.G. (2000). A DNA transfection system for generation of influenza A virus from eight plasmids. Proc. Natl. Acad. Sci. USA *97*, 6108–6113.

Huleatt, J.W., Nakaar, V., Desai, P., Huang, Y., Hewitt, D., Jacobs, A., Tang, J., McDonald, W., Song, L., Evans, R.K., et al. (2008). Potent immunogenicity and efficacy of a universal influenza vaccine candidate comprising a recombinant fusion protein linking influenza M2e to the TLR5 ligand flagellin. Vaccine *26*, 201–214.

Ilyinskii, P.O., Gambaryan, A.S., Meriin, A.B., Gabai, V., Kartashov, A., Thoidis, G., and Shneider, A.M. (2008). Inhibition of influenza M2-induced cell death alleviates its negative contribution to vaccination efficiency. PLoS ONE *3*, e1417.

Jang, Y.H., and Seong, B.L. (2012). Principles underlying rational design of live attenuated influenza vaccines. Clin. Exp. Vaccine Res. *1*, 35–49.

Krammer, F., and Palese, P. (2015). Advances in the development of influenza virus vaccines. Nat. Rev. Drug Discov. *14*, 167–182.

Lamb, R.A., Lai, C.J., and Choppin, P.W. (1981). Sequences of mRNAs derived from genome RNA segment 7 of influenza virus: colinear and interrupted mRNAs code for overlapping proteins. Proc. Natl. Acad. Sci. USA *78*, 4170–4174.

Maher, J.A., and DeStefano, J. (2004). The ferret: an animal model to study influenza virus. Lab Anim. (NY) *33*, 50–53.

Matsuoka, Y., Lamirande, E.W., and Subbarao, K. (2009). The ferret model for influenza. Curr. Protoc. Microbiol. *Chapter 15*, 2.

Neirynck, S., Deroo, T., Saelens, X., Vanlandschoot, P., Jou, W.M., and Fiers, W. (1999). A universal influenza A vaccine based on the extracellular domain of the M2 protein. Nat. Med. *5*, 1157–1163.

Reuman, P.D., Keely, S., and Schiff, G.M. (1989). Assessment of signs of influenza illness in the ferret model. J. Virol. Methods *24*, 27–34.

Schnell, J.R., and Chou, J.J. (2008). Structure and mechanism of the M2 proton channel of influenza A virus. Nature *451*, 591–595.

Schotsaert, M., De Filette, M., Fiers, W., and Saelens, X. (2009). Universal M2 ectodomain-based influenza A vaccines: preclinical and clinical developments. Expert Rev. Vaccines *8*, 499–508.

Shahangian, A., Chow, E.K., Tian, X., Kang, J.R., Ghaffari, A., Liu, S.Y., Belperio, J.A., Cheng, G., and Deng, J.C. (2009). Type I IFNs mediate development of postinfluenza bacterial pneumonia in mice. J. Clin. Invest. *119*, 1910–1920.

Tompkins, S.M., Zhao, Z.S., Lo, C.Y., Misplon, J.A., Liu, T., Ye, Z., Hogan, R.J., Wu, Z., Benton, K.A., Tumpey, T.M., and Epstein, S.L. (2007). Matrix protein 2 vaccination and protection against influenza viruses, including subtype H5N1. Emerg. Infect. Dis. *13*, 426–435.

Wang, L., Hess, A., Chang, T.Z., Wang, Y.C., Champion, J.A., Compans, R.W., and Wang, B.Z. (2014). Nanoclusters self-assembled from conformation-stabilized influenza M2e as broadly cross-protective influenza vaccines. Nanomedicine (Lond.) *10*, 473–482.

Watanabe, S., Watanabe, T., and Kawaoka, Y. (2009). Influenza A virus lacking M2 protein as a live attenuated vaccine. J. Virol. *83*, 5947–5950.

WHO (2003). Influenza: fact sheets. http://www.who.int/mediacentre/factsheets/fs211/en/.